DEVELOPMENT AND VALIDATION OF A DRYING MODEL FOR *RASTRINEOBOLA ARGENTEA* FISH IN AN INDIRECT FORCED CONVECTION SOLAR DRYER

BY

GEORGE ODHIAMBO ONYINGE

A THESIS SUBMITTED IN FULFILLMENT OF THE REQUIREMENTS FOR THE DEGREE OF DOCTOR OF PHILOSOPHY IN PHYSICS

DEPARTMENT OF PHYSICS AND MATERIALS SCIENCE

MASENO UNIVERSITY

DECLARATION

I, GEORGE ODHIAMBO ONYINGE declare that the work presented in this thesis is my original work and that it has not been submitted in part/ full for an award in any other University.

Declaration by Student

George Odhiambo Onyinge
PG/ PhD/ 050/ 2010

Sign …… Date ……

Declaration by Supervisors

This thesis has been submitted for examination by our approval as University supervisors.

1. Prof. Andrew O. Oduor
   Department of Physics and Materials Science
   Maseno University.

Sign …….. Date…….

2. Prof. Herrick E. Othieno
   Department of Physics and Materials Science
   Maseno University.

Sign …….. Date ……

ACKNOWLEDGEMENT

I first and foremost thank the almighty God for the precious gift of life, his love and grace that enabled me to undertake my PhD studies. My sincere gratitude goes to my supervisors, Prof. Andrew Oduor and Prof. Herrick Othieno, for taking their time to read through the many drafts and for their valuable guidance, suggestions and criticisms that have been very useful in ensuring that this work meets the standards required by the examiners.

My special gratitude goes to Prof. Andrew Oduor, who originated the idea and the National Commission for Science, Technology and Innovation for availing the research grant for implementing the research project.

My appreciation also goes to the entire staff of the Department of Physics and Materials Science for their moral support, my special thanks goes to the chief technologist, Mr. John Otiato and all the technical staff; Mr. G. Ndinya, Mr. Edward Atito, Mr. A. Muhali, Mr. A. Orwa, Miss Valary Okudo and Mr. W. Ngunyi. I acknowledge with gratitude the assistance accorded to me by Mr. George Ndinya and Mr. Edward Atito in the programming and setting up of the data logging system during the data collection stage. My acknowledgement also goes to Mr. Samwuel Apima of Masinde Muliro University of Science and Technology for the assistance he offered me on Mat-lab programming.

I am also extremely grateful to Maseno University for offering me the opportunity to serve as a Tutorial Fellow in the Department of Physics and Materials Science, thereby enabling me to undertake PhD studies.

To my wife Mrs. Dorothy Odhiambo and children; Tigana, Timothy, Titus and Troy thank you for the understanding and patience during the entire period of undertaking my studies. Finally my appreciation also goes to my parents and the larger Onyinge family, thank you all for your encouragement, may the almighty God bless and keep you all.

DEDICATION

This work is dedicated to my parents Mzee Francis Onyinge and Mama Mary Onyinge; my wife Dorothy Odhiambo and all my children; Tigana, Baraka, Imani and Mwamba.

ABSTRACT

Rastrineobola argentea, (*R. argentea*) is a commercially important fish species in Lake Victoria, with a characteristically smaller size compared to the other fish and high surface moisture content. However the prevalent preservation method of the fish is open sun drying, in which the fish is laid uncovered on the ground for a prolonged period exposed to; contamination, attack by bacteria, molds, rodents, birds and adverse weather conditions. Often huge losses estimated at between 20 % and 50 % occur especially during the rainy season, because of the slow drying process that lasts several hours or even days depending on the prevailing weather. Although studies have been conducted on solar drying of *R. argentea* fish, none has been reported on modeling of its drying process. Moreover existing drying models of food products have been formulated based on internal moisture diffusion as the sole mass transfer mechanism, which is a falling rate period phenomenon. Studies have however shown that high moisture products exhibit both constant and falling rate drying periods, and therefore a linear section in their drying curves, that is not accounted for by the diffusion models. Thus in the present study, a drying model based on evaporation was formulated for *R. argentea* fish in an indirect forced convection solar dryer. The model results were compared with experimental data obtained from a prototype solar dryer and the tests revealed a reduction in moisture content of the fish from 73 % (w. b.) to between 8 % and 10 % (w. b.) after a period of 11 hours in the solar dryer whereas the open sun samples took 18 hours to reach the same moisture levels. Effective moisture diffusivities of $(1.65 \pm 0.02) \times 10^{-3} m^2 / s$ and $(0.91 \pm 0.05) \times 10^{-3} m^2 / s$ were obtained for the fish in the solar dryer and open sun, respectively. The activation energy of the drying process of *R. argentea* fish was also found to be: $-15.954 kJ / mol$, a much lower value than for other similar high moisture food products thus indicating that the energy threshold for drying the product that can be provided by the available solar energy. Statistical analysis carried out based on the moisture ratio of the fish in the solar dryer gave: $R^2 = 0.946, RMSE = 0.0383$, and $R^2 = 0.839, RMSE = 0.0533$, for the top and bottom trays, thus confirming the prediction reliability of the model. The simulations of the model further revealed that the drying time of this product can be reduced to 5 hours (the period after which deterioration of the product occurs if adequate drying has not occurred) in the solar dryer by increasing the air mass flow rate to $0.06\ kg / s$.

TABLE OF CONTENTS

LIST OF SYMBOLS AND ABBREVIATIONS

Y : Instantaneous air humidity

X : Instantaneous moisture content in the product

C_{pa} : Specific heat of air

ρ_a : Density of air

k : Drying constant

v_a : Velocity of air

L_v : Latent heat of evaporation of water

WS-**1**: First drying test series conducted during the wetter season; May – June 2014

WS-**2**: Second drying test series conducted during the wetter season; May – June 2014

WS-**3**: Third drying test series conducted during the wetter season; May – June 2014

DS-**4**: Fourth drying test series conducted during the dryer season; Jan – March 2015

DS-**5**: Fifth drying test series conducted during the dryer season; Jan – March 2015

RH_a : Relative humidity of ambient air (%)

RH_c : Relative humidity of drying chamber air (%)

m1L : Moisture ratio fish in the top left tray

m1R : Moisture ratio fish in the top left tray

m6L : Moisture ratio fish in the top left tray

m6R : Moisture ratio fish in the top left tray

m10L: Moisture ratio fish in the top left tray

m10R: Moisture ratio fish in the top left tray

mOSD: Moisture ratio fish for open sun dried sample

d 1L: Drying rate of fish in the top left tray (ghr^{-1})

d 1R: Drying rate of fish in the top right tray

d 6L: Drying rate of fish in the middle left tray

d 6R: Drying rate of fish in the middle right tray

d 10L: Drying rate of fish in the bottom left tray

d 10R: Drying rate of fish in the bottom right tray

d OSD: Drying rate of fish of open sun dried sample

$m\,d$: Mean drying rate (g/ hr)

Tc: Collector outlet temperature (^{o} C)

$T2$: Bottom tray temperature (^{o} C)

$T6$: Top tray temperature (^{o} C)

$T8$: Ambient air temperature (^{o} C)

$T13$: Middle tray temperature (^{o} C)

T_{bc}: Chamber bottom temperature (^{o} C)

V_i: Inlet air volume flow rate (m^3/ hr)

V_o: Outlet air volume flow rate (m^3/ hr)

$C.Eff.$: Collector efficiency on a typical drying day (%)

IR : Incident solar radiation intensity on a typical drying day (W /m^2)

$mdOSD$: mean drying rate of open sun dried sample (kg/ s)

1R: top right tray

1L: top left tray

6R: middle right tray

6L: middle left tray

10R: bottom right tray

10L: bottom left tray

A_c: Area of cover material

A_f : Area of concrete floor

A_p : Area of product

A_{in}: Cross section area of air inlet

A_{out}: Cross section area of air outlet

C_{pp}: Specific heat of product

C_{pv}: Specific heat of water vapor

C_{pas}: Specific heat of dry air

C_{pc}: Specific heat of cover material

C_{pl}: Specific heat of liquid

C_{pf} : Specific heat of floor

C_{pp} : Specific heat of wet product

C_{pa} : Specific heat of humid air

D: Average distance between floor and cover

D_{eff} : effective moisture diffusivity m^2/s

D_p : Thickness of the product

F_p : Fraction of solar radiation falling on product

G_a : Mass flow of air in a control volume

G_p : Mass flow of product in a control volume

$G_{p_{in}}$: Inlet mass flow of product

$G_{p_{out}}$: Outlet mass flow of product

H_{in} : Humidity ratio of air entering dryer

H_{out}: Humidity ratio of air leaving dryer

h_w : Convective heat transfer between cover and ambient

$h_{c,c-a}$: Convective heat transfer between air and cover

$h_{c,f-a}$: Convective heat transfer between floor and air

$h_{c,p-a}$: Convective heat transfer between air and product

$h_{r,p-c}$: Radiative heat transfer between product and cover

$h_{l,f-g}$: Conductive heat transfer between floor and underground

$h_{r,c-f}$: Radiative heat transfer between cover and sky

I_s : Incident solar radiation

K_a : Thermal conductivity of air

K_c : Thermal conductivity of insulation material

K_f : Thermal conductivity of floor material

L_p : Latent heat of vaporization of product

m_a : Mass of air inside the dryer

m_c : Mass of cover

m_f : Mass of concrete floor

m_p : Mass of product

M_p : Mass of product in the control volume

q_{lat} : Latent heat of vaporization of water in product

Q_p : Heat loss through dryer walls in the control volume

R_w : The drying rate

t_t : Residence time in the dryer

T_a : Ambient temperature

T_c : Cover temperature

T_f : Floor temperature

$T_{out,ch}$: Chimney outlet temperature

T_p : Product temperature

T_s : Sky temperature

U_c : Overall heat loss coefficient from cover to ambient

U_{va} **:** Volumetric heat transfer coefficient between air and product

V : Volume of drying chamber

V_a : Volume of air in the dryer

ν : Viscosity of air

V_{in} : Inlet air flow rate

V_{out} : Outlet air flow rate

ν_{in} : Inlet air speed

ν_{out} : Outlet air speed

V_w : Wind speed

W : Instantaneous moisture content

W_{in} : Moisture content of product entering dryer

Y_i : Absolute humidity of air

Y_{in} : Relative humidity of air entering dryer

α_c : Absorptance of cover material

α_f : Absorptance of floor material

ρ_c : Density of cover material

ρ_d : Density of dry product

ρ_p : Density of product

τ_c : Transmittance of cover material

ε_c : Emissivity of cover material

ε_p : Emissivity of product

ΔT_{lm} **:** Logarithmic mean temperature difference

α_p: Absorptance of product

∂_c: Thickness of cover

σ: Stefan Boltzmann constant

ρ_a: Density of air

MR: Moisture ratio

LIST OF TABLES

Page

LIST OF FIGURES

Page

LIST OF APPENDICES

Page

CHAPTER ONE: INTRODUCTION

1.1 Background of the Problem

Although fish is a major source of animal protein and an important food item in many countries, its high levels of moisture and unsaturated fatty acid makes it highly perishable during processing and preservation (Davies, 2009). It is estimated that 10 % or about 13 million tons of the world's total fish production is lost through spoilage, in spite of the existing high global demand (Abila, 2003). However when dried to moisture contents of less than 15 % (w. b.), fish products have a longer shelf life, better marketability and maintain a steady price (Morris, 1981). In order to achieve continuous availability of fish to the population all year round in developing countries, where dried fish is more popular, up to 40 % of the fish landings could be preserved by solar drying technologies rather than by open sun drying (Abila, 2003; Mustapha et al, 2014).

The fishing sector is particularly important in Kenya as it provides lively-hood, income and employment to more than 2 million people, with Lake Victoria providing 95 % of the total fish landings. The fishing is carried out by artisan fishermen who operate small boats in inland lakes and marine waters. A fraction of the fish harvested is sold fresh, while a significant portion is processed for later consumption. The main fish landed in Lake Victoria are: *Rastrineobola argentea*/ Dagaa (62.9 %), Nile perch/ *Lates niloticus* (29.9 %), Tilapia/ *Oreochromis niloticus* (5.3 %) *Halplochromines*/ Fulu (1 %) and others (0.8 %) (Nyeko, 2008).

Rastrineobola argentea (R. argentea), is a popular fish food for the low-income households in Eastern and Central Africa and is readily available at affordable price. It is the second commercially important among the fish species in Lake Victoria, owing to its high landings and wide use. But despite its higher landings, the value of the catch is often very low due to the huge

post harvest losses arising from poor transport systems and inadequate preservation facilities. Many artisan fish farmers resort to indigenous preservation methods such as smoking, salting and open sun drying (Owaga et al, 2011). However, open sun drying which involves spreading of the fish on the open ground over a large land space, is the most widely applied method. But the major limitation of this method is the lack of mechanisms for controlling the drying process, which is often slow and wholly dependent on the availability of sunshine. The method is also laborious as the fish layers have to be turned over periodically in order to achieve uniform drying. Moreover the duration of drying is often prolonged which exposes the fish to contamination, infestation by insects, rodents, birds and adverse weather conditions, leading to loss of quality and huge economic post-harvest losses, estimated at between 20 % and 50 %, especially during the rainy seasons (Owaga et al, 2011). At times the fish also loses some of the more fragile vitamins during the exposure to direct sunlight (Madhlopa et al, 2002) as per a survey that has revealed that most of the open sun dried *R. argentea* fish currently available in the market do not meet the quality requirements articulated in the KS 05-1470 standards (KIRDI, 2008).

Solar drying is a better preservation option for food products since it utilizes the solar energy more efficiently with the drying taking place in enclosed units under controlled conditions of temperature and air flow. The drying times are also shortened by up to 35 % of time taken by open sun drying. Solar dryers perform in humid as well as arid climates, and are operated in direct, indirect or mixed modes. In direct mode dryers, the food is placed in a chamber covered with a transparent plastic or glass and is exposed to direct sunlight; heat is thus trapped inside the dryer creating a "green house effect". Indirect mode dryers, on the other hand consists of separate solar heating units where air is preheated before being passed over the food products

stacked in trays, inside a drying chamber. Mixed mode dryers combine the use of the direct solar radiation with the preheated air from the solar collectors (Tripathy and Kumar, 2009). Solar dryers are further classified according to their mode of air flow as being either natural or forced convection. While natural convection dryers make use of the air buoyancy to maintain the air flow (do not require a fan) and are suited for rural areas, where there is no grid electricity, forced convection solar dryers require electricity to operate the incorporated fans.

When properly designed, solar dryers can solve the problems associated with open sun drying (Mohammed et al, 2005) since they have mechanisms for controlling and optimizing the drying process (Amer et al, 2010). However the design of an efficient drying technology for any product must involve mathematical modeling and simulation of the drying process of the product. The modeling entails formulating a set of equations that adequately characterize the drying system and whose solution allows the prediction of the process parameters as a function of time at any point in the dryer, based only on a set of initial conditions (Jindal and Gunasekaran, 1982). The main object of modeling and simulation is usually to obtain optimum dryer design and operating parameters for a particular set of conditions (Zomorodian and Moradi, 2010), that can be used in designing new drying systems or improving existing ones.

The most common modeling technique involves the subdivision of the drying system into equipment and material model components. The equipment component is formulated based on external heat transfer factors; which are a function of the dryer design (physical size and mode) and operating parameters (temperature, air relative humidity, air flow rate and the incident solar radiation) as well as the product thickness, quantity and moisture content (Kemp and Oakley, 2002). The material component on the other hand is based on the nature and internal thermal characteristics of the product to be dried. It therefore describes the heat and mass transfer

phenomena during thin layer drying processes of products, the fundamental mechanisms and distribution of moisture and temperature within the product. They are evolutions of density as a function of moisture content, since density is directly linked to quality, depends on moisture content and thus affects most of the thermo-physical and transport properties of a material (Giner, 2009).

A majority of the existing drying models are semi-theoretical/ thin layer, in which the drying time is related to measured moisture content of the product (Kemp and Oakley, 2002). While these models have capabilities of predicting the drying times and the drying characteristics of food / agricultural products, as a function temperature, air velocity and material characteristics (Afzel and Abe, 2000), they are formulated based on the assumption that drying processes of food products occurs solely by diffusion, starting with a decreasing drying rate while neglecting the effects of surface moisture evaporation. Although diffusion models can provide fairly accurate predictions of drying time, studies have shown that they cannot predict moisture distribution within the material, under non-uniform drying conditions (Srikiatden, 2007).

Moreover while diffusion-based models are based on the assumption that the drying of agricultural and food products occurs only during the falling rate period, it has been observed that drying of high moisture content foods occurs in both the constant and falling rate periods, where externally controlled surface evaporation rather than diffusion is the major moisture transport mechanism (Giner, 2009). Furthermore other studies have also shown that in rigid and highly porous products, where liquid water is located in large pores and channels, only heat transport rather than diffusion of liquid within the material is permitted (Srikiatden, 2007). The drying of high moisture content products cannot therefore be adequately described by diffusion models which are based solely on falling rate drying phenomena.

Notwithstanding their shortcomings, diffusion models have been used to simulate thin layer drying of many food and agricultural products including: Tilapia fish, green Beans, Tomato slices, Pistachio, red Pepper, Mint leaves, tarragon, Potato, Chilli pepper, Carrot, Citrus, Aurantium leaves, Vegetable by-product, Tropical fruits, surgical Cotton, Wood, Herbal and medicinal plants, Sardine fish, Cocoa beans, Herbs and spices and Strawberry. It is thus observed that the diffusion models adequately describe the drying characteristics of food products whose initial moisture contents are less than the critical moisture content, but are inadequate for products which exhibit both constant and falling rate periods of drying, and whose initial moisture contents are higher than the critical moisture content.

Like other fish, *R. argentea* is a high moisture content product with an initial moisture content of 73 % (w. b.) greater than the critical moisture content of 30 % (w. b.). Studies have thus reported its drying characteristics as exhibiting both constant and falling rate drying periods (Odour-Odote et al, 2010), which suggests that its drying cannot be adequately be described by a diffusion based model. Even though evaporation-based drying models are still largely scarce in literature, a study by Giner, (2009) has proposed a drying model for high moisture foods by adopting an analytical solution of the unsteady state diffusion equation for a plane sheet, by taking into account both internal and external resistances while neglecting the internal moisture gradients. Whereas the model provides a prediction of the linear behavior of the average moisture content, as a function of time for the surface and several positions within the plane sheet, at early stages in the drying curve, under certain conditions the curves are found to differ from one another and none is linear, thus suggesting that the linear drying behavior is restricted to the average moisture content for only a limited period. The study therefore failed to establish whether or not the constant rate period of drying in high moisture content foods, is a purely

convective and externally controlled process. Moreover it also fell short of establishing the dominance of the surface evaporation over diffusion as a moisture transport mechanism in high moisture content foods. The present study was carried out with the aim of formulating an evaporation-based model that would adequately describe the drying of *R. argentea* fish in an indirect solar dryer, and then not only compare the theoretical and experimental data but also determine through experiment the thermal properties of the product such as; effective moisture diffusivity coefficient and activation energy, that cannot be predicted theoretically and are also unavailable in physical property data banks.

1.2 Statement of the Problem

The majority of existing material models are thin layer based, for which the drying time is related to measured moisture content of the product (Afzel and Abe, 2000). Although these models adequately describe the drying characteristics of food products whose initial moisture content are lower than the critical value, they are inadequate for high moisture foods that exhibit both constant and falling rate periods of drying and whose initial moisture contents are much greater than the critical value (Kemp and Oakley, 2002).

The major weakness of diffusion-based models being that they are based on the assumption that drying processes of food products occurs in the falling rate period with diffusion as sole moisture transfer mechanism, starting with a decreasing drying rate while neglecting completely the effects of surface moisture evaporation.

But as some authors have observed, the drying of high moisture content foods actually occurs in both constant and falling rate periods and where in the former period it is known that externally controlled surface evaporation is the main transport mechanism and not internal moisture diffusion. Furthermore that in rigid and highly porous products, liquid water is located in large

pores and channels with only heat transport rather than diffusion of liquid within the material being permitted. The drying of such products cannot therefore be adequately described by diffusion models which are based wholly on the falling rate drying phenomena.

1.3 Objectives of the Study

The study was undertaken with the broad objective of formulating a drying model for *R. argentea* fish in an indirect forced convection solar dryer.

1.3.1 Specific Objectives

1. Formulating a drying model, based on evaporation, for the drying process of *R. argentea* fish in an indirect forced convection solar dryer.
2. Comparison of the results of the model with those of experimental tests on the prototype solar dryer.

1.4 Justification of the Study

The drying model for *R. argentea* fish would be a useful tool in the design process of an efficient solar dryer that is capable of drying this product in a much shorter drying time. Its application in the solar drying process of the fish product could therefore lead to improvement of the preservation and reduce the risks of attack by bacteria, molds, insects, rodents and contamination. Overall the implementation of the recommendations of this study would lead to a significant reduction in the economic losses currently encountered by the fish farmers, estimated at 50 % of the catch (Owaga et al 2011) as well as the improvement of quality of the dried fish product and hence the need for the study.

1.5 Limitations of the Study

One limitation of the study was the relatively short time span of the experimental tests, where a prolonged period would have captured the seasonal variation of the operating parameters but which was not possible in the present study due to budget and time constraints. The other limitation was the lack of appropriate instrument for measuring the moisture content of the fish directly, where instead indirect measurements were carried out through weighing at regular intervals of time.

CHAPTER TWO: LITERATURE REVIEW

2.1 Understanding the Drying Process

Drying is a heat and mass transfer process involving the migration of moisture from the interior of the individual material to the surface and subsequent evaporation to the surrounding air. The material absorbs heat increasing its vapor pressure above that of the surrounding air, creating thermal and pressure gradients that causes the liquid and vapor to move to the surface where the evaporation takes place (Ghaba et al, 2007). Drying requires heat to draw out the moisture from the material and dry air with adequate circulation to absorb and carry away the released moisture. The energy consumed by the drying process depends on the drying rate and the moisture content distribution within the thin layer of the material. The internal liquid flow within the product occurs by diffusion in continuous/ homogenous solids, where the liquid diffusion coefficient is a function of moisture content and by capillarity for granular/ porous solids.

Drying occurs in two phases; constant and falling rate periods. During constant rate drying, the moisture movement within the solid is rapid enough to maintain a saturation condition at the surface and so the drying rate is controlled by the rate at which heat is transferred to the evaporating surface (Chandrakumar and Jiwanlal, 2013). During this phase the mass transfer occurs by diffusion of vapor from the stagnant air film into the surrounding atmosphere while the temperature of the surface remains constant. Constant rate drying therefore depends on the heat and mass transfer coefficients, the area of material exposed to the drying medium and the difference in temperature and humidity between the gas stream and the wet surface of the solid material (Murthy, 2009). The falling rate drying phase on the other hand begins at the critical moisture content and occurs in two sectors; unsaturated surface drying and internal moisture controlled drying. In the first sector, the entire evaporating surface cannot be maintained at

saturation by moisture movement within the solid so the drying rate decreases (Saleh and Badran, 2009). Here the drying rate is affected by factors that govern diffusion and moisture movement away from the evaporating surface. The second sector which determines the overall drying time, occurs when the evaporating surface is unsaturated and the point of evaporation moves inside the solid, hence the drying rate is controlled by the rate of internal moisture movement and not the external variables (Raju et al, 2013) and thus the total drying time is the sum of the constant and falling rate periods.

2.1.1 Modeling the Drying Process of Food Products

Mathematical modeling of drying characteristics is based on the physical mechanisms of heat /mass transfer conditions that are external as well as those inside the material, in which thermodynamic relationships involving the drying air and product moisture are applied in solving the heat and mass balance equations (Saleh and Badran, 2009). Some of the physical mechanisms that describe the moisture transport within the capillary porous product include: diffusion (liquid movement due to moisture concentration difference), capillarity (liquid movement due surface forces), surface tension (liquid movement due to diffusion of moisture on the pore surfaces), thermal diffusion (vapor movement due to temperature difference), vapor diffusion (vapor movement due to moisture concentration difference), hydrodynamic flow (water and vapor movement due total pressure difference) (Sagagi and Enaburekhan, 2007). Based on these physical mechanisms, models are constituted consisting of a set of partial differential equations, that describe the moisture transfer in capillary porous materials /cereals grains (Brooker et al, 1978)

Drying is a complex process in which more than one mechanism (which may also vary during the drying process), contributes to the total mass transfer rate (Ghaba et al, 2007). The inlet conditions are dependent on metrological factors and are strong functions of time, although most of the simulation models consider them as being constant. Some of the parameters involved in simulation models and prediction of dryer performance include: equilibrium moisture content, drying rate constant, physical properties of agriculture products / moist air and psychometric parameters.

Materials are classified as belong to either type A (fast drying) or type B (slow drying) where in the former the drying rate is dependent on gas velocity (air flow rate) and is accelerated by higher gas velocities and gas inlet temperatures but reduced by bed depth. On the other hand for class B materials their drying rate is independent of gas velocity and bed depth but is affected by gas temperature, except wheat most materials exhibit a mixture of type A and B characteristics (Kemp and Oakley, 2002).

There are three types of models for describing the drying characteristics of agricultural products; theoretical, semi-theoretical and empirical models; theoretical models consist of diffusion/ simultaneous heat and mass transfer equations, semi-theoretical models consist of approximated theoretical equations while empirical models are based on simulations of experimental data. For theoretical and semi-theoretical models the assumption is that the ratio of the volumes of air and the product are infinitely large, so that the drying rate depends only on the properties of the material to be dried; the size, drying temperature and moisture content. While theoretical models take into account the internal resistance to moisture transfer, semi-theoretical models account only for the external resistance to moisture transfer between the air and product. Semi-theoretical/ thin layer model equations, analogous to Newton's law of cooling are however more

popular than theoretical model equations, which are more complex and involve heavy computations.

2.1.2 Semi-theoretical/ Thin Layer Drying Models

Semi-theoretical or thin layer drying models are formulated based on Fick's second law of diffusion given by (Christie, 2008):

$$\frac{\partial X}{\partial t} = D_{eff} \frac{\partial^2 X}{\partial y^2} \tag{2.1}$$

for an infinite slab, assuming one-dimensional moisture transfer, no shrinkage, constant temperature and diffusivity coefficients and negligible external resistance. These models describe the drying process of most biological/ food materials that occur in the falling rate period, where the moisture transfer process is controlled by internal diffusion and influenced by moisture content and temperature of the product (Youcef et al, 2001).

Thus thin layer drying models assume that all resistance to moisture flow is concentrated on a thin layer at the surface of the material, with the drying rate being directly proportional to the difference between the instantaneous and equilibrium moisture content with the surrounding air. The rate of moisture loss during thin layer drying of agricultural / food products is thus given by:

$$\frac{dX}{dt} = -k[X(t) - X_e] \tag{2.2}$$

For the drying characteristics of biological products, the solution of the Fick's diffusion equation is the moisture ratio (MR) equation given by (Sagagi and Enaburekhan, 2007):

$$\frac{X(t)}{X_o} = \frac{8}{\pi^2} \exp\left[-D_{eff} \left(\frac{\pi}{2L} \right)^2 \right] t = \exp(-kt) \tag{2.3}$$

where X_e is the equilibrium moisture content (%) dry basis (d. b.), X_o is the initial moisture content (%) d. b. and $X(t)$ is the moisture content (%) d. b., at any time, D_{eff} is the effective moisture diffusivity, t is time and L is the characteristic diameter of the product and where the drying rate constant k is given by (Babalis and Belessiotis, 2004):

$$k = -D_{eff}\left(\frac{\pi}{2L}\right)^2 \tag{2.4}$$

Equation 2.3 is therefore the most basic drying equation known as the logarithmic or exponential model. The presence of the exponential term in model indicates the contribution of the diffusion mechanism in thin layer drying; which involves the moisture removal from the porous media through evaporation by passing excess drying air over a thin layer of the material, until the equilibrium moisture content is reached.

Thin layer drying models have thus been more widely applied in the design process and optimization of food/ crop dryers in the food industry because the final dried products usually record minimal loss of their native nutritional, chemical and physical qualities with the extension of shelf life and onset of microbial spoilage (Akpinar and Bicer, 2008). A number of these models have been developed for the drying characteristics of various agricultural products, some of which are given in Appendix, Table A2.

2.2 Some Existing Drying Models

2.2.1 Model for the Drying of Tilapia Fish, (*Oreochromis niloticus*) in a Solar Tunnel Dryer

The formulation of this model was based on thin layer drying assumptions of: unidirectional moisture movement by diffusion and negligible effect of air velocity on drying (Kituu et al,

2010). A drying rate equation in the form of Fick's diffusion model (Equation 2.1) was applied based on the following boundary conditions:

$$X(t=0,y)=X_o,\ X(t=t_\infty,y)=X_e \text{ and } \frac{\partial X}{\partial y}(y=0,)=0 \tag{2.5}$$

The solution of the model equation for thin layer drying of fish in trays with planar geometry representing the moisture ratio was thus obtained as:

$$MR=\frac{X-X_e}{X_o-X_e}=\frac{8}{\pi^2}\sum_{n=0}^{\infty}\left(\frac{1}{2n+1}\right)^2\exp\left[-(2n+1)^2\frac{\pi^2}{d^2}D_{eff}t\right] \tag{2.6}$$

For large values of time, the solution was taken as the first term of the series ($n=0$) and given by:

$$MR=\frac{8}{\pi^2}\exp\left[-\frac{\pi^2}{d_s{}^2}D_{eff}t\right] \tag{2.7}$$

A shrinkage-dependent drying rate constant k was also developed through analysis of the structural properties, as a function of moisture content and temperature and given by:

$$k=D_o\left(\frac{\pi X_o}{d_o(1+\beta_s'X)(X_o-\beta_s'X}\right)^2\exp\left(\frac{-E}{RT_p}\right)\Delta t \tag{2.8}$$

where d_s shrinkage thickness of drying fish at any time was defined in terms of the shrinkage coefficient and moisture content as:

$$d_s=d_o\left(1-\beta_s'\frac{X}{X_o}\right) \tag{2.9}$$

where d_o initial thickness of drying fish and β_s' the linear shrinkage coefficient, was given by:

$$\beta_s' = \left(\frac{\rho_s}{\rho_s + \rho_w X_o} \right)^{1/3} \tag{2.10}$$

where ρ_s solid density of fish ρ_w density of water X_o initial moisture content.

.

The effect of shrinkage (reduction in the dimensions of the product) on the drying kinetics of the drying fish as represented by the shrinkage dependent effective diffusivity D_{sf} was thus given by:

$$D_{sf} = D_{eff} \left(\frac{1}{1 + \beta_s' X} \right)^2 \tag{2.11}$$

where D_{eff} is the effective moisture diffusivity of the drying fish.

The effective diffusivity dependency on drying temperature deduced from the Arrhenius relation, (Equation 3.35) with the values of D_o and E was defined by the relations:

$$D_o = \exp\left(-1308.795 + \frac{6072317}{T_p - 273} + 195.799 In(T_p - 273) \right) \tag{2.12}$$

$$E = \left(1554.946 - 0.059(T_p - 273) + 0.299271(T_p - 273)\right)^2 (a_x + b_x M) \tag{2.13}$$

where a_x and b_x are exponential factors, T_p the drying temperature. The model was thus simulated using Visual Basic program with an input parameter I_c dependent on solar energy reception.

2.2.2 Modeling of Wood Solar Drying under the Moroccan Climate

The main assumptions of the model were: uniform temperatures of the wood, dryer and the moisture, unidirectional air flow and constant values of transfer coefficients (Bentayab et al, 2011). The model is based on global balance that takes into account the transfer exchange

between the wood, drying air, walls of the dryer and ambient medium and was used for determining the temperature, moisture content distribution of the timber and air moisture content inside the drying room. The moisture rate in the drying air was given by:

$$\frac{dY_i}{dt} = -\frac{Q}{V}(Y_i - Y_e) - \frac{M_o}{V}\frac{dX}{dt} \tag{2.14}$$

where Q volumetric flow rate of air through the dryer, V volume of the dryer Y_i and Y_e are the absolute values of air humidity inside and outside the dryer.

The drying rate was of the form of Fick's law equation for moisture transport in solids that considers the in-homogeneity of the wood and multitude of moisture transport mechanisms in the drying of wood, and was given by:

$$m_0 \frac{dX}{dt} = -K\rho_o S(X - X_e) \tag{2.15}$$

where K moisture transfer coefficient in the timber X_e and X are equilibrium and absolute humidity of the timber respectively and which on applying Taylor's relation was given by:

$$\frac{dX}{dt} = -fKS\frac{(X - X_e)}{d} \tag{2.16}$$

where d is thickness of the wood while f is the saturation coefficient given by:

$$f^2 = \frac{Y_s - Y}{\overline{Y_s} - \overline{Y}} \tag{2.17}$$

where Y and Y_s are the absolute and saturated humidity, while $\overline{Y}$ and $\overline{Y_s}$ are their average values during the drying period. The solar energy input to the dryer was thus deduced from a thermal balance about the solar radiation through the glass walls, the ground and the north facing wall.

2.2.3 Modeling of a Mixed Mode Natural Convection Solar Crop Dryer

The drying phenomena was modeled by taking a thin layer of a slab shaped crop bed of thickness dz and then combining many of these thin layers to form a deep bed thickness of z_o (Forson et al, 2007). By consecutively calculating the air and moisture changes occurring during short intervals of time, as drying air passes from one layer to another, the continuous drying process was simulated assuming that each layer is dried for a short time interval dt using air leaving the preceding layer. The process was repeated with consecutive short increments of time until the desired final moisture content was achieved. The four independent partial differential equations used to predict changes in crop temperature, moisture content, air temperature and relative humidity were:

1. Drying rate of crop
2. Mass balance on the drying air
3. Heat balance on the drying air
4. Heat balance on the crop

This model considered the drying chamber walls to be dia-thermic thus requiring a fifth equation for the energy balance on the chamber walls, an expression for determining the steady state operating temperature of the drying chamber wall. The rate of moisture removal from the bed was modeled using the diffusion model for slab shaped bed, (Equation 2.32) in which the diffusion coefficient is a function of moisture content, drying air temperature and drying air relative humidity. The diffusion coefficient, modified based on preliminary experimental results was given by:

$$D = \psi\left(-0.0274 - 5.74\times10^{-6}X + 5.98\times10^{-6}e^{X} + 0.0275e^{-\frac{1}{T}} + 2.23\times10^{-6}\{-2RH + 1.2\}\right) \quad (2.18)$$

where ψ is a multiplying factor whose value depends on the range of moisture content of the product. The equilibrium moisture content of hygroscopic materials was thus computed from the generalized relation below:

$$In\frac{X_e}{P_o + P_1RH + P_2RH^2 + P_3RH^3} = q_o + \left(q_1 + q_o + q_1RH + q_2RH^2 + q_3RH^3 + q_4RH^4\right)T \tag{2.19}$$

where P_i and q_i are product dependent constants, while RH and T are the relative humidity and temperature respectively.

2.2.4 Model of the Drying Process of Vegetable Wastes from a Wholesale Market in a Rotary Dryer

The model was derived based on the following assumptions that: the products have a rectangular geometry whose dimensions remain unchanged during the drying process, the drying process consists only of the falling rate phase, the air mass flow rate being constant throughout the dryer, which works in optimal load conditions (3 % to 7 % of the total dryer volume) and with each control volume the inlet flow rate of product being equal to the outflow rate of product from previous control volume (Iguaz et al, 2003).

Thus the model equations were:

1. Mass balance of the product

$$\frac{dM_p}{dt} = G_{P_{in}} - G_{P_{out}} \tag{2.20}$$

where M_p mass of product in the control volume, $G_{P_{in}}$ inlet mass flow of product and $G_{P_{out}}$ is the outlet mass flow of the product is given by

$$G_{P_{out}} = \frac{M_p}{t_t} \tag{2.21}$$

where t_t is the residence time in the dryer.

2. Moisture balance in the product:

[Change in amount of water in product] = [water entering into dryer with product] – [water leaving dryer with product] – [water evaporated from product]

$$\frac{dM_p}{dt} = G_{P_{\text{int}}} X_{in} - G_{P_{out}} X - R_w M_p \tag{2.22}$$

or
$$M_P \frac{dX}{dt} + X \frac{dM_P}{dt} = G_{P_{in}} X_{in} - G_{P_{out}} X - R_w M_P \tag{2.23}$$

giving the mass balance for the product as

$$\frac{dX}{dt} = \frac{1}{M_P}\left[G_{P_{in}} X_{in} - G_{P_{out}} X_{out} - R_w M_P - X \frac{dM_P}{dt} \right] \tag{2.24}$$

where X is the instantaneous moisture content, X_{in} moisture content of product entering the dryer, R_w is the drying rate.

3. Moisture balance in the air

[Change in amount of water in inlet air] = [water entering into dryer with air] – [water leaving dryer with air] + [water evaporated from product]

$$\frac{d\left(M_{a,} Y\right)}{dt} = G_{a_{in}} Y_{in} - G_{a_{out}} Y + R_w M_P \tag{2.25}$$

or
$$M_a \frac{dY}{dt} + Y \frac{dM_a}{dt} = \dot{G}_{a_{in}} Y_{in} - \dot{G}_{a_{out}} Y + R_w M_P \tag{2.26}$$

by considering
$$\frac{dM_a}{dt} = 0 \tag{2.27}$$

yields
$$\frac{dY}{dt} = \frac{1}{M_a}\left[G_a (Y_{in} - Y) + R_w M_P \right] \tag{2.28}$$

4. Heat balance for product

   [Enthalpy change of product] = [enthalpy of product entering dryer] – [enthalpy of product leaving dryer] + [heat transferred from air to product] – [heat required to vaporize moisture from the product] - [heat needed to heat water vapor to air temperature] – [heat lost through walls of the dryer]

$$\frac{d\left(M_P C_{pp} T_P\right)}{dt} = G_{P_{in}} C_{pp_{in}} T_{P_{in}} - G_{P_{out}} C_{pp} T_p + U_{va} V\left(T_a - T_p\right) - R_w M_P q_{lat} - R_w M_b C_{pv}\left(T_a - T_p\right) - Q_p \tag{2.29}$$

where the expansion of the left hand was given by:

$$\frac{d\left(M_p, C_{pp}, T_p\right)}{dt} = M_p C_{pp} \frac{dT_p}{dt} + M_p T_p \frac{dC_{pp}}{dt} + T_p C_{pp} \frac{dM_p}{dt} \tag{2.30}$$

The heat balance for the product was thus given by:

$$\frac{dT_p}{dt} = \frac{1}{M_p C_{pp}} \left[\begin{array}{l} G_{P_{in}} C_{pp_{in}} T_{p_{in}} - G_{P_{out}} C_{pp} T_p + U_{va} V\left(T_a - T_p\right) - R_w M_p q_{lat} - R_w M_b C_{pv}\left(T_a - T_p\right) - \\ Q_p - M_p T_p \frac{dC_{pp}}{dt} - T_p C_{pp} \frac{dM_p}{dt} \end{array} \right] \tag{2.31}$$

5. Heat balance for the air

[Enthalpy change of the air] = [enthalpy of air entering dryer] – [enthalpy of air leaving dryer] – [heat transferred from air to product] + [enthalpy of water evaporated from product]

$$\frac{d\left(M_a C_{pa} T_a\right)}{dt} = G_a C_{pa_{in}} T_{a_{in}} - G_a C_{pa} T_a - U_{va} V \Delta T_{ml} + R_w M_p C_{pv} T_a \tag{2.32}$$

where the expansion of the left hand side was given by:

$$\frac{d\left(M_a C_{pa} T_a\right)}{dt} = M_a C_{pa} \frac{dT_a}{dt} + C_{pa} T_a \frac{dM_a}{dt} + T_a M_a \frac{dC_{pa}}{dt} \tag{2.33}$$

By assuming constant conditions of M_a and C_{pa}, the heat balance for air was thus given by:

$$\frac{dT_a}{dt} = \frac{1}{M_a C_{pa}}\left[G_a\left(C_{pa_{in}} T_{a_{in}} - C_{pa} T_a\right) - U_{va} V \Delta T_{ml} + R_w M_p C_{pv} T_a - T_a M_a \frac{dC_p}{dt} \right] \quad (2.34)$$

6. The drying rate equation was given by

$$R_w = k\left(X - X_e\right) \quad (2.35)$$

The drying constant k was related to the temperature through the equation:

$$k = 0.00719 \exp\left(\frac{-130.64}{T_a}\right) \quad (2.36)$$

where C_{pa} is specific heat of humid air, C_{pas} specific heat of dry air, C_{pp} specific heat of wet product, C_{pv} specific heat of water vapor, G_a mass flow of air in the control volume, T_a ambient temperature, T_p is the temperature of the product, G_p is the mass flow of product in a control volume, q_{lat} latent heat of vaporization of water in the product, Q_p heat loss through dryer walls in the control volume, X_e is equilibrium moisture content, ΔT_{lm} logarithmic mean temperature difference, U_{va} is the volumetric heat transfer coefficient between air and product, Y, absolute humidity of air and Y_{in} relative humidity of air entering dryer.

2.2.5 Model of Walk-in-type Solar Tunnel Dryer for the Drying of Surgical Cotton

The assumptions made in the model development were: non-stratification of air in the dryer, thin layer based computations, constant values of specific heats for the air, cover and product, negligible absorptivity of air and radiative transfer from floor to the product (Panwar et al, 2013): The components of the model were:

1. Energy balance for cover

[Heat energy accumulation on tunnel cover] = [convective heat transfer between air inside tunnel and cover] + [radiative heat transfer between cover and ambient air] + [radiative heat transfer between product and cover] + [solar radiation absorbed by cover]

$$m_c C_{pc} \frac{dT_c}{dt} = A_c h_{c,c-a}(T_a - T_c) + A_c h_{r,c-s}(T_s - T_c) + A_c h_w(T_o - T_c) + A_p h_{r,p-c}(T_p - T_c) + A_c \alpha_c I_s \quad (2.37)$$

2. Energy balance in the air inside tunnel

The air inside the tunnel dyer was heated through convective transfer among the floor, product and air hence:

[Thermal energy accumulation of air inside dryer] = [convective heat transfer between floor and air] + [thermal energy gain of air from product due to sensible heat transfer] + [thermal energy gain by air inside dryer due to inflow and outflow of the air in drying chamber] + [overall heat loss from the air inside the dryer to ambient air] + [solar energy absorbed by the air inside the dryer]

$$m_a C_{pa} \frac{dT_a}{dt} = A_p h_{c,p-a}(T_p - T_a) + A_f h_{c,f-a}(T_f - T_a) + D_p A_p C_{pv}(T_p - T_a)\frac{dM_p}{dt} + \rho_p V_{out} C_{pa} T_{out} - \rho_a V_{in} T_o + U_c A_c (T_o - T_a) + [(1 - F_p)(1 - \alpha_f) + (1 - \alpha_f)F_p] I_s A_c \tau_c \quad (2.38)$$

3. Energy balance on the product

Convection and radiation being the main heat transfer modes that contribute to the energy balance of the product inside the solar dryer, hence:

[Thermal energy accumulation in the product] + [convective heat transfer between product and air] + [radiative heat transfer between product and cover] + [thermal energy lost from product due to sensible heat and latent heat transfer] + [thermal energy gained by product]

$$m_p\left(C_{pp}+C_{pl}m_p\right)\frac{dT_p}{dt}=A_p h_{c,p-a}\left(T_a-T_p\right)+A_p h_{r,p-c}\left(T_c-T_p\right)+D_p A_p \rho_p L_p \frac{dM_p}{dt}+ F_p \alpha_p I_s A_c \tau_c \tag{2.39}$$

4. Energy balance on the concrete floor

$$m_f C_{pf}\frac{dT_f}{dt}=Ah\left(T-T\right)+\left(1-F_p\right)\alpha_f I_s A_f \tau_c \tag{2.40}$$

5. Mass balance equations

The air inside the dryer has an increased moisture picking capacity since temperature is higher than the corresponding ambient air, thus:

[Moisture accumulation rate in the air inside the dryer] = [moisture inflow into the dryer carried by entering] + [moisture in the air flowing out of the dryer] + [moisture removed from product inside the dryer]

$$\rho_a V\frac{dH}{dt}=A_{in}\rho_a H_{in}v_{in}-A_{out}\rho_p H_{out}v_{out}+D_p A_p \rho_p \frac{dM_p}{dt} \tag{2.41}$$

The heat transfer and loss coefficient are calculated as follows:

Radiative heat transfer coefficient from cover to the sky, (Duffie and Beckman, 1991):

$$h_{r,c-s}=\varepsilon_c \sigma\left(T_c^{\,2}+T_s^{\,2}\right)\left(T_c+T_s\right) \tag{2.42}$$

Radiative heat transfer coefficient between the product and cover to the sky

$$h_{r,p-c}=\varepsilon_p \sigma\left(T_p^{\,2}+T_c^{\,2}\right)\left(T_p+T_c\right) \tag{2.43}$$

where the correlation between sky and the ambient temperatures is given by:

$$T_s=0.0552T_a^{\,1.5} \tag{2.44}$$

The convective heat transfer coefficient from cover to ambient due to wind is given by:

$$h_w=2.8+3.0V_w \tag{2.45}$$

The convective heat transfer coefficients inside the solar greenhouse dryer, for the cover, product and floor were computed from the relationship:

$$h_{r,c-s} = h_{c,c-a} = h_{c,p-a} = h_c = \frac{Nuk}{D_h} \tag{2.46}$$

Since the wind speed outside the dryer and the speed of drying were very low, it was assumed that the overall heat loss coefficient of heat transfer from air inside the dryer to ambient air was approximately equal to the conductive heat transfer coefficient of the cover given by:

$$U_c = \frac{k_c}{\delta_c} \tag{2.47}$$

1. The drying rate equation

Thin layer drying equation for agricultural products under greenhouse type solar dryer similar to tunnel dryer was used to estimate the moisture as

$$MR = \frac{X - X_e}{X_o - X_e} = \exp\left(-At^n\right) \tag{2.48}$$

where A is the drying rate constant and n the drying coefficient

2.2.6 A Model for the Drying of Fruit and Vegetable Material undergoing Shrinkage.

The drying material was considered as a thin slab of thickness $L = 2b$ at a uniform temperature T_o and moisture content X_o exposed to an air flow of temperature T_a

and relative humidity RH.

The following simplifying assumptions were: one-dimensional moisture movement and heat transfer, no chemical reactions occurring during drying, shrinkage of the material during the drying process and uniform air distribution inside the dryer.

The modeling was done from principles, involving mass conservation, using Fick's second law as follows (Afolabi, 2004):

1. Moisture transport

Input – Output = Accumulation

$$0 - \frac{\partial J}{\partial X}(Ax) = \left(u\frac{\partial X}{\partial x} + \frac{\partial X}{\partial t} \right) Ax \tag{2.49}$$

thus yielding

$$-\frac{\partial J}{\partial x} = u\frac{\partial X}{\partial x} + \frac{\partial X}{\partial t} \tag{2.50}$$

where the mass transfer flux was given by:

$$J = -D\frac{\partial C}{\partial x} \tag{2.51}$$

where C is the concentration and X is moisture content.

hence

$$u\frac{\partial X}{\partial x} + \frac{\partial X}{\partial t} = D\frac{\partial^2 X}{\partial x^2} \tag{2.52}$$

2. The mass transfer equation

The medium was considered to be the superposition of two continuous interactive media, and hence mass of the medium during a transformation between two phases were considered. The liquid phase was characterized by the velocity of liquid diffusion $\overline{v_e}$ while the solid phase was characterized by the velocity of the diffusion of the solid is $\overline{v_s}$.

In the liquid phase

$$\frac{\partial \rho_e}{\partial t} + div\left(\rho_e, \overline{v_e}\right) = 0 \tag{2.53}$$

while in the solid phase

$$\frac{\partial \rho_s}{\partial t} + div\left(\rho_s, \overline{v_s}\right) = 0 \tag{2.54}$$

The mass transfer in the liquid and solid phases was thus given by:

$$\frac{\partial \rho_s}{\partial t} + \bar{v}\frac{\partial \rho_s}{\partial x} = D\frac{\partial^2 \rho_s}{\partial x^2} \tag{2.55}$$

where $D$is diffusion coefficient, ∂t change in time, ∂x change in distance and X is defined as $\frac{\rho_\theta}{\rho_e}$ while $\frac{\theta}{\theta_t}$is the time derivative following the movement of the solid.

Since for materials that undergo shrinkage, the diffusion coefficient is not constant but varies moisture content. The shrinkage effect was taken into account by incorporating the volume change into the diffusion coefficient and introducing an effective diffusion coefficient D_{eff}

$$\frac{\partial \rho_e}{\partial t} + \overline{v}_e\frac{\partial \rho_e}{\partial x} = D_{eff}\frac{\partial^2 \rho_e}{\partial x^2} \tag{2.56}$$

and
$$\frac{\partial \rho_e}{\partial t} + \overline{v}_e\frac{\partial \rho_e}{\partial x} = D_{eff}\frac{\partial^2 \rho_e}{\partial x^2} \tag{2.57}$$

the functional dependence of D_{eff} on moisture content was given by:

$$\frac{D_{ref}}{D_{eff}} = \left(\frac{b_o}{b}\right)^2 \tag{2.58}$$

where b is the thickness of material (half of the length).

The thickness ratio was obtained according to the relation:

$$b = b_o\left(\frac{\rho_e + \overline{X}\rho_e}{\rho_e + \overline{X}\rho_s}\right) \tag{2.59}$$

By assuming a linear distribution of shrinkage velocity was given by:

$$u(b) = \frac{b - b_{old}}{\Delta x} \tag{2.60}$$

where b_{old} is half thickness of sample at the previous time step.

At the beginning of drying, the density of the specimen was assumed to be uniform while in the middle, the density gradient is considered to be zero $(x=0)$ thus the boundary conditions were given by:

At $x=0$ $$\frac{\partial \rho_e}{\partial x}\Big|_{x=0} \quad \text{and} \quad \frac{\partial \rho_s}{\partial x}\Big|_{x=0} = 0 \tag{2.61}$$

At $x=b$ the liquid density balance was given by:

$$-D_{eff}\frac{\partial \rho_e}{\partial x}\Big|_{x=b} + u\rho_e\Big|_{x=b} = h\rho_e(\rho-\rho_e)\Big|_{x=b} \tag{2.62}$$

while the solid phase density balance was given by:

$$-D_{eff}\frac{\partial \rho_s}{\partial x}\Big|_{x=b} + u\rho_s\Big|_{x=b} = h\rho_s(\rho-\rho_s)\Big|_{x=b} \tag{2.63}$$

where h_ρ mass transfer coefficient was determined from the relationship for laminar and turbulent flow respectively given by Eqns. 2.64 (a) and 2.64 (b) below (Karim et al, 2005):

$$sh = \frac{h_\rho L}{D} = 0.332\mathrm{Re}^{0.5}\, Sc^{0.33} \tag{2.64a}$$

and $$sh = \frac{h_\rho L}{D} = 0.029\mathrm{Re}^{0.8}\, Sc^{0.33} \tag{2.64b}$$

3. The heat transfer equation was derived as:

[Heat gained in control vol - heat out of control vol] + [generation] = [heat storage]

$$\frac{\partial T}{\partial t} + u\frac{\partial T}{\partial x} = \alpha\frac{\partial^2 T}{\partial x^2} \tag{2.65}$$

The applicable boundary conditions were:

$$T\Big|_{t=0} = T_o \quad \text{and} \quad \frac{\partial T}{\partial x}\Big|_{x=0} = 0 \tag{2.66}$$

The heat balance at boundary $x=b$ was given by:

$$k\frac{\partial T}{\partial x} \quad \rho C_m u T \,|_{x=b} \quad = \quad h(T_a - T) \;\; |_{x=b} - h_m \rho (X - X_e) h_f g \;|_{x=b} \tag{2.67}$$

where the heat transfer coefficient are estimated from the relationships for laminar and turbulent flows respectively

$$Nu = \frac{hL}{k} = 0.332 \mathrm{Re}^{0.5} \mathrm{Pr}^{0.33} \tag{2.68a}$$

and $$Nu = \frac{hL}{k} = 0.029 \mathrm{Re}^{0.5} \mathrm{Pr}^{0.33} \tag{2.68b}$$

2.3 A Review of the Existing Drying Models

There are various techniques that have been applied in mathematical modeling of solar dryers, while some treat the dryer as one complete unit, others subdivide the system into equipment and material components. Most of the techniques apply one-dimensional treatment except the Computational Fluid Dynamics (CFD) which involves 3-D effects and swirl, suited for systems where localized flow patterns have a major effect on the overall performance of the dryer, but not appropriate for well-mixed systems dominated by the falling rate kinetics, in which local conditions have minimal effect on dryer performance (Kemp and Oakley, 2002).

The most widely applied however has been the modeling technique of drying systems involving the subdivision into equipment and material model components. The equipment component involves parameters that depend on the dryer type, particle transport through the dryer, external heat transfer from hot gas to the solids and vapor-phase mass transfers, external to the solid and can be modeled theoretically for different dryers (Kemp and Oakley, 2002). The material component on the other hand incorporates parameters dependent on the nature of the solid being dried, the product kinetics and equilibrium moisture content relationships, product quality and materials handling. Although some of the material parameters can be obtained from data banks,

others are highly dependent on the nature and structure of the solid and must be measured experimentally.

Mathematical modeling studies on solar dryers tend to either focus on the behavior of the product during the drying process, leading to the determination of the product parameters (coefficient of diffusion, heat and mass transfer coefficients, and drying constants) or on the general behavior of the dryer, by applying heat and mass balances with variations in the operating and dryer design parameters, as the drying efficiency of the system is monitored.

Studies that have been conducted on modeling of drying of products in direct tunnel solar dryers include: a model for the drying of chilli, encompassing an economic component (Hossain et al, 2005), for which the application of the adaptive search pattern technique gave optimum dryer design parameters and a cost saving of 15.9 %, a walk-in-type model of tunnel dryer, described in section 2.2.5 (Panwar et al, 2013) developed for the drying of surgical cotton. Unlike previous models, this model incorporated heat losses within the components of the drying system. Other models of tunnel dryers have been formulated for simulating the drying of food / agricultural products including: tropical fruits (Karim and Hawlader, 2005), tilapia fish; described in section 2.2.1 (Kituu et al, 2010) where for the models, their drying rate equations accounted for shrinkage during drying, through a shrinkage dependent effective moisture diffusivity based on the Fick's diffusion law, that assumes drying occurs in the falling rate period. In case of the drying model by Kituu et. al. (2010) a computer program was developed for simulating the drying process of the tilapia fish. Other studies have also been conducted involving the performance testing of various types of dryers including: testing of a new convective flow dryer (Pangevahane et al, 2002), testing of a fruit and vegetable solar drying system (Al-Juamily et al, 2007), testing of a natural convection solar dryer (Ghaba et al, 2007) testing of a solar tunnel

dryer for drying surgical cotton (Panwar et al, 2013), testing of mixed mode and indirect mode natural convection solar dryer (Simante, 2003), testing of a forced convection solar dryer for Moringa leaves (Amedorme et al, 2013), testing of mixed mode forced convection dryers (Chandrakumar and Jiwanlal, 2013), testing of a domestic solar dryer (Saleh and Badran, 2009), testing of a chimney dependent solar crop dryer (Afriyie et al, 2009) and testing of a hybrid solar dryer for banana (Amer et al, 2010).

Some of these past studies have led to the formulation of models for the solar drying process of various food and agricultural products that include: a model for drying of cassava chips in a mixed mode natural convection solar dryer (Forson et al, 2007), model for drying herbs and spices in a roof-integrated solar dryer (Janjai et al, 2008), a model for the drying process in a chimney dependent solar crop dryer (Afriyie et al, 2013), model for drying of wood in Morocco in a green house type solar dryer (Bekkioui et al, 2011), model for drying of vegetable wholesale by-products in a rotary dryer (Iguaz et al, 2003).

It is noted that the model for the drying process of species and medicinal plants in a solar tunnel dryer (Hossain et al, 2005) predicted moisture loss from the product over a wider range of temperatures and air recirculation percentages in comparison with the model for drying of herbs and spices in the roof-integrated (Bahnasawy et al, 2011). It is also noted that the models cited above were formulated alongside experimental tests with the effects of various parameters on the drying rate being investigated. It is also observed that in some cases (Bekkioui et al, 2011) the simulations were applied to experimental data from previous studies where the models were used as refining tools in the design process of dryers with optimum performance. Although the models by Smitabhindu et. al. (2008) and Kituu et. al. (2010), even incorporated economic components for optimization and computer programs for aiding the simulations the drying process, the main

weakness is that their simulations make use of drying rate equations that almost invariably apply to the falling rate drying period where drying process is wholly controlled by internal mass transfer factors. Further, although the formulation of these models is based only on internal mass transfer factors, they are used to predict externally controlled conditions such as temperature, gas velocity and bed width by making use of a driving force associated with externally controlled factors.

The major flaw of the models being that they are wholly based on type B material characteristics in which air flow rates are considered to have little effect on the drying process, but where in reality most materials are found to exhibit a mixture of type A and B material rules, where the drying times being accelerated by both higher air flow velocities and temperature (Kemp and Oakley, 2002).

Further some of the drying models (section 2.2.1 - 2.2.6) make use of distributed parameters which are very sensitive to errors in basic parameters such as those encountered in real dryers, (wide range particle sizes and shapes occur with errors in measurement of particle sizes exceeding 10%) in modeling the material drying characteristics in the falling rate period. Even though distributed parameter based models are constituted from fundamental physical equations and quantities, they can only work well when all the parameters required can be measured for a given material, within limits of experimental error. But drying processes are characterized by non-linear simultaneous equations containing many quantities, some of which are difficult to measure and hence the limited use of these models only to solid products for which needed parameters in the governing equations have been measured. In contrast lumped parameter based models are most preferred since they involve a smaller number of equations, where the material being dried is characterized by a few parameters that combine several aspects of physical

phenomena, e.g. the various transport processes in a solid can be modeled using a pseudo diffusion coefficient, in a system controlled by gas or liquid phase diffusion.

The most widely applied in studies involving mathematical modeling of solar dryers has been the drying characteristics curve, a lumped parameter based model in which the moisture content is related to the drying time. However in spite of the perceived advantage, lumped parameter based models unlike distributed parameter based models suffer the weaknesses of limited theoretical basis (Kemp and Oakley, 2002).

The drying characteristics curve has thus been used in the formulation of thin layer solar drying processes of many agricultural and food products that include: green beans (Doymaz, 2005), tomato slices (Baghari et al, 2013), Pistachio (Midilli and Kuculk, 2003), red pepper (Akpinar et al, 2003), mint leaves (Akpinar, 2010), tarragon (Arabhosseni et al, 2008), potato (Aghbasho et al, 2009), chilli pepper (Tunde-Akirtunde, 2011), carrot (Berufi et al, 2009), citrus aurantium leaves (Mohamed et al, 2005), Vegetable by-product (Iguaz et al, 2003), tropical fruits (Afolabi, 2014), surgical cotton (Panwar et al, 2013), wood (Awadalla et al, 2004 and Bentayab et al, 2008), talipia (Kituu et al, 2010), herbal and medicinal plants (Ali and Bahnasawy, 2011), sardine fish (Darvishi et al, 2013), cocoa beans (Forson et al, 2007), herbs and spices (Janjai, 2008) and strawberry (El-Beltaji et al, 2007).

Because if the fact that the simulations of these models make use of drying rate equations that are wholly a falling rate drying phenomena based on diffusion as the sole moisture transport mechanism and ignores the effects of surface evaporation of moisture, the effective moisture diffusivity coefficient derived from the experimental moisture curves using from Fick's second law does not account for the constant rate drying phase, which is dominated by external heat and

mass transfer factors. Diffusion based models can only therefore be applied for drying of food products that occurs predominantly in falling rate period but not those that exhibit both constant and falling rates periods of drying for which the initial moisture contents are much greater than the critical moisture content.

Despite the vast literature available on mathematical modeling of thin layer drying of various agricultural/ food products in solar dryers, the models developed tend to relate to specific equipment and products and there is no one general theory for describing the drying characteristics of all products and mechanism of solar dryers.

There is so far no reported study on modeling of the drying process of *R. argentea* fish in a solar dryer, although some experimental investigations have been conducted on the drying of various products including *R. argentea* fish in solar dryers some of which include: drying of crops in a mixed mode solar dryer (Forson et al, 2007), drying of Amaranth grains in a natural convection solar tent dryer (Abalone et al, 2006), drying of Chilli in an indirect forced convection dryer (Ahmed, 2011), drying of *R. argentea* fish in a direct solar tunnel dryer (Oduor-Odote et al, 2010), drying of Okra in an indirect, direct and natural convection dryers (Sobukola, 2009), drying of Jameed in a natural convection solar dryer (Ghassan et al, 2014), drying of Cuminium Cyminium in a forced convection solar dryer (Zomorodian and Moradi, 2011), drying of Tilapia fish in a solar tunnel dryer (Kituu et al, 2010), drying of Kales in a natural convection solar dryer (Onyinge et al, 2014), drying of Tomato in a solar tunnel dryer (Goken et al, 2009), drying of Sardine fish in a microwave heater (Darvishi et al, 2013), drying of tropical fruits (Karim and Hawlader, 2005), drying of herbs and spices in a roof integrated solar dryer (Janjai et al, 2008), walk-in-type hemi-cylindrical solar tunnel dryer for industrial use (Saveda. 2012).

These experimental studies on drying of most food products have revealed that the process is dominated by the falling rate period where internal moisture transport, a complex combination of several processes that include: convection, diffusion in both liquid and vapor phases, capillary action in pores, adsorption and chemisorptions all play role. However the studies have also revealed that the internal moisture transport within the material is dependent on the structure and the drying parameters within the solid and which cannot be predicted by theory only so that the main purpose of the experimental investigations is not only to validate the models but also measure the parameters; diffusion coefficient, activation energy and equilibrium moisture content that are often difficult to obtain from physical data banks.

Like other high moisture food products, experimental studies on the drying of *R. argentea* fish in solar dryers have revealed that the product exhibits both constant and falling rate drying periods, in a drying time of about 14 hours (Oduor-Odote et al, 2010). Other studies have also revealed the physical nature and characteristics of the product as being; highly perishable, with high surface moisture content and a relatively small diameter. Surface evaporation rather than diffusion is therefore likely to be an important factor in its drying process (KIRDI, 2008). Thus with prolonged drying times, the product is likely to be exposed to spoilage. Despite the fact that studies have been done on drying of this product, some of the drying parameters such as effective moisture diffusivity and activation energy, that are useful in designing and optimizing the drying processes are still unavailable in physical property data banks.

The objective of the present study therefore was to develop a drying model of *R. argentea* fish in an indirect forced convection solar dryer and simulate it based on an evaporation drying rate equation rather than Fick's diffusion model, so as to obtain vital information that could be useful in developing an efficient commercial solar drying technology for the product. The evaporation

based drying rate equation was developed from thermodynamic principles of energy exchanges, assuming adiabatic conditions during the drying process.

CHAPTER THREE: METHODOLOGY

3.1 General Procedures

The procedure adopted for developing the mathematical model of the drying process of *R. argentea* fish in an indirect forced convection solar dryer involved the formulation of heat and mass balance equations for the drying air and the product in the drying chamber based on the following assumptions:

1) Non-stratification of the air in the dryer,

2) Constant values of the specific heats of air, cover and product,

3) Negligible absorptivity of the air

4) Thin layer model drying based computations.

Consequently simulations of the model were carried out by varying the design and operating parameters, computed according to the relations outlined in section 3.4 below, in order to optimize the drying process. The information obtained from the model was used to construct a prototype solar dryer and theoretical drying data generated by the simulations validated by conducting experimental drying tests of *R. argentea* fish on the dryer. Statistical analysis was applied to determine the model prediction reliability and the goodness of fit between the theoretical and experimental data.

3.2 Procedure for Formulating the Drying Model of the Product

From Thermodynamics, the change in enthalpy of air is equal to the heat transferred convectively to the product and the heat supplied by air to evaporate the moisture, thus the energy required to dry a given product is given by (Youcef-Ali et al, 2001):

$$m_w L_v = m_a C_{pa}(T_i - T_e) \tag{3.1}$$

where m_w is the mass of water evaporated, T_i is the temperature of air entering product, T_e is the temperature of air leaving product, C_{pa} is the specific heat capacity of air, m_a is the mass of air and L_v is latent heat of evaporation from product.

The total mass of water evaporated in the drying process of a product is given by (Raju et al 2013):

$$m_w = m_s \frac{X_i - X_f}{1 - X_f} \tag{3.2}$$

where m_s is the mass of wet product, X_i is the initial moisture content and X_f is the initial moisture content.

In a time interval, dt during which moisture content of product decreases by dX',

the energy required is given by:

$$E_w \approx \rho_d A L_v \frac{\dot{dX_d}}{100} dx \tag{3.3}$$

where dx is the thickness of the product, X_d is moisture content (d. b.), ρ_d is the product matter density and A is the area of the product exposed to the air

The energy lost by heated air is given by:

$$E_a = m_a A \dot{C_{pa}} dT_a dt \tag{3.4}$$

where T_a is temperature of the air, by assuming an adiabatic process in which no heat is lost or gained, the energy lost by the air is equal to that gained by the product hence:

$$E_w = E_a \tag{3.5}$$

which leads to

$$\frac{dX_d}{dt} = \frac{100\dot{m}_a C_{pa}}{\rho_d L_v}\frac{dT_a}{dx} \tag{3.6}$$

Equation 3.7 is the drying rate equation that can be written in the form:

$$\frac{dX_d}{dt} = D_f \frac{dT_a}{dx} \tag{3.7}$$

where D_f is the drying factor and is given by:

$$D_f = \frac{100\dot{m}_a C_{pa}}{\rho_d L_v} \tag{3.8}$$

and is constant for a set of drying conditions.

If the time is converted into hours (from seconds) then we have that:

$$D_f = \frac{3600\times 100\dot{m}_a C_{pa}}{\rho_d L_v} \tag{3.9}$$

The drying rate equation (Eqn. 3.7) satisfies the boundary conditions:

$$X_d - X_{d.eq} = (X_{di} - X_{d.eq})e^{-kt} \quad \text{when } x = 0 \tag{3.10}$$

$$T_a - T_{a.eq} = (T_{ai} - T_{a.eq})e^{-cx} \qquad \text{when } t = 0 \tag{3.11}$$

The drying constant k and the constant c are related according to the equation:

$$c = \frac{k\left(X_{di} - X_{deq}\right)}{D_f\left(T_{ai} - T_{aeq}\right)} \tag{3.12}$$

The nature of the model equation, unlike the diffusion model Equation 2.1, suggests it has two interdependent solutions obtained through the separation procedure below:

$$D_f \frac{dT_a}{dx} = \frac{dX_d}{dt} = -Bf_g\left[X_d - X_{deq}, T_a - T_{aeq}\right] \tag{3.13}$$

where B is a constant

by applying the equilibrium approximation conditions (Zomorodian and Dadashzadeh, 2009); $T_{aeq} \approx 0^{\circ}$ C and $X_{deq} \approx 0$ % (w. b.), and where the interdependence of the moisture content and temperature during the drying process is represented by the function f_g, it is shown that the solutions that satisfy the model Equation 3.8 are:

$$X_d = X_{di}\left[\frac{e^{cx}}{e^{cx} + e^{kt} - 1}\right] \tag{3.14}$$

and

$$T_a = T_{ai}\left[\frac{e^{kt}}{e^{cx} + e^{kt} - 1}\right] \tag{3.15}$$

if we differentiate Equations 3.14 and 3.15 to obtain

$$\frac{dX_d}{dt} = X_{di}\left[\frac{-ke^{kt}e^{cx}}{(e^{cx} + e^{kt} - 1)^2}\right] \tag{3.16}$$

and

$$\frac{dT_a}{dx} = T_{ai}\left[\frac{-ce^{kt}e^{cx}}{(e^{cx} + e^{kt} - 1)^2}\right] \tag{3.17}$$

respectively.

where by multiplying Equation 3.17 by the factor D_f from the relation given in Equation 3.12, we obtain the function f_g and constant B as:

$$f_g\left[X_d - X_{deq}, T_a - T_{aeq}\right] = \frac{e^{kt}e^{cx}}{(e^{cx} + e^{kt} - 1)^2} \tag{3.18}$$

and

$$B = -cT_{ai} \tag{3.19}$$

respectively.

3.3 Procedure for Obtaining the Equation for the Drying Time

Assuming a constant temperature with time during the drying process as applied to Equation 3.17, the temperature gradient function across the material reduces to:

$$\frac{dT_a}{dx} = T_{ai}\left[\frac{-ce^{cx}}{(e^{cx})^2}\right] = -T_{ai}ce^{-cx} = -cT_a \tag{3.20}$$

The differential equation can be thus modified to a simple O.D.E solvable by separation of variables:

$$\frac{dX_d}{dt} = -cD_f T_a \tag{3.21}$$

The solution of equation 3.21 which gives the change in moisture content of the product as a function of time was obtained through the integration procedure below given below:

$$\int_{M_1}^{M_f} dX_d = -cD_f T_a \int_0^t dt \tag{3.22}$$

$$X_f - X_i = -cD_f T_a t \tag{3.23}$$

from which the drying time was obtained as:

$$t = \frac{X_f - X_i}{-cD_f T_a} \tag{3.24}$$

3.4 Computation of Parameters for the Prototype Solar Dryer and the Product

1. The collector tilt angle γ is linked to the geographical latitude of the site location, and for maximum incident solar radiation it obtained from relation (Forson et al, 2007):

$$\gamma = 10^o + lat\varphi \tag{3.25}$$

where for the present site location (Maseno, Kenya), $lat\varphi = 0^o$ and therefore a value of

$\gamma = 10^o$ was adopted to allow for the drainage of rain water.

2. The quantity of water to be evaporated from the product was computed from Equation 3.2 as follows:

$$m_w = 10.0\left(\frac{0.73-0.15}{1-0.15}\right)$$

$$= \quad 6.8 \text{ kg}$$

by assigning the values; $X_i = 0.73$, $X_i = 0.15$ and $m_s = 10.0kg$.

3. The Equilibrium Moisture Content (EMC) for *R. argentea* fish was computed from the relation (Chukwuka et al, 2009):

$$M_e = \frac{M_i M_f - (M_m)^2}{M_i + M_f - 2M_m} \tag{3.26}$$

$$= \frac{(270.39 \times 17.65) - (38.89)^2}{270.39 + 17.65 - 2(38.89)}$$

= 15.5 % (d. b.) or 13.42 % (w. b.)

where initial moisture content at $t = 0$, $M_i = 73\%$ (w. b.) = 270.39 % (d. b.), final moisture content $M_f = 15\%$ (w. b.) = 17.65 % (d. b.) and moisture content at half time

$M_m = 38.89$ % (d. b.) or 28.0 % (w. b.).

4. The heat needed for drying a given quantity of food product is given by:

$$Q = m_w L_v \tag{3.27}$$

$$= 6.8 \times 226000$$

$$= 15370kJ$$

where m_w is mass of water evaporated from the product, L_v latent heat of vaporization of water.

5. The total mass of air needed for drying was computed from Equation 3.1 as follows:

$$m_a = \frac{15370kJ}{1007\times(311-301.5)} = 1526.3kg$$

with the values of specific heat capacity of air C_{pa}, the final and initial temperatures T_o and T_i respectively being substituted from Table A1.

6. The volume flow rate of air was then computed as follows:

$$\dot{v} = \frac{V_a}{t_d} \tag{3.28}$$

$$= \frac{1526.3kg}{1.17kg/m^3 \times 14hrs}$$

$$= 93.18 \text{ m}^3/\text{hr}$$

where the values of total volume of air used in drying V_a and total drying time were substituted from Table A1.

7. The average drying rate was evaluated according to the relation:

$$M_{dr} = \frac{m_w}{t_d} \tag{3.29}$$

$$= \frac{6.8kg}{14}$$

$$= 0.486 \text{ kg/ hr}$$

where the values of total drying time t_d and mass of water evaporated were substituted from Table A1.

8. The collector area A_c was computed from the relation (Bolaji and Olalusi, 2008):

$$\eta_c = \frac{\dot{m}_a C_{pa}(T_o - T_i)}{A_c I_m} \times 100 \quad (3.30)$$

where η_c thermal efficiency of the collectors, $\dot{m}_a$ is air mass flow rate, C_{pa} specific heat capacity of air, T_i collector inlet air temperature, T_o outlet air temperature and I_m the predicted incident solar radiation, were assigned theoretical values given in Table A2, (Appendices). A value of 5.0 m^2 was thus obtained for the collector area.

9. With the ratio of length to width of the air collectors taken as being greater than 1.5, the length of the drying chamber was given by (Forson et al, 2007):

$$L_s = \frac{A_c}{w} \quad (3.31)$$

$$= \frac{2.5m^2}{1.29} = 1.9 \text{ m}$$

where A_c is taken to half of the total surface area of the collectors while w is width of the collector substituted from Table A1.

10. The electric power (P_f) of the fan was computed from the equation (Bolaji and Olalusi, 2008):

$$\eta_p = \frac{m_w L_v}{IA_c + P_f} \quad (3.32)$$

$$P_f = \frac{15370kJ}{(14\times 3600)\times 0.121} - (496\times 5)$$

$$= 40.33 \text{ W}$$

with the values of mass of water evaporated from the product m_w, latent heat of vaporization of water L_v , theoretical value of solar radiation intensity I_m and total

collector area A_c being substituted from Table A1.

11. The chimney length taken as greater than $1/15$ of the collector length, e.g. 30 cm

12. The aggregate thin layer drying thickness, $h_L \leq 200mm$, was assumed for the *R. argentea* fish (Forson et al, 2007).

13. For the diffusion model, the drying rate constants were computed as the gradients of the graph of In *MR* versus time according to the equation:

$$MR = \exp(-kt) \tag{3.33}$$

14. The effective moisture diffusivity D_{eff} representing the overall mass transport property of moisture in the material including liquid, vapor diffusion and other transport mechanism was estimated from the drying rate constant according to the relation (Simante, 2003):

$$k = \frac{\pi^2 D_{eff}}{4L} \tag{3.34}$$

where L is the characteristic length of the product.

15. The activation energy of food product was calculated according to the Arrhenius Equation (Akipnar et al, 2003):

$$D_{eff} = D_o \exp -E/RT \tag{3.35}$$

where T (K) plenum chamber temperature $E\,(J/mol)$ activation energy, R universal gas constant $J/mol/K$ and D_o (m^2/s) is the pre-exponential factor for the Arrhenius equation

3.5 Model Simulation Procedure

The model equations were simulated based on theoretical parameters whose values were obtained from the design calculations using the relations outlined in Section 3.4 and given in Table A2 and other information obtained in literature. The drying model equation representing drying process was solved and simulated to predict the drying time, moisture ratios and drying rates among other parameters.

3.6 Description of the Prototype Solar Dryer

The materials used in the construction of the proto-type indirect forced convection cabinet solar dryer were: well-seasoned cedar timber, galvanized iron sheets, transparent glass (5.0 mm thickness), white polythene sheets, PVC waste pipes (diameter 8.5 cm), electric fan and a solar photovoltaic module. The drying system consists of a drying chamber, two solar air heaters with a total glazing area of 5.0 m^2 made from wooden frames and transparent glass (5.0 mm thickness), the two collectors arranged perpendicular to each other, were connected to the drying chamber by an air duct system made using PVC waste pipes. The two solar collectors each had a tilt angle of 10 ^{o} based on design calculations to allow for rain water drain.

The drying chamber measuring 2.1 m by 1.2 m by 1.8 m, had a mounted door and was divided into two sections, left and right each consisting of 10 trays, made of wooden frames and aluminum gauzing, spaced 0.20 m apart, each with a drying area of 1.0 m^2. The drying chamber had an inner lagging of foam material, a 30.0 cm tall chimney, an exhaust fan mounted on the dome of the chamber and a 50-W solar photovoltaic module, Figure 3.1. The dome of the drying chamber was made of un-insulated galvanized iron sheet. The bottom of the chamber was connected to the solar collectors using PVC waste pipes, with an air inlet on each of its four

sides. The exhaust fan was connected to the solar photovoltaic module via insulated electric power cables with internal diameter of 2.5 mm.

The design details of the prototype indirect forced convection solar dryer and photographic view are presented in Figures 3.1 and 3.2 respectively below;

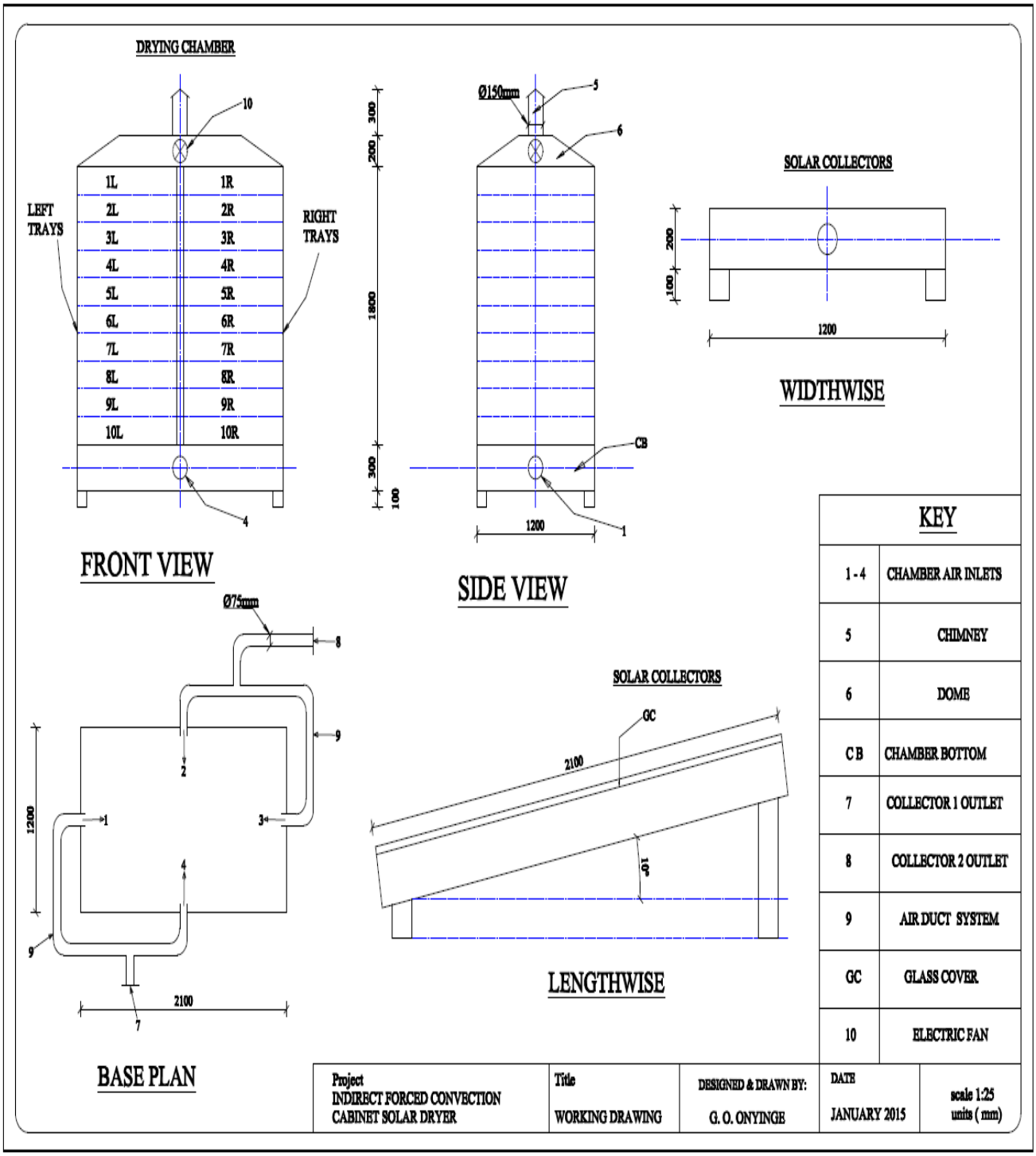

Figure 3.1: The design drawings of the proto-type indirect, forced convection cabinet solar dryer.

Figure 3.2: Pictorial view of the prototype indirect cabinet forced convection solar dryer, developed at Maseno University, Kenya.

3.7 Experimental Methods and Procedures

3.7.1 Full Load Tests

The indirect forced convection solar dryer shown in figure 3.1, was used to conduct a series of five drying tests for *R. argentea* fish during the periods; May - June 2014 and January - March 2015 during which fish samples were dried and the performance evaluated. During the experimental tests the air temperature at the collector outlets, at various locations in the drying

chamber and ambient temperatures were measured by the use of type "J" thermocouples connected to a data logging system at regular intervals of 1 hour between the hours of 09:00 hours and 16:00 hours local time. The solar radiation intensity was measured during the hours of drying by means of a portable solarimeter placed horizontally. The dryer was loaded with 1 kg *R. argentea* fish with initial moisture content 73% w. b. laid in thin layers onto each tray. The food samples were removed from the dryer, the weights measured at the start and at two-hourly intervals thereafter using an electronic balance.

Measurements of relative humidity of air in the ambient and drying chamber were taken at hourly intervals using a Psychrometer. The initial weight and the final weight of the fish up to the stage when no further weight loss occurred were recorded, drying was only stopped when there was no significant differences in the weight of the samples after three consecutive weighing. Weight measurements were also taken from control samples dried to approximately the same moisture content using open sun method. The fish was left in the solar dryer overnight and before beginning drying on the second day, weight measurements were taken in the morning

3.7.2 Measurement of Temperature

Temperatures readings were taken at intervals of 10 minutes for the ambient air and at various locations in the collectors and drying chamber using thermocouples connected to a data logging system, Fluke model 2286A (Everett WA, USA), consisting of type J (Iron - Constantan), K (Chromel - Alumel) and E (Chromel - Constantan) thermocouples with measurement ranges - 200 to 760 ° C, - 225 to 1350 ° C and - 250 to 1000 ° C, respectively.

3.7.3 Measurement of the Incident Solar Radiation

The instantaneous incident solar radiation was measured at intervals of 1 minute using a solariometer model SL 200, (e-instruments, France), with measurement range of 1 - 1300 W/ m^2, accuracy ± 5 %, measurement frequency: 2 Measurement per second.

3.7.4 Measurement of Relative Humidity

The relative humidity of air inside and outside the chamber was measured at 1-hourly intervals using two digital Pyschrometer: model 5105 (JENWAY, U.K.) with one being placed inside the drying chamber and the other outside.

3.7.5 Measurement of Air Flow Rates

The air speed and volume flow rates were measured at the collector outlets and chimney at hourly intervals using an anemometer: VELOCICAL model 8357 (T.S.I., USA), with measuring ranges: $0.0424 - 1.17\times10^{8} m^3/s$ for volume flow rates and accuracy ranges: ± 0.05 for 2.5 - 10 m/s, ± 0.025 m/s for 10 - 30 m/s and ± 0.5 for 30 - 50 m/s air velocities.

The following is a pictorial view of the prototype solar dryer showing the various trays loaded with *R. argentea* fish during the experimental tests

Figure 3.3: Pictorial view of the indirect cabinet solar dryer loaded with *R. argentea* fish

3.8 Model Testing Procedure

The mathematical model of the solar drying process of *R. argentea* fish was validated through the application of statistical methods of regression and correlation analysis to test the fitting of the model. The coefficient of determination (R^2), reduced chi-square (χ^2) and root mean square error (*RMSE*) were computed in order to determine the quality of fit, where the value of reduced chi-square was computed from the equation given below:

$$\chi^2 = \sum_{i=1}^{N} \frac{(MR_{\exp i} - MR_{prei})^2}{N - p}, \tag{3.36}$$

The coefficient of determination (R^2) was also obtained from the following relation:

$$R^2 = \frac{\left[\left(\sum_{i=1}^{N} MR_{\exp i} - \overline{MR}_{pre}\right)\left(\sum_{i=1}^{N} MR_{prei} - \overline{MR}_{pre}\right)\right]^2}{\sum_{i=1}^{N}\left(MR_{\exp i} - \overline{MR}_{\exp}\right)^2 \sum_{i=1}^{N}\left(MR_{prei} - \overline{MR}_{pre}\right)^2} \tag{3.37}$$

while the root mean square error (*RMSE*) was computed from the relation:

$$RMSE = \left[\frac{1}{N}\sum_{i=1}^{N}(MR_{\exp i} - MR_{prei})^2\right]^{\frac{1}{2}} \tag{3.38}$$

where $MR_{\exp i}$ is the i^{th} experimentally observed moisture ratio, MR_{prei} is the i^{th} predicted moisture ratio, $\overline{MR}_{\exp i}$ is the mean value the experimental moisture ratio, n is the number of constants and N is the number of observations (Bentayab et al, 2008).

CHAPTER FOUR: RESULTS AND DISCUSSION

4.1 The Mathematical Drying Model

The mathematical drying model of *R. argentea* fish consists of four equations formulated using the procedures described in Chapter three, section 3.2. These are the drying rate equation which is a first order Ordinary Differential Equation (O.D.E), the moisture and temperature ratios respectively, which are the two solutions of the drying rate equation and a drying time equation, which is a special solution of the drying rate equation, when equilibrium conditions are assumed to occur very close to zero.

4.1.1 The Drying Rate Equation

The Equation 3.8, derived in section 3.2 represents the drying rate of the product and is the basic model equation from which other equations were derived. This equation is

analogous to the Fick's diffusion model, Equation 2.1 with the drying factor D_f corresponding to the effective moisture diffusivity D_{eff}. However, whereas in the diffusion model, the effective moisture diffusivity (D_{eff}) cannot be predicted theoretically and is determined through experimental measurements, the drying factor D_f in the present model can be computed since the constituting parameters; air flow rate, specific heat capacity of air, material density and latent heat of vaporization of water are easily obtainable. Furthermore in contrast with the Fick's diffusion model which provides no information on dryer design parameters, the present model contains a parameter D_f (drying factor) whose main variable is the air flow rate, which is an important design parameter of solar dryers.

4.1.2 Moisture Ratio and Temperature Ratio Equations

The moisture and temperature ratios were obtained from the two solutions of Equation 3.8 based on the boundary conditions Equations 3.10 and 3.11. By assuming that equilibrium moisture and temperature conditions to occur close to zero, the moisture and temperatures ratio were obtained as

$$MR = \frac{X_d - X_{deq}}{X_{di} - X_{deq}} = \frac{e^{cx}}{e^{cx} + e^{kt} - 1} \tag{4.1}$$

and

$$\theta = \frac{T_a - T_{ai}}{T_{ai} - T_{aeq}} = \frac{e^{kt}}{e^{cx} + e^{kt} - 1} \tag{4.2}$$

respectively:

Equation 4.1 is the ratio of instantaneous to initial moisture contents of the *R. argentea* fish, representing the rate of moisture removal from the product. The two drying constants *c* and *k* related according to Equation 3.12 depend on the product characteristics and drying conditions, *k* is the drying rate constant representing the heat and mass transfer mechanism while *c* is a constant representing the physical characteristics of the product, both constants therefore have physical significance. Equation 4.2 provides a prediction of the instantaneous temperature of the product as function of product thickness *x*, constant *c* and the drying time *t*.

4.1.3 The Drying Time Equation

The drying time equation was obtained from the solution of the simplified form of the drying rate equation, Equation 3.21,

The integration procedures outlined in section 3.3, therefore gave rise to the drying time Equation 3.22, but where the constant *c* defined according to Equation 3.12 was simplified by assuming that equilibrium conditions occur very close to zero;

$T_{aeq} \approx 0$ K, $X_{deq} \approx 0$ % (w. b.) to:

$$c = \frac{kX_{di}}{D_f T_{ai}} \tag{4.3}$$

It is observed that the present drying time model equation is similar to that of an evaporation based model in a past study by Chukwuka et. al. (2009) although with the constituting parameters in the models being different. It is further noted that while in the earlier model the driving force was the difference in vapor pressure of the water at the surface and in the surrounding atmosphere, in the present model it is the air flow rate.

4.2 Model Results

4.2.1 Variation of Drying Time with Temperature

The variation of drying time with temperature as derived from the model Equation 3.22 for the air mass flow rates; 0.022 kg/s, 0.03kg/s 0.04 kg/s, 0.05kg/s and 0.06 kg/s have been presented in the following table:

Table 4.1: Model simulations of drying times with air mass flow rate and temperature

Temperature $T_a(K)$	**Drying time at** $0.022kg/s$	**Drying time at** $0.03kg/s$	**Drying time at** $0.04kg/s$	**Drying time at** $0.05kg/s$	**Drying time at** $0.06kg/s$
308	12.1	8.9	6.7	5.3	4.4
318	11.7	8.6	6.4	5.2	4.3
328	11.4	8.3	6.2	5.0	4.2
338	11.0	8.1	6.1	4.9	4.0
348	10.7	7.9	5.9	4.7	3.9
358	10.4	7.6	5.7	4.6	3.8

As can be observed from the table, there is a decreasing trend of drying time with increasing temperature. It is further observed that increasing the air mass flow rate from 0.022 kg/s to 0.06 kg/s causes an average reduction of 7 hours in the drying time whereas an increase in temperature from 308 K to 358 K causes an average reduction in the drying time of less than 2 hours. The least drying times predicted by the model occur at 0.06 kg/s for which the minimum drying was 3.8 hours at a temperature of about 360 K. However since drying food products is recommended at temperatures below 343 K, the optimum set of drying parameters would be: 340 K, 0.06 kg/s and 4.0 hours being temperature, air mass flow rate and drying time respectively.

Further from the table a comparative graphical variation of the drying time with temperature for different air mass flow rates have been presented in Figure 4.1 below:

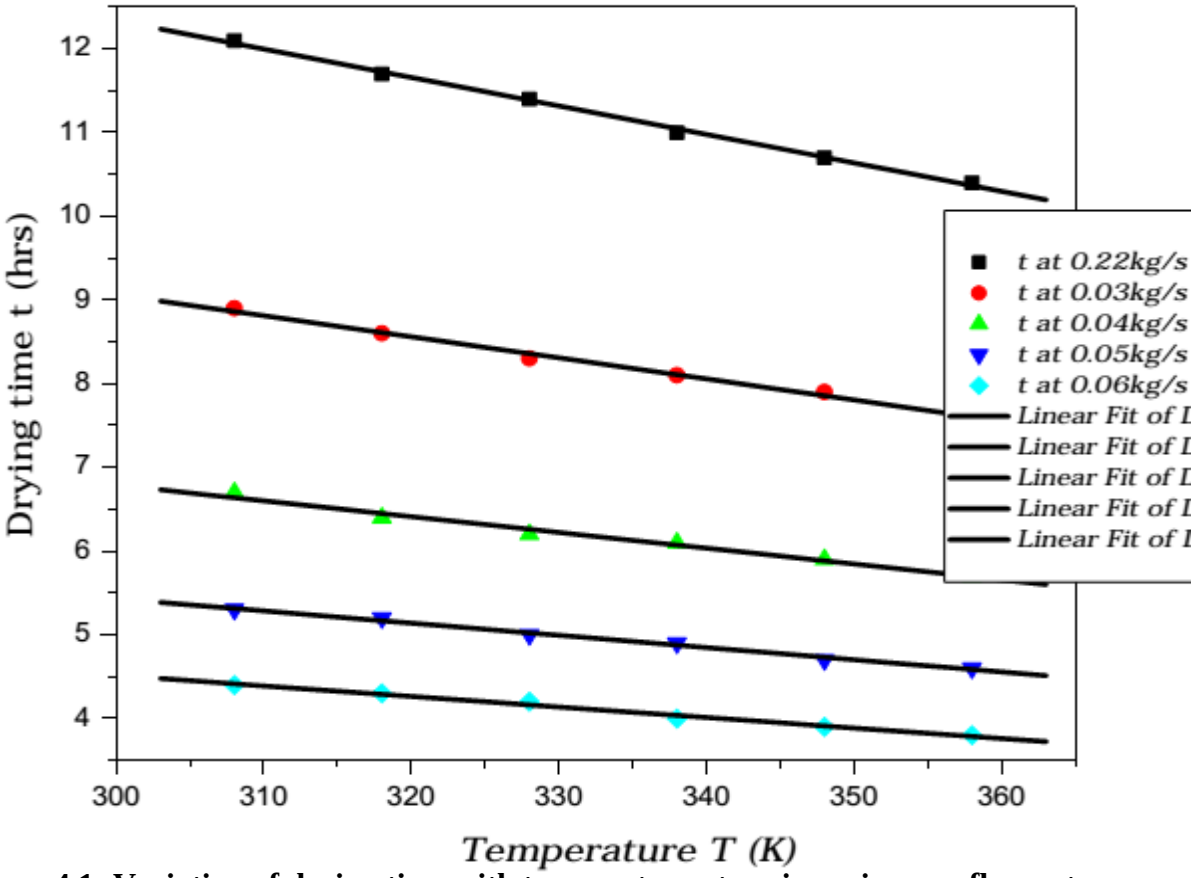

Figure 4.1: Variation of drying time with temperature at various air mass flow rates.

As can be observed from the figure, the drying time decreases linearly with increasing temperature. The longest drying times predicted by the model are for air mass flow rate of 0.022 kg/s and range from 10.4 to 12.4 hours for the different temperatures. The shortest drying times are predicted for 0.06 kg/s air mass flow rates and range between 3.8 and 4.4 hours. At the simulated experimental drying temperature of 320 K, and air mass flow rate of 0.022kg/s the model predicts a drying time of 11.7 hours. Although the least predicted drying time is 3.8 hours for 0.06 kg/s air flow rate at the drying temperature 358 K (Table 4.1) the recommended maximum temperature for drying of food products should not exceed 343 K. But within the

experimental drying temperature of 320 K, the model predicted that the drying time could be reduced by 7 hours just by enhancing the air mass flow rates to 0.06 kg/s. The shortest drying time of 3.8 hours predicted by the model is observed to be much shorter than 14 hours which has been obtained by a past study on *R. argentea* fish, (Oduor-Odote et al, 2010). Thus the set of optimum drying parameters for this product would be 0.06 kg/s air flow rate and 340 K temperature for which the model predicts a drying time of about 4 hours.

4.2.2 Variation of Drying Time with Air Mass Flow Rate

The variation of drying time with air mass flow rate for various temperatures as derived from the simulations of the model, Table 4.1, have been presented in Figure 4.2 below;

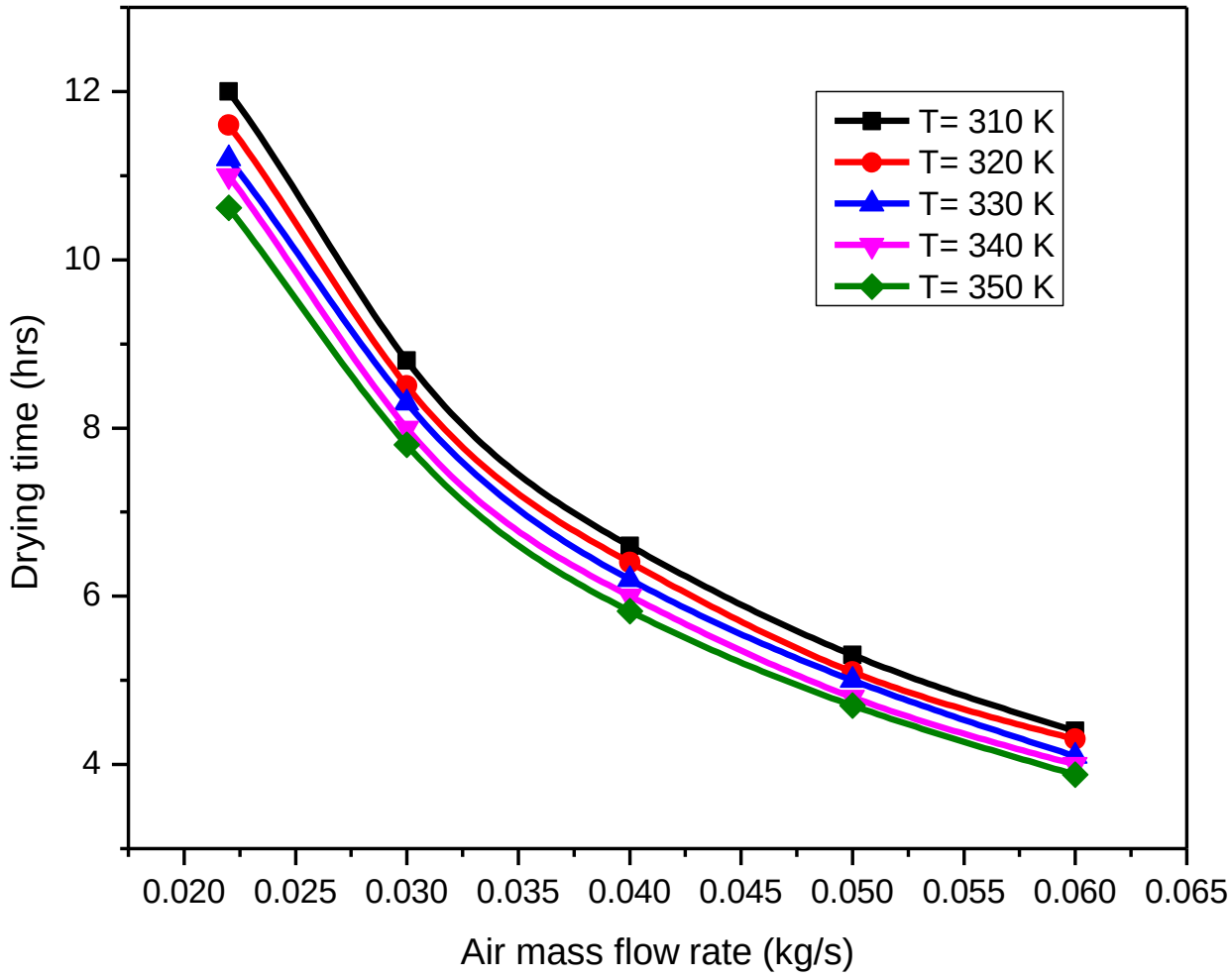

Figure 4.2: Variation of drying time with air mass flow rate at various temperatures

From the figure above, it is observed that there is an exponential decrease of drying time with increasing air mass flow rate. However there is an apparent critical air mass flow rate above which no further decrease in the drying time can be achieved, suggesting that the minimum drying time of about four hours for the *R. argentea* fish product. The model thus predicts a reduction of about 7 hours in the drying time of this product, when air the mass flow rate is enhanced to 0.06 kg/s. However there was no significant variation observed between the drying time and temperature, suggesting that the air mass flow rate is a more influential parameter than temperature in determining the drying time, this has also been observed by past studies involving

evaporation models (Babalis and Belessiotis, 2004) who have also observed the strong influence of air temperature and velocity of air at early stages of drying, however the authors observed that the influence of air flow rate vanished after a period of between 4 to 5 hours.

4.2.3 Variation of the Moisture Ratio with Time

The model simulations of the moisture ratio of the fish with time derived from Equation 3.14, for the product thickness $x = 0.004m$, at various *k* (drying rate constant) and *c* (the product constant) are presented in the table below:

Table 4.2: Model predictions of the moisture ratio of fish in the solar dryer

Time (hrs)	**MR for (*k* = 0.202hr^{-1} *c* = 9.92)**	**MR (*k* = 0.205hr^{-1} *c* = 9.92)**	**MR (*k* = 0.215hr^{-1} *c* = 9.92)**	**MR (*k* = 0.296hr^{-1} *c* = 9.29)**	**MR (*k* = 0.392hr^{-1} *c* = 9.89)**	**MR (*k* = 0.569hr^{-1} *c* = 11.49)**	**MR (*k* = 0.589hr^{-1} *c* = 9.93)**
0	0.73	0.73	0.73	0.73	0.73	0.73	0.73
2	0.68	0.67	0.66	0.56	0.47	0.33	0.32
4	0.46	0.45	0.44	0.31	0.22	0.11	0.10
6	0.30	0.30	0.28	0.18	0.10	0.03	0.03
8	0.20	0.20	0.19	0.10	0.05	0.01	0.00
10	0.14	0.13	0.12	0.05	0.02	0.00	0.00
12	0.09	0.09	0.08	0.03	0.01	0.00	0.00
14	0.06	0.06	0.05	0.02	0.00	0.00	0.00
16	0.04	0.04	0.03	0.01	0.00	0.00	0.00

As can be seen from Table 4.2, the moisture ratios of the fish decrease with the drying time, but the decrease is comparatively more rapid for larger values of the drying rate constants. It is observed that moisture ratios of the fish for the drying rate constants; 0.202 hr^{-1}, 0.205 hr^{-1} and 0.215 hr^{-1} are almost identical, which can be explained by the fact they have the same value of drying factor, $1.76\times10^{-3} m^3/s/K$. The model predicts that moisture ratio lower than 0.15 or 15 % (w. b.) moisture content, the recommended safe value for food products, can be attained by the

fish in less than 6 hours for the drying rate constants; 0.392 hr^{-1}, 0.569 hr^{-1} and 0.589 hr^{-1}. However near the simulated experimental conditions corresponding to drying rate constants; 0.202 hr^{-1}, 0.205 hr^{-1} and 0.215 hr^{-1} the model predicts that the safe moisture content / ratios is only attained after more than 8 hours of drying.

Further, variations of the model moisture ratio of the fish with time derived from Table 4.2 have been presented in the Figure 4.3 below:

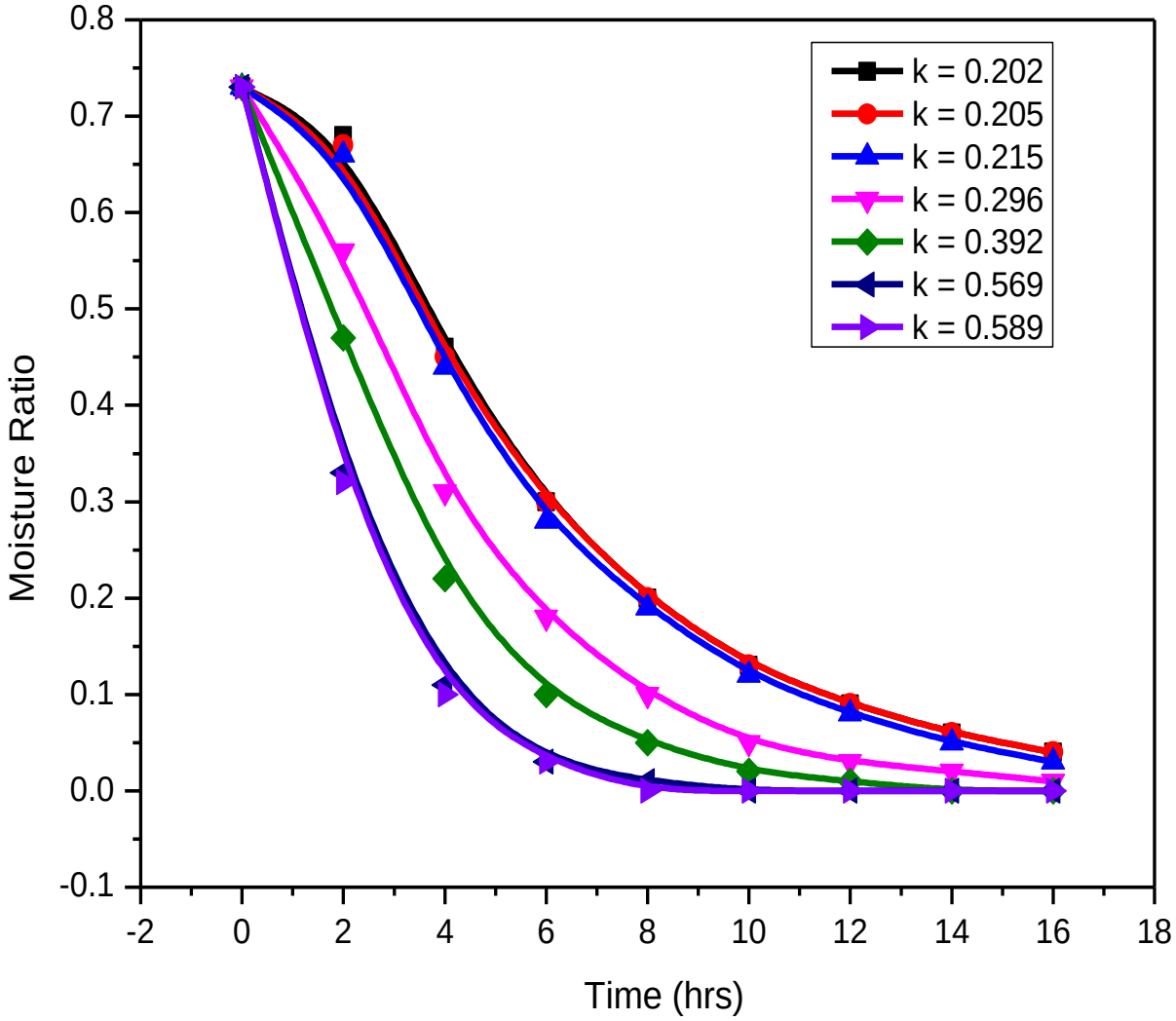

Figure 4.3: Variation of the model moisture ratio of the fish with time for various drying rate constants

It is observed from Figure 4.3, that the moisture ratio for the fish for the various drying factors; ($D_f = 1.76\times10^{-3}\ m^3/s/K$ for k = 0.202 hr^{-1}, 0.205 hr^{-1} and 0.215 hr^{-1}, $D_f = 2.56\times10^{-3}\ m^3/s/K$ for k = 0.296 hr^{-1}, $D_f = 3.21\times10^{-3}\ m^3/s/K$ for k = 0.392 hr^{-1}, $D_f = 4.01\times10^{-3}\ m^3/s/K$ for k = 0.569 hr^{-1} and $D_f = 4.81\times10^{-3}\ m^3/s/K$ for k = 0.589 hr^{-1}) show an approximately linear section at the beginning of drying (time interval 0 - 4 hours) before an exponential decay with increasing drying time. In the linear region the graphs have slopes

indicating higher drying rates as unlike in the exponential section. It is observed that the moisture curves denoting the drying rate constants; k = 0.202 hr^{-1}, 0.205 hr^{-1} and 0.215 hr^{-1} are almost coincident which is attributable to the fact that they have the value of drying factor, $D_f = 1.76\times10^{-3}\ m^3/s/K$. A similar trend was observed for the drying curves representing; k = 0.569 hr^{-1} and k = 0.589 hr^{-1}, with drying factors $D_f = 4.01\times10^{-3}\ m^3/s/K$ and $D_f = 4.81\times10^{-3}\ m^3/s/K$ respectively. This observation suggests that there is a diminishing effect of the drying factor on the drying rates beyond some critical value. Since the drying factor is proportional to the air mass flow rate it affects the heat and mass transfer rates between the product and drying medium (heated air) this observation therefore suggests that beyond certain air flow rates, other parameters such as temperature have a greater effect on the drying rates than air flow rate. It is also observed that for air mass flow rates of 0.05 kg/s and 0.06 kg/s, the moisture ratio of the fish is decreased to safe moisture content; 10 % (w. b.) in a drying time of less than 5 hours, suggesting that larger moisture losses occur for higher values of drying factors. This result implies that the fish could be dried in a period of 5 hours attaining the safe moisture content; 25 % (w. b.) at which bacterial activity is inhibited in the first 3 hours and then to 15 % (w. b.), at which mould activity is halted (Basunia et al, 2011) in a further 2 hours at an enhanced air mass flow rate of 0.05 kg/ s.

4.2.4 Variation of Drying Rate Constant with Air Mass Flow Rate

By assigning values to; c , X_{di} and T_{ai} based on the product characteristics and operating conditions, the variations of drying rate constant k (hr^{-1}) with the air mass flow rate for various temperatures by the model were obtained and have been presented in the table below:

Table 4.3: Variations of the drying rate constant with temperature and air mass flow rates.

Temperature (K)	**Drying rate constant *k* (hr^{-1}) at 0.022 kg/s**	***k*** **(hr^{-1}) at 0.03 kg/s**	***k*** **(hr^{-1}) at 0.04 kg/s**	***k*** **(hr^{-1}) at 0.05 kg/s**	***k*** **(hr^{-1}) at 0.06 kg/s**
310	0.199	0.290	0.362	0.526	0.545
320	0.205	0.280	0.374	0.543	0.562
330	0.212	0.289	0.386	0.560	0.580
340	0.219	0.298	0.397	0.577	0.598
350	0.225	0.306	0.409	0.594	0.615
360	0.232	0.315	0.421	0.611	0.633

From the table, it is observed that for a particular temperature, the drying rate constants increase with the air flow rates and a similar trend is seen where at particular air flow rate the drying rate constants increase with rising temperature. It is however noted that greater changes in drying rate constants result from variations in the air flow rates produces as compared to temperature, where for example at 320 K, (temperature) enhancing the air flow rate from 0.022 kg/s to 0.06 kg/s results in change of 0.367 hr^{-1} in the drying constant but while increasing the temperature to 360 K results in a change of only 0.033 hr^{-1} in the drying rate constant. This observation in the present model would appear to suggest that although both temperature and air flow rates affect the rate of drying of a product, air flow rate is a more influential factor than temperature.

Further, graphical variation of the drying rate constants with air mass flow rate, at various temperatures have also been presented in the figure below:

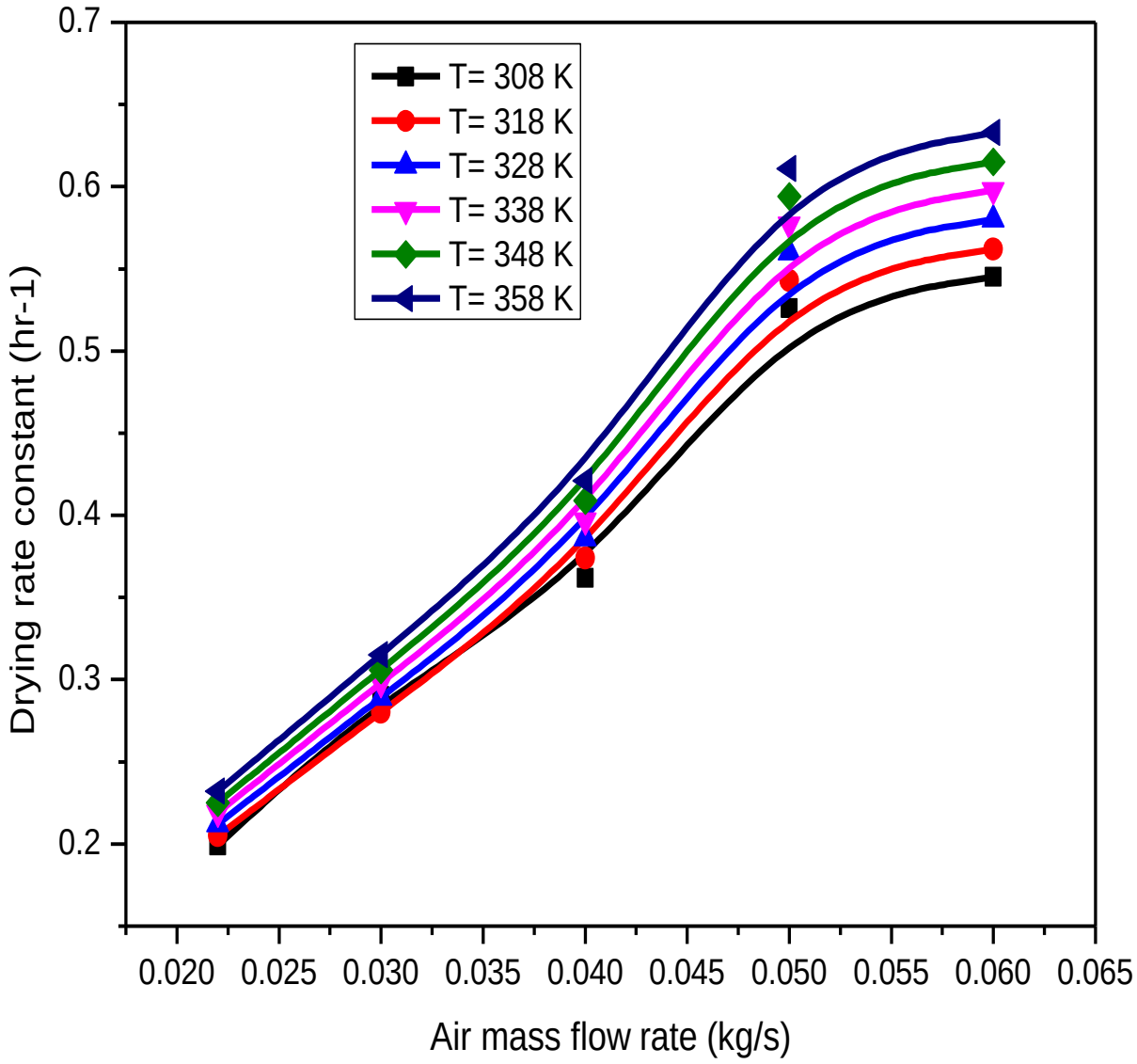

Figure 4.4: Variation of drying rate constant with air mass flow rate for various temperatures

From Figure 4.4 above, it is observed that there is an almost linear relationship between the drying rate constants and the air mass flow rate at lower air mass flow rates but a non-linear trend for higher flows. It is also apparent that at higher flows the curves each approach a maximum value of drying rate constant with further increases in air flow rates.

However the figure shows that a minimal influence of temperature, especially at lower air mass flow rates, thus suggesting that air mass flow rate is a more influential factor on the drying rate as compared to temperature. This observation is consistent with results of past studies on constant rate drying (Srikiatden, 2007) whose authors have also observed that the drying rate in this phase of drying is largely controlled by the rate of air flow over the product rather than internal diffusion factors. The model therefore predicts; 0.06 kg/s as the value for which there is a maximum drying rate constant; 0.640 hr^{-1} but beyond which there is a diminishing effect of air mass flow rate on the drying rate constant. This observation is consistent with findings of the study by Babalis and Belesiotis (2004) who have also reported the strong influence of air velocity on drying rates during the early stages of drying, but which influence diminishes after approximately 4 to 5 hours.

4.2.5 Variation of Drying Rate Constant with Temperature

The influence of temperature on the drying rate constant was also investigated using the model and the results have been summarized in the table below:

Table 4.4: Influence of temperature on the model drying rate constant for different air mass flow rates

Temp (K)	k **(hr^{-1}) at** $\dot{m}_a = 0.022kg/s$	k **(hr^{-1}) at** $\dot{m}_a = 0.03kg/s$	k **(hr^{-1}) at** $\dot{m}_a = 0.04kg/s$	k **(hr^{-1}) at** $\dot{m}_a = 0.05kg/s$	k **(hr^{-1}) at** $\dot{m}_a = 0.06kg/$
310	0.199	0.290	0.362	0.526	0.545
320	0.205	0.280	0.374	0.543	0.562
330	0.212	0.289	0.386	0.560	0.580
340	0.219	0.298	0.397	0.577	0.598
350	0.225	0.306	0.409	0.594	0.615
360	0.232	0.315	0.421	0.611	0.633
mean k (hr^{-1})	0.215 $\pm$ 0.00015	0.296 $\pm$ 0.00016	0.392 $\pm$ 0.00048	0.569 $\pm$ 0.0010	0.589 $\pm$ 0.0011

From the table, it is observed that there is an increasing trend in the drying rate constant with increase in temperature, for the air flow rates under consideration. However at particular air flow rates the ranges of the drying rate constants caused by temperature variation is much smaller compared to the ranges produced by variation in air flow rates. For example at 0.022 kg/s air flow rate and 310 K, increasing the temperature by 50 K (15 %) results in only a change of 0.016 hr^{-1} (10 %) while enhancing the air flow rate by 0.008 kg/s (36 %) results in a comparatively greater change of 0.081 hr^{-1} (40 %) in the drying rate constant.

Further, the variation of drying rate constants with air mass flow rate has been presented in Figure 4.5 below;

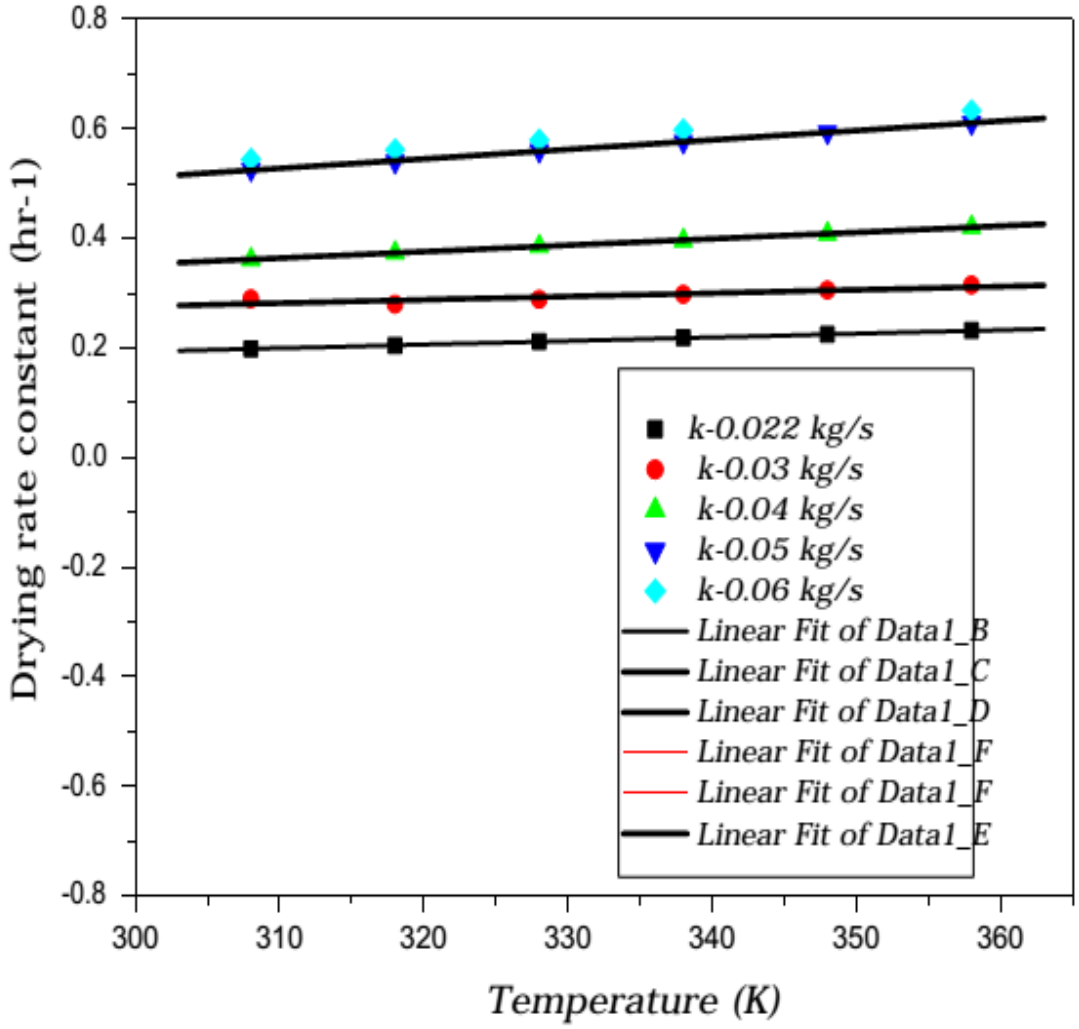

Figure 4.5: Variation of drying rate constants k with temperature for the different air mass flow rates

From the figure above, it is observed that there is a direct linear proportionality between the drying rate constants and temperature and that the drying rate constants are generally larger for higher air flow rates. The fact is that increasing the temperature raises the absolute humidity of air but lowers its relative humidity hence increasing the drying rates. There is therefore agreement between the present model and the Fick's diffusion model as far as the prediction of the drying rate constant with temperature is concerned and Akoy (2007) has also observed the same trend. However there is an apparent convergence in the drying rate constants at higher air

flow rates as observed in the overlapping of the drying constants for air mass flow rates; $0.05kg/s$ and $0.06kg/s$ and confirmed by statistical analysis using Student-"t' and one-way Anova tests whose results; $t = 1.1054$ and $p = 2.949$: $F = 1.222$ and $P = 0.2949$ respectively indicated no significant differences of the means of the drying rate constants at 5 % significance levels. This observation therefore implies that there is a limit to which increasing the air flow rate contributes to increasing the drying rate.

It is also observed that the values of drying rate constants are larger at higher temperatures, where at the simulated experimental conditions; 0.022 kg/s and 310 K for air mass flow rate and drying temperature respectively, the model predicted a drying rate constant of between 0.200 hr^{-1} and 0.230 hr^{-1} at 310 K and 360 K temperatures respectively. These values are within the range of 0.22 hr^{-1} and 0.23 hr^{-1} for *R. argentea* fish obtained in direct tunnel solar dryer by a past study (Odote et al, 2010). However larger drying rate constants than these values for the product have been predicted by the model as are obtainable at air mass flow rates of between 0.03 kg/s and 0.06 kg/s for the temperature range 310 K to 360 K.

In conclusion the drying rate constant is a function of both air and material properties, it describes the heat and mass transport mechanism and is therefore a useful design and optimization tool since it embodies all the transport properties into a simple exponential function (Akoy, 2007).

4.2.6 Variation of Drying Rates with Time

The variation of drying rates with time as predicted by the model were computed from the moisture ratios using Equation 3.29 and the results have been presented in Figure 4.6 below:

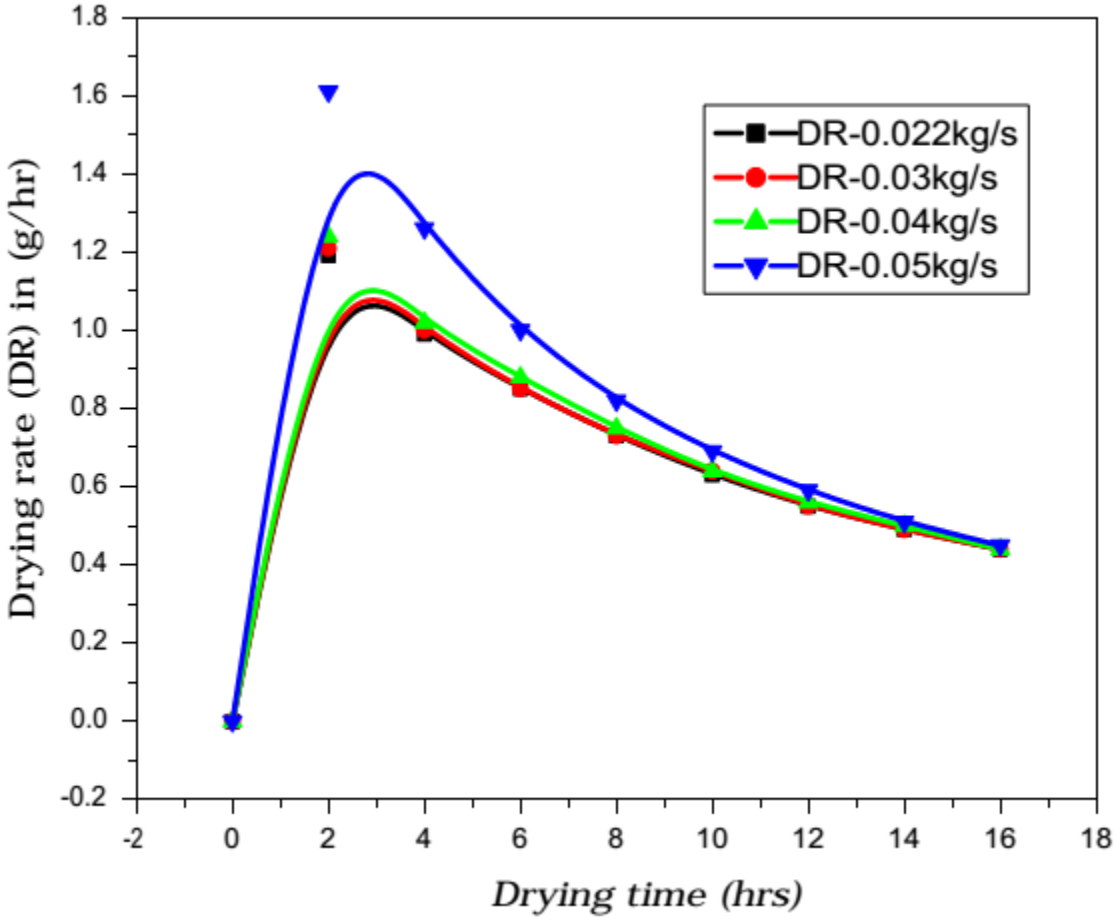

Figure 4.6: Variation of the model drying rates with time

It is observed from the figure that the drying rates initially increase to a maximum value but begin to decrease after about 2 hours of drying. The falling rate drying period during which the drying rate decreases is observed to be much longer than the constant rate drying period. At the simulated experimental value of the drying rate constant 0.205 hr^{-1}, the model predicts that the drying rates begins to decrease after about 3 hours of drying, with the falling rate period lasting about 6 hours.

4.2.7 Variation of Drying Rate Constant with Drying Factor

The influence of the drying factor D_f on the drying rate constant k at various temperatures was investigated by the model and the results have been presented in Figure 4.7 below:

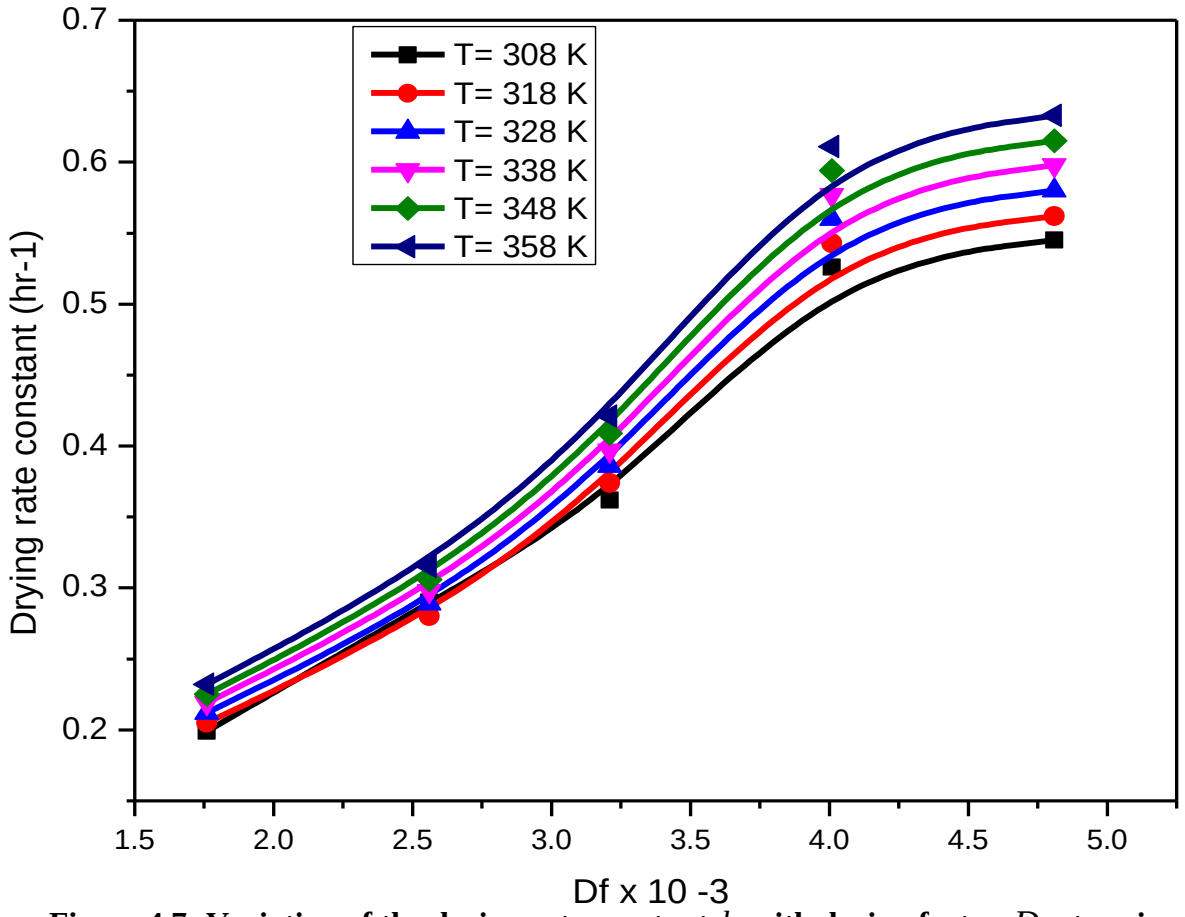

Figure 4.7: Variation of the drying rate constant k with drying factor D_f at various temperatures

It is observed that there is a similarity between the variations of drying rate constant with air mass flow rate and drying factor, as seen in the similarities of Figures 4.4 and 4.7. The observation confirms that the drying factor, Equation 3.9, contains only one variable; air mass flow rate. There is an apparent similarity between the present model and the diffusion model,

with the drying factor D_f in the former and moisture diffusivity coefficient D_{eff} in the latter both having a linear relationship with the drying rate constants, Equations 3.34 and 4.6. However the advantage for the present model is that D_f is easily computable from Equation 3.9, where the only variable is the air flow rate unlike in the Fick's diffusion model where coefficient of moisture diffusivity D_{eff} is measured through experimental tests.

4.2.8 Variation of Drying Factor with Drying Time

The influence of the drying factor D_f on the drying times at various temperatures as predicted by the model, have been presented in Table 4.5 below:

Table 4.5: Influence of drying factor D_f on the drying time at different temperature

$D_f \times 10^{-3}$ $(m^3/s/K)$	**Drying time (hrs) t-310K**	**t-320K**	**t-330K**	**t-340K**	**t-350K**	**t-360K**	**Mean drying time t_d (hrs)**
1.76	12.1	11.7		11.4	11.0	10.4	11.22
2.56	8.9	8.6		8.3	8.1	7.6	8.23
3.21	6.7	6.4		6.2	6.1	5.7	6.17
4.01	5.3	5.2		5.0	4.9	4.6	4.95
4.81	4.4	4.3		4.2	4.0	3.8	4.10
Δt_d	7.6	7.3		7.1	7.0	6.7	

It is observed that the drying times are much shorter for larger values of the drying factor, whereas an increase in D_f from $1.76\times10^{-3} m^3/s/K$ to $4.81\times10^{-3} m^3/s/K$ results in the reduction of drying time by about 7 hours, a temperature change from 310 K to 360 K causes a reduction of less than 2 hours in the drying time. It is apparent that the drying factor whose main constituting variable is air flow rate affects the drying rates more than temperature. Further the

graphical variation of the drying time with the drying factor has also been presented in the figure below:

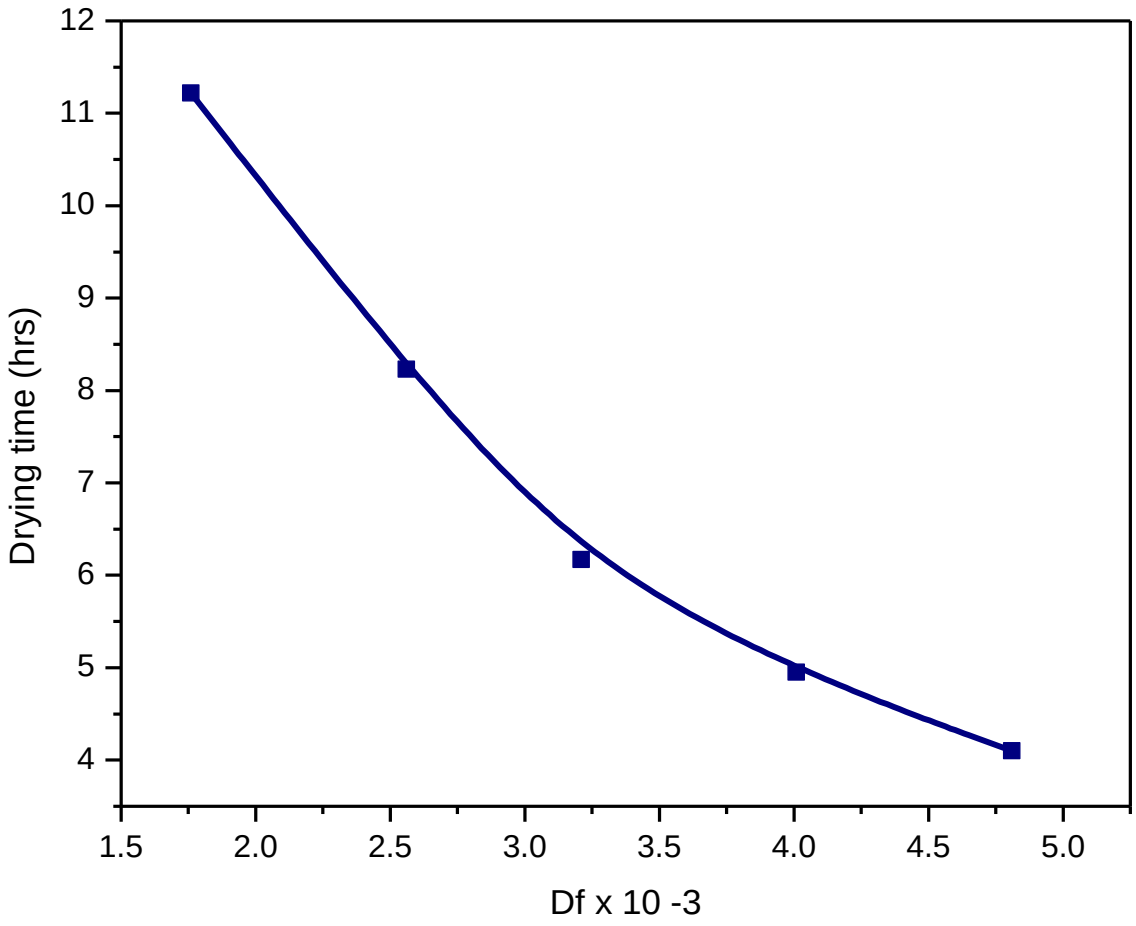

Figure 4.8: Variation of the mean drying time t_d with the drying factor D_f

The figure shows an exponential decrease in the drying time with drying factor. Increasing the drying factor drastically reduces the drying time from about 12 hours to 4 hours. This observation suggests a strong influence of the drying factor on the drying time and since drying factor is a lumped parameter containing air mass flow rate as the main variable, its variation with time must therefore reflect that of the air flow rate.

From Figure 4.8, it is also apparent that there is a critical value of drying factor beyond which no further reduction in the drying time can be achieved. The model thus suggests a minimum drying time of about 4 hours for the *R. argentea* fish product.

4.3 Experimental Results

4.3.1 Variation of Ambient and Drying Chamber Air Relative Humidity with Time

The variations of the mean relative humidity of ambient and chamber air against time experiment during the first phase of drying has been presented in Figure 4.9 below:

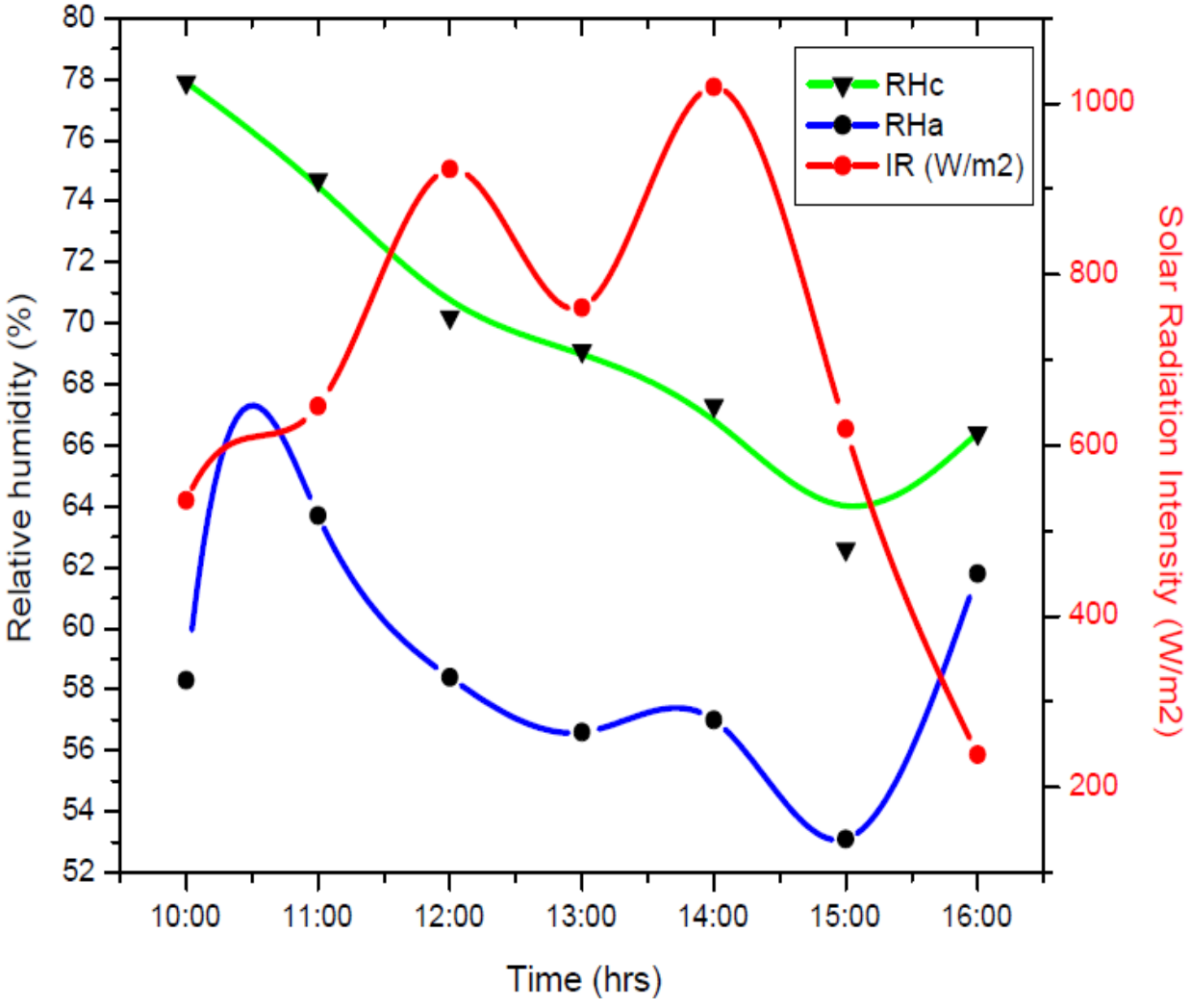

Figure 4.9: Variation of the mean relative humidity of ambient and chamber during the first phase of drying.

It is observed from the figure that the values of relative humidity of air in the drying chamber obtained by the experimental tests ranges from 66.5 % to 77.9 %, while for the ambient air the range was from 52.6 % and 67.4 %, during the first phase of drying (the first 5 hours). During this phase, the relative humidity of air is greater for the drying chamber than the ambient, even though both decrease with increasing time of the day. The comparatively higher relative humidity of air in drying chamber is attributed to the fact that at the beginning of the drying, the fish was heavily laden with moisture which increased moisture of air in the drying chamber. However, the decrease in the relative humidity of air in the drying chamber appears to be more uniform and steady as compared to that of the ambient.

At about 15:00 hrs, there is shift in the trend where an increase is observed; with the rise in ambient value being sharper than the value for the drying chamber. This observation can be attributed to the marked decrease in the solar radiation intensity after 14:00 hours, which in turn causes a drop in the temperature of both the ambient and drying chamber. In general the relative humidity of air in the ambient and drying chamber is observed to be higher at beginning of drying 10:00 hours but decrease to a minimum value at about the instant when there marked decreasing trend in the solar radiation intensity.

The figure also shows that while the values of relative humidity of air in both ambient and drying chamber decreases with the drying time, the solar radiation intensity increases with a peak value occurring at about 14:00 hours. This observation suggests an inverse relationship between relative humidity of the air and solar radiation intensity, which is accounted for by the fact that increase in solar radiation intensity causes an increase in temperature in the ambient air entering the collectors, the fact is that although the absolute humidity of the air is constant at a particular temperature, it can be increased by raising the temperature of air thus lowering the relative

humidity of the air. The above explanation therefore leads to the observation that relative humidity in ambient air reduces with increasing solar radiation.

Further the variation of the mean relative humidity of ambient and chamber during the second phase of drying (last 6 hours) is presented in Figure 4.10 below:

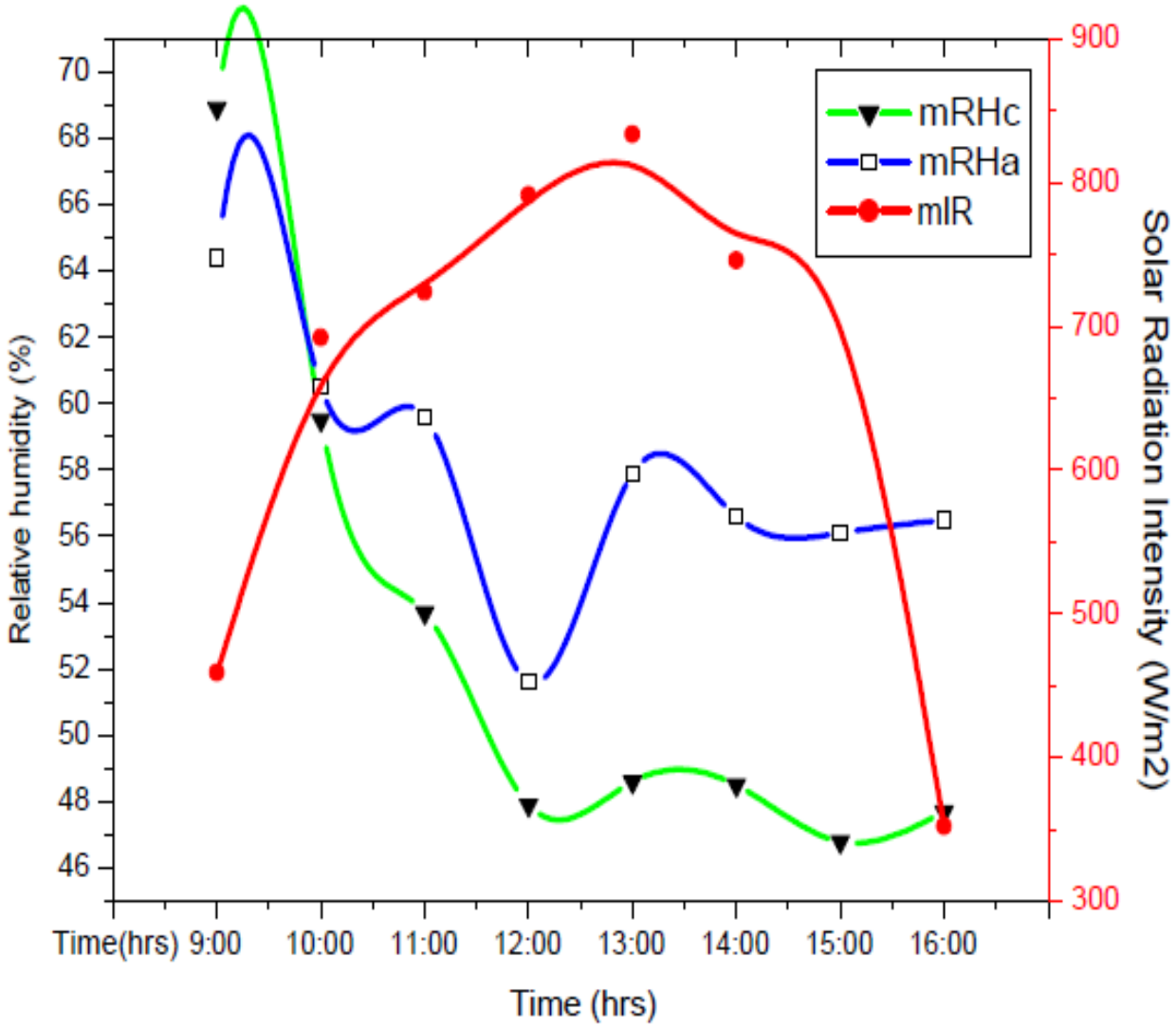

Figure 4.10: Variation of the mean relative humidity in the ambient and chamber during the second phase of drying

From Figure 4.14, it is observed that during the second phase of the drying tests, the mean relative humidity of the chamber air ranged from 47.2 % to 69.2 % while that of ambient air

varied from 51.0 % to 68.0 %. It is therefore apparent that the relative humidity of the chamber air was lower than that of ambient. But as can be been observed from the Figures 4.13 and 4.14, both the relative humidity in the ambient and chamber air showed a general decreasing trend with increasing time of the day. It is also further observed that whereas there were fluctuations in mean relative humidity of the ambient air, a decreasing trend in the relative humidity of the chamber air to an almost constant value was observed. There was therefore an overall reduction in relative humidity of air in the drying chamber by 23.4 % below the ambient value during the days of drying. In addition, it was observed that between 10:00 hours and 16:00 hours, the solar radiation intensity and therefore temperatures were relatively higher while the relative humidity of air during this period was lower, a condition that tended to enhance the drying process.

The observed decrease in relative humidity of air in the chamber and ambient with time of the day was caused by increased temperature of the ambient air, through heating by the incident solar radiation, with the absolute humidity of the air increasing with temperature but the relative humidity is lowered due to expansion of the air. This decreasing trend of air relative humidity with solar radiation intensity has the effect of increasing drying rates during solar drying, as has been observed by past studies (Aghbasho et al, 2008; Kaplanis, 2006).

The properties of the air flowing around the product are therefore major factors that determine the rate of removal of moisture, with the capacity of air to remove moisture principally depending on its initial temperature and humidity. This has been observed by by past studies which have reported that higher temperatures coupled with lower humidity tends to enhance moisture removal capacity of the air, (Raju et al, 2013)

4.3.2 Variation of Temperature and Solar Radiation Intensity with Time

The variations of temperature and incident solar radiation intensity with time for various locations in the drying system under load are presented in Figure 4.11 below;

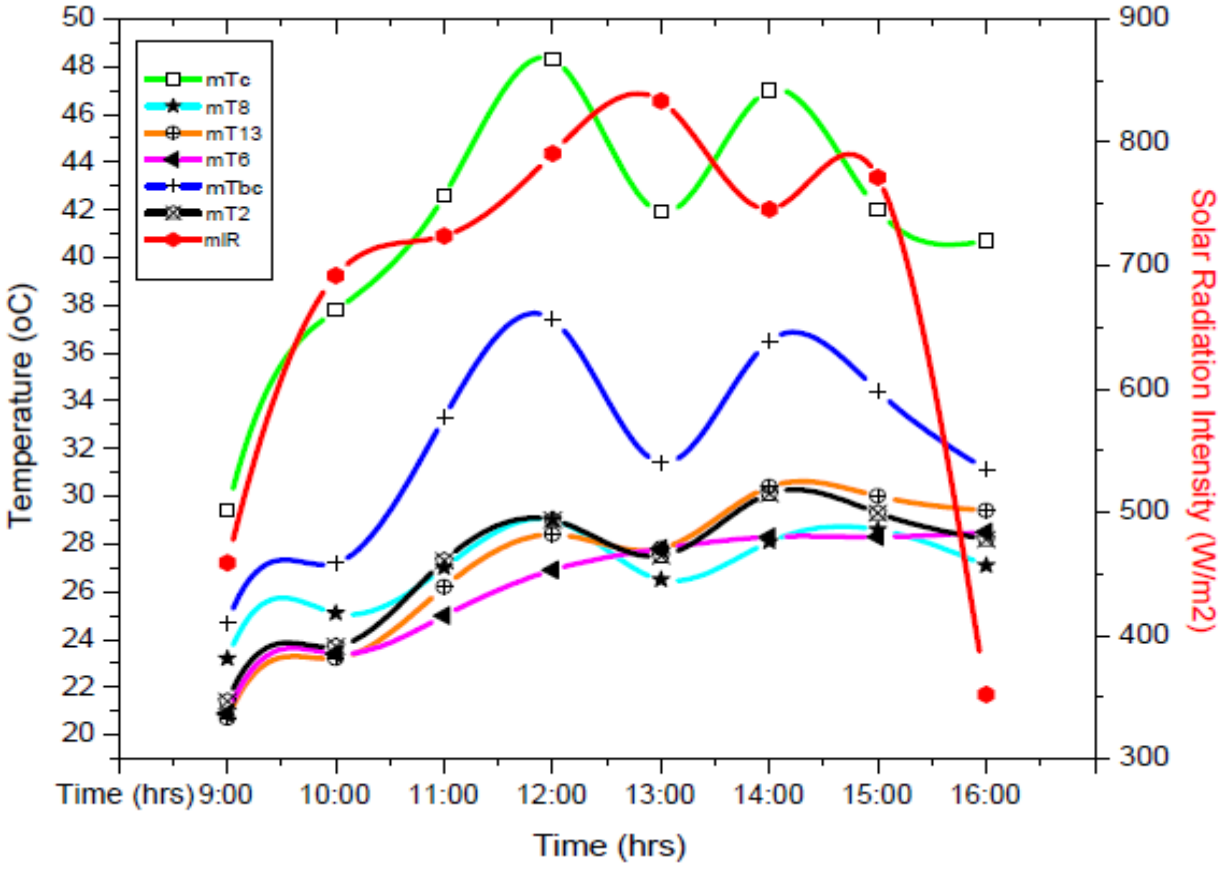

Figure 4.11: Variation of mean temperatures at various locations in the collectors and drying chamber with time during drying.

It is noted that there is a fluctuating pattern of temperature of the components of the drying system with time of the day. The chamber temperature increases from relatively lower values in the morning and attains maximum values between 12 noon and 13:00 hrs, with the peaks of temperature corresponding to the period when the global solar radiation is maximum an observation which agrees with findings of other studies, (Kaplanis, 2006).

It is observed further that the mean outlet temperatures of the collector system was 44.85 $\pm$ 15.89 ^{o} C, which was higher than 32.0 $\pm$ 9.71 ^{o} C and 28.7 $\pm$ 3.23 ^{o} C, the mean values for bottom chamber and ambient air temperatures respectively, although the mean bottom chamber temperature was observed to be higher than the ambient value. This is explained by the fact that as the solar radiation falls on the glass cover of the collectors, a part of this energy is absorbed by the glass but the portion transmitted by the glass is exchanged through radiation and convection between the absorber and air in the collectors, causing heating of the air as it flows in the collectors hence the higher temperature of air in the collectors as compared to the ambient. There are therefore convection and conduction thermal losses between the collector walls, metal absorber, collector walls and the glass leading to attenuation of heat energy transmitted to the drying chamber by the flowing air and hence the observation that temperatures are lower in the drying chamber than at the collectors.

It was also observed that as the solar radiation intensity increased, so did the outlet temperature of the collectors and hence the difference in temperature between the collector outlet and the ambient air. The maximum values of outlet temperatures of the collector system and solar radiation intensity occurred at about the same time (s) of the day, Figure 4.11. The mean temperatures at the bottom, middle, top trays and the chimney were found to be; 29.1 $\pm$ 3.00 ^{o} C, 27.0 $\pm$ 3.46 ^{o} C, 26.1 $\pm$ 2.79 ^{o} C and 26.6 $\pm$ 4.23 ^{o} C respectively. Although there was an observed general decreasing trend in temperature from the bottom chamber to the top tray of the dryer, the temperature of the chimney was found to be slightly higher than that of the top tray. The higher temperature of the chimney is attributed to the good thermal absorption properties of the metallic material used in its construction.

The variation of the solar radiation intensity assumed a parabolic shape, (though not perfectly), with the peak occurring at about 13:00 hrs, with increase and decrease before and after the peak respectively. The variation of solar radiation intensity with the time of the day was not perfectly parabolic as expected but fluctuated near the peak, an observation that was attributed to the movements and intensity of the clouds. It was also observed that the temperature of the air in the drying chamber was higher than the ambient for most hours of the drying day. The graph of the temperature profiles of the various components in the drying system followed the pattern of the incident solar radiation with their maxima and minima occurring at about the same times with that of the incident solar radiation, an observation which suggests that temperature is an evolution of the instantaneous incident solar radiation, and which has been observed by previous studies (Ghaba et al, 2007).

4.3.3 Variation of Air Volume Flow Rate and Solar Radiation Intensity with Time

The variations of the air inlet and outlet flow rates through the drying chamber and the solar radiation intensity have been presented in Figure 4.12 below:

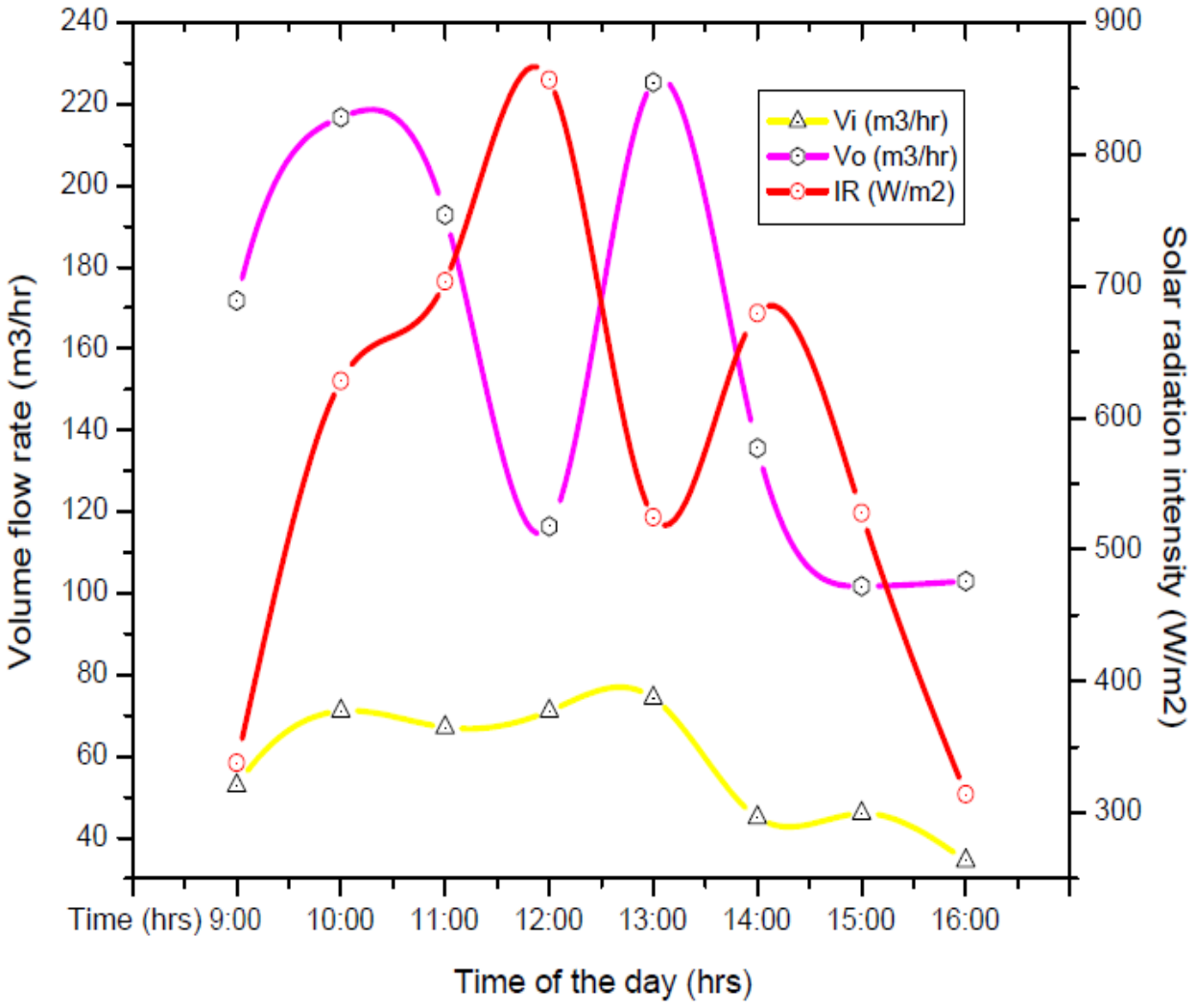

Figure 4.12: Variation of the mean inlet and out let air volume flow rates with time during drying.

From the figure, it is observed that the mean air mass flow rate from the combination of collectors into the drying chamber was 0.0190 ± 0.0048 kg/s while the air flow rate out of the chimney was 0.051 ± 0.0153 kg/s, during the drying period. The flow rate of air into the drying chamber was observed to be much lower than the flow rate out of the chimney. Greater fluctuations were also observed in air flow rate out of the chimney than in the inlet air entering

the chamber. There was an initial period of increase in the air inflow rates followed by an almost constant phase and then a decrease at about 13:00 hrs.

There was no observed relationship between the variation of the intensity of the solar radiation and the air flow rates with time. The air inflow rate into the drying system was observed to be nearly constant for most hours of the day, an observation that can be attributed to the exhaust fan incorporated within the dome of the dryer which maintained a steady air flow rate in the collectors and drying chamber. The relatively higher flow rate of the air at the chimney can be attributed to the positioning of the suction fan at the dome of the drying chamber, where the air nearest to it is sucked out faster than air at farther locations in the drying system. On the other hand, the inflow rate of air upward through the drying chamber is lower since the fish stacked in the trays reduces suction power of the electric fan.

It is observed that the inlet air mass flow rates of 0.0190 ± 0.0048 kg/s obtained in the experiments based on the specifications of the fan were lower than lower than 0.022 kg/s, the least value predicted by the model. The observed flow rates were similarly lower than 0.0401 kg/s, that have been obtained by a past study involving a similar type of dryer (Ahmed, 2011) but where this difference could be attributed to the lower power ratings of the electric fan employed in the present study.

4.3.4 Variation of Thermal Efficiency and Solar Radiation Intensity with Time

The thermal efficiencies of the collectors were computed according to Equations 3.30, for which variations of the mean efficiency for the collectors, the instantaneous solar radiation intensities with time during the days of drying have been presented in the figure below:

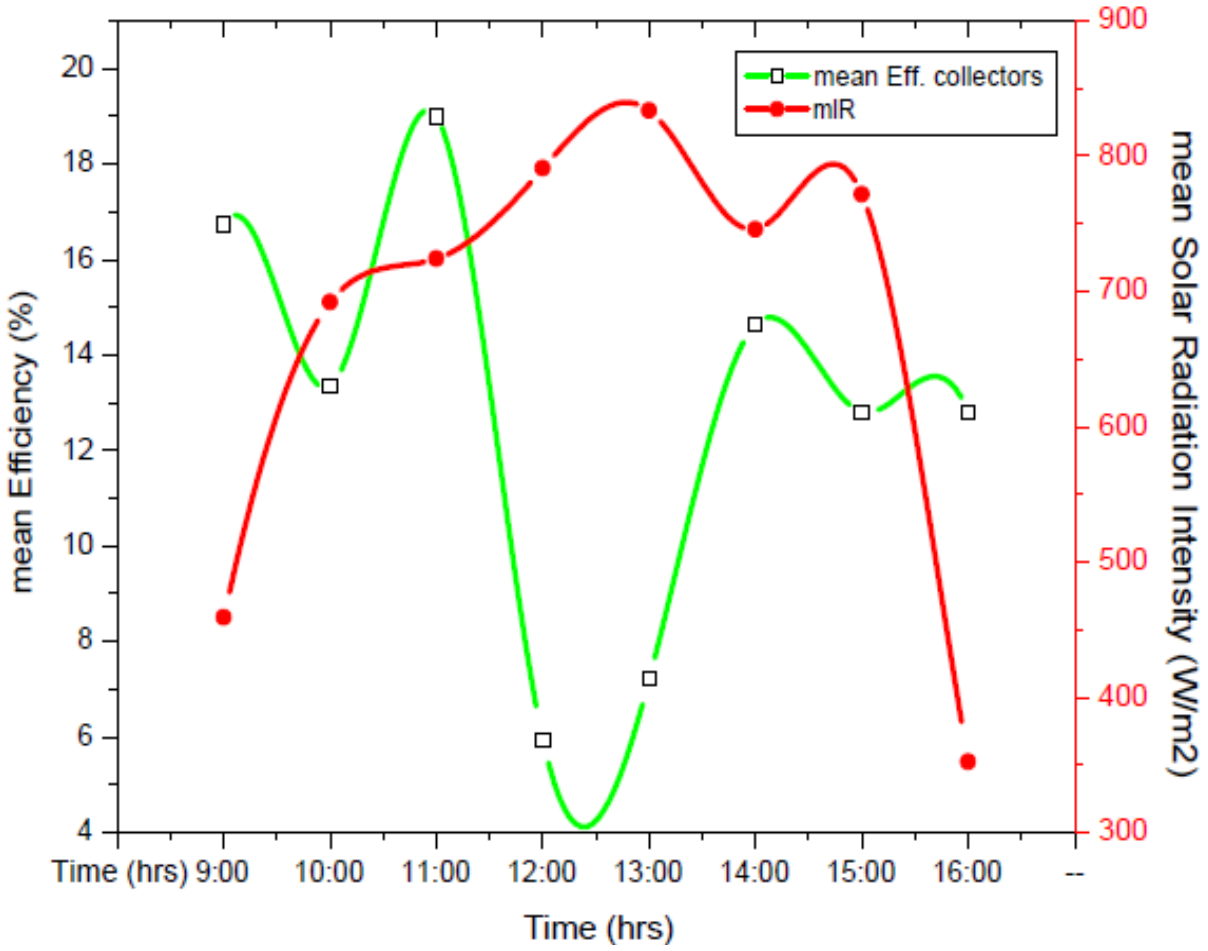

Figure 4.13: Variation of mean thermal efficiency of the collectors with time during drying

The efficiency of the collector system was observed to increase with the incident solar radiation intensity with the peaks occurring between 11:00 hrs and 12:45 hrs. There is observed a time lag interval of about 1 hour 45 minutes between the peaks of efficiencies and the solar radiation intensity. This lag in time between the peaks can be explained by the fact that when there is an increase in solar radiation intensity this is first detected as an increase in the air temperature at collector inlets and then after an interval of time has lapsed the same temperature change is realized at the collector outlets.

The mean thermal efficiency of the collector system, as computed according to Equation 3.30, was found to have maximum and minimum values of 15.96 % at about 11:30 hrs and 5.30 % at 16:00 hrs respectively during the drying period. The mean thermal efficiency of the collector system was thus found to be: 9.93 ± 3.45 %, although this value was lower than the predicted value of 43.5 %, Table A1, (Appendices) it was closer to 21.0 %, the value obtained by a previous study involving a similar type of dryer (Bala and Janjai, 2009). The differences in the values can be attributable to the differences in optical transmittance of the glass material used which determines the fraction of the incident solar radiation on the collectors that is (visible spectrum) transmitted by the glass material and converted to useful thermal energy absorbed by the air in the collectors. There are also probable convection, conduction and radiation thermal losses within the collectors and air duct system which tends to lower the mean thermal efficiency.

The overall drying system efficiency, computed according to Equation 3.32, was found to be: 11.0 %, and although this value was lower than the expected values of between
20 % and 30 % for forced convection drying systems (Forson et al, 2007), it was however comparable to typical values of 18.41 % obtained by a past study involving a similar dryer (Ahmed, 2011). The difference between the expected and the experimental values can be attributed to the relatively low heat transfer coefficients between the air and glass cover of the collectors and between air and the fish product, which leads to only a relatively small fraction of the incident solar radiation on the collectors being converted to useful energy transferred to the product for the evaporation of moisture.

4.3.5 Variation of the Moisture Ratio for *R. argentea* Fish

The experimental moisture curves of *R. argentea* fish samples in open sun and fish in the bottom, middle and top trays of the solar dryer, for the five experimental tests conducted in the wetter season May –June 2014 denoted by: WS-**1,** WS-**2** and WS-**3** and drier season Jan- March 2015 denoted by DS-**4** and DS-**5** have been presented in figures 4.14 - 4.18.

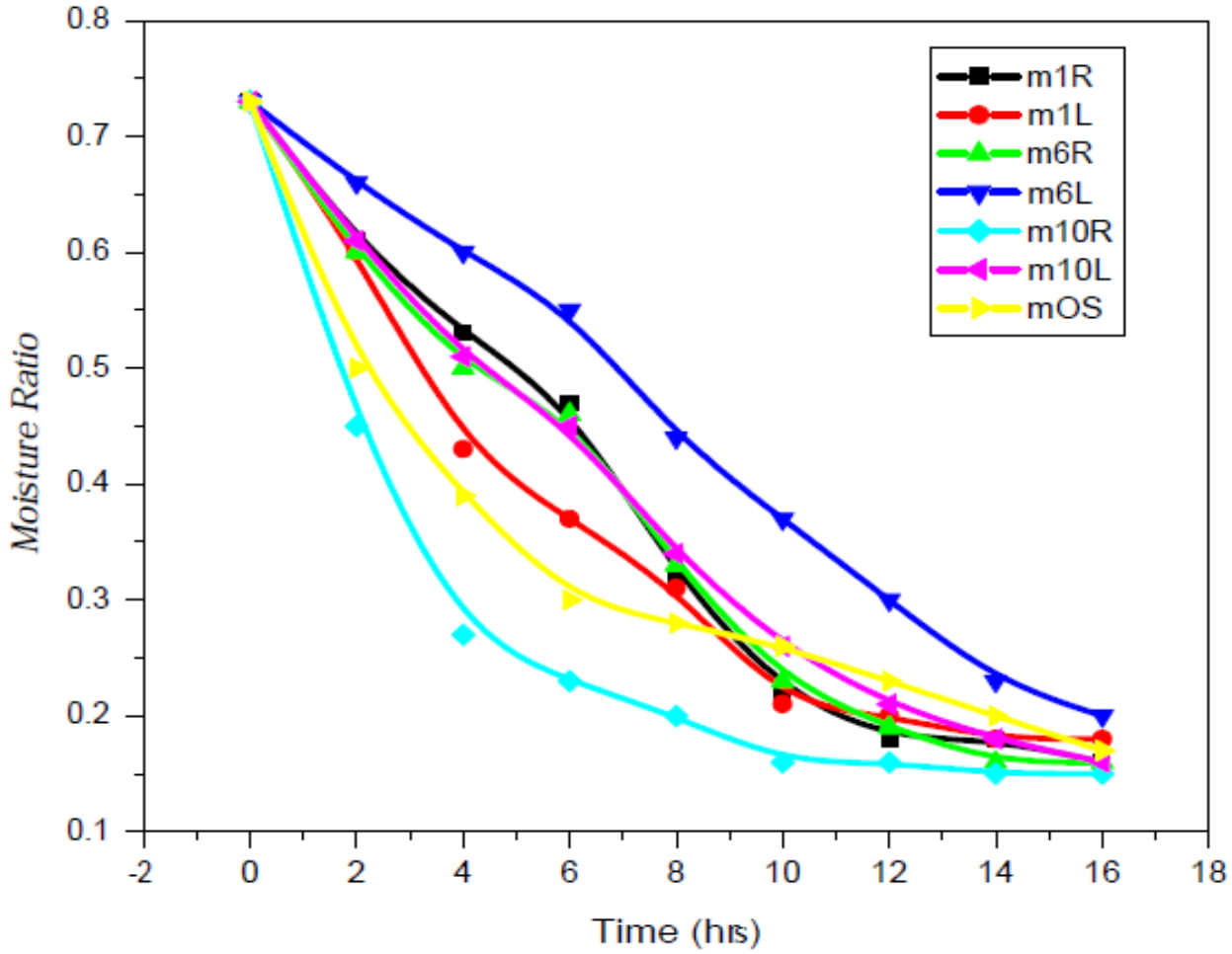

Figure 4.14: Variation of moisture ratios of the fish with time, WS-1

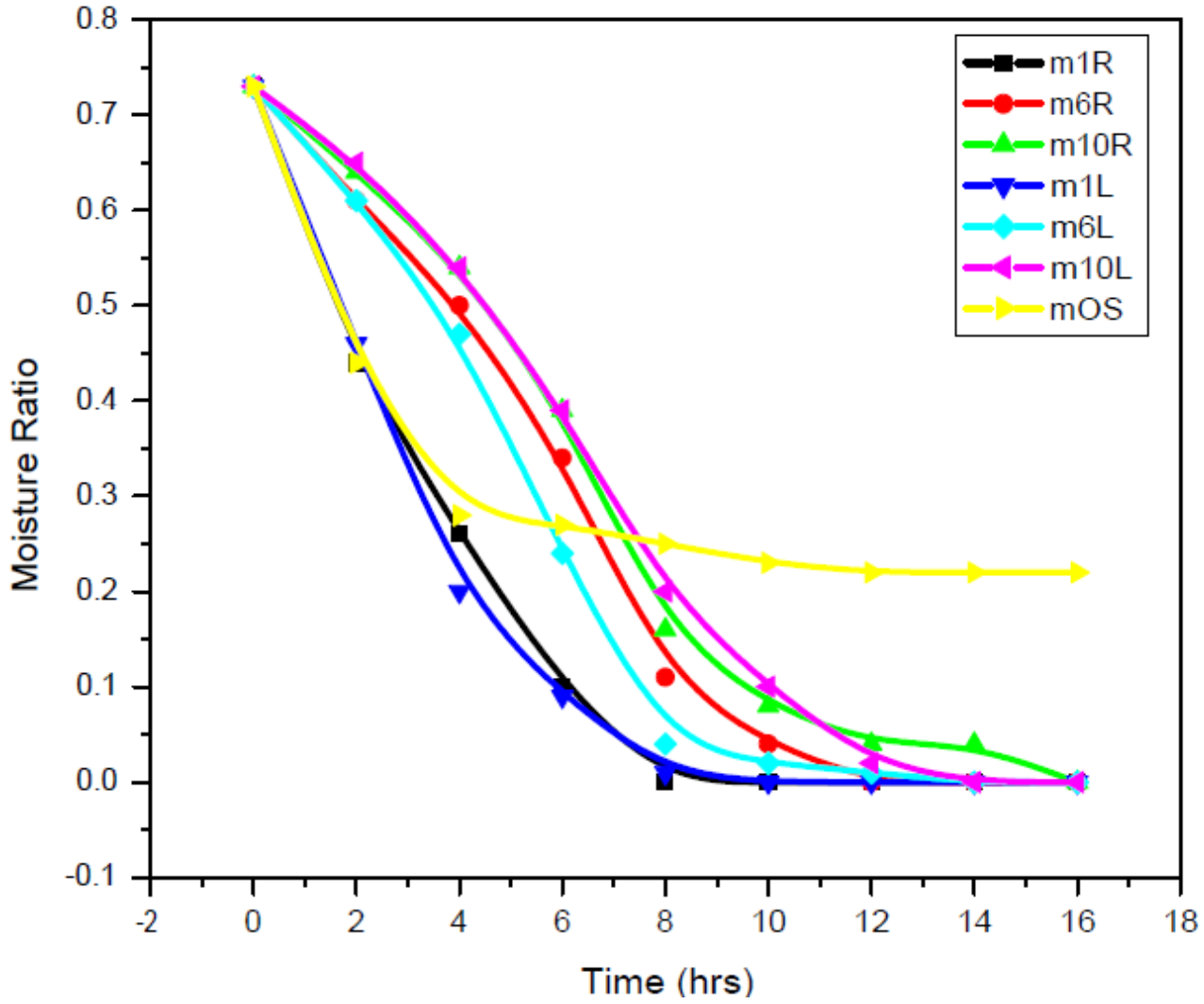

Figure 4.15: Variation of moisture ratios of the fish with time, WS-2

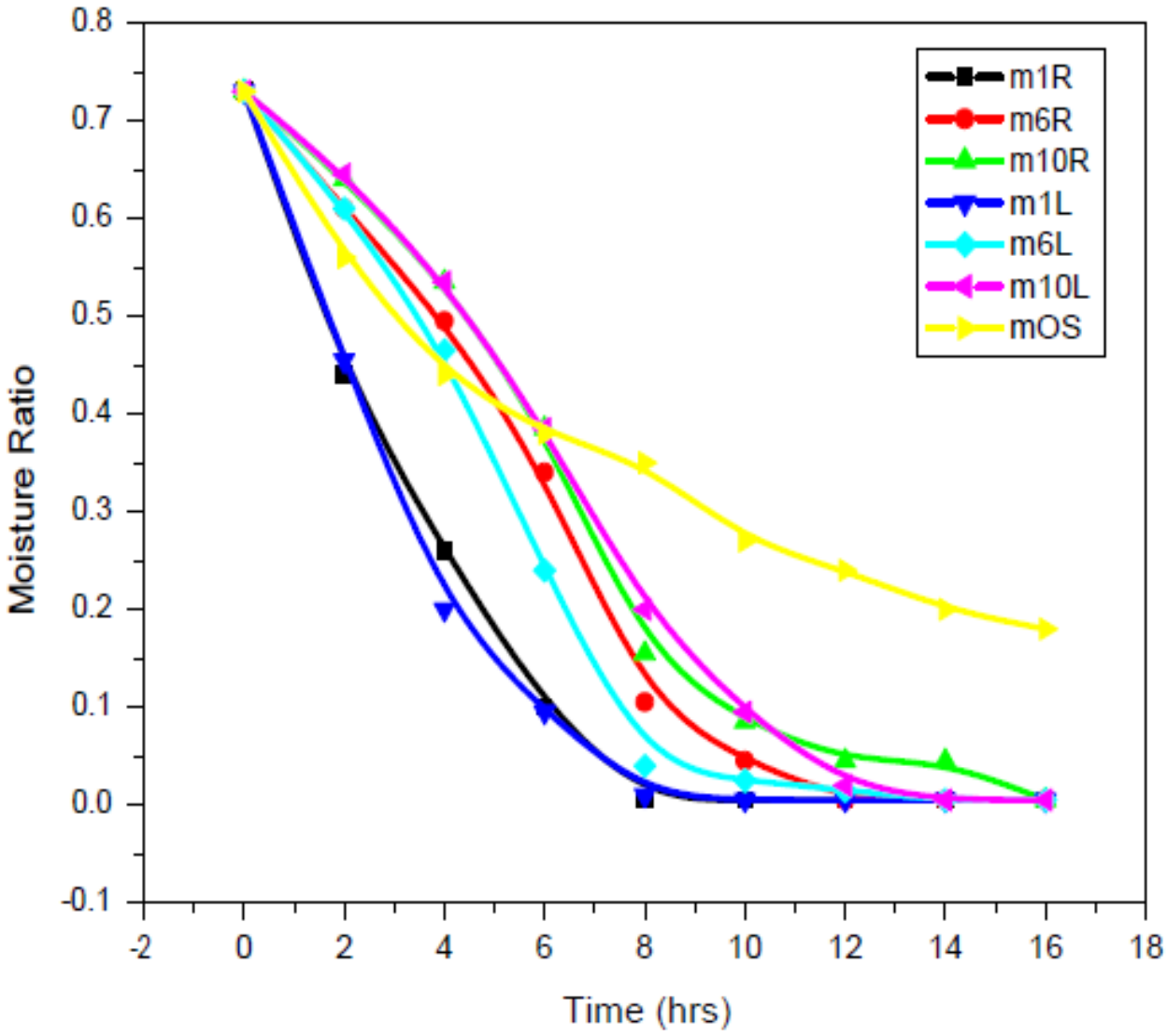

Figure 4.16: Variation of moisture ratios of fish with time, WS-3

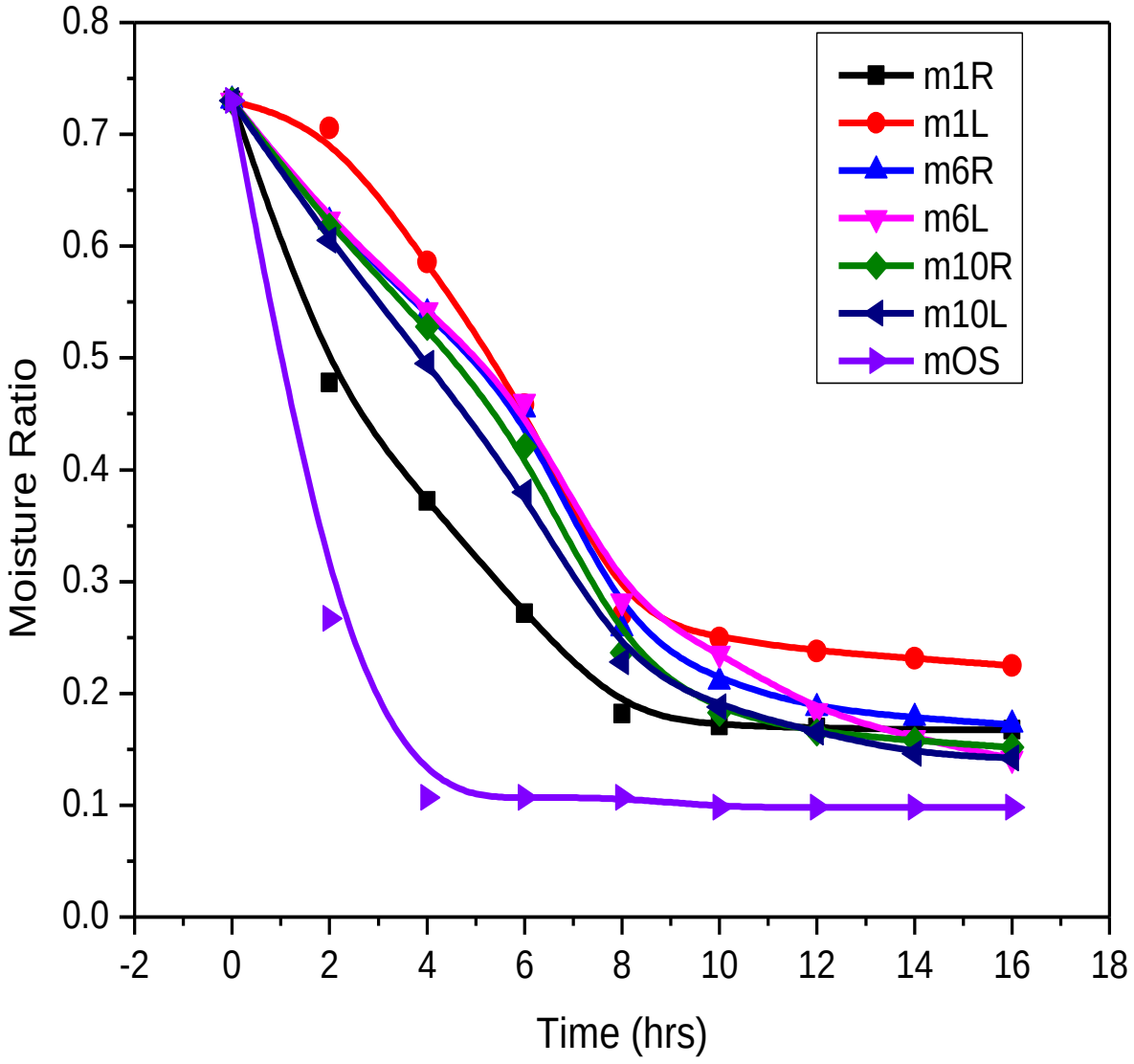

Figure 4.17: Variation of moisture ratios of fish with time, DS-4

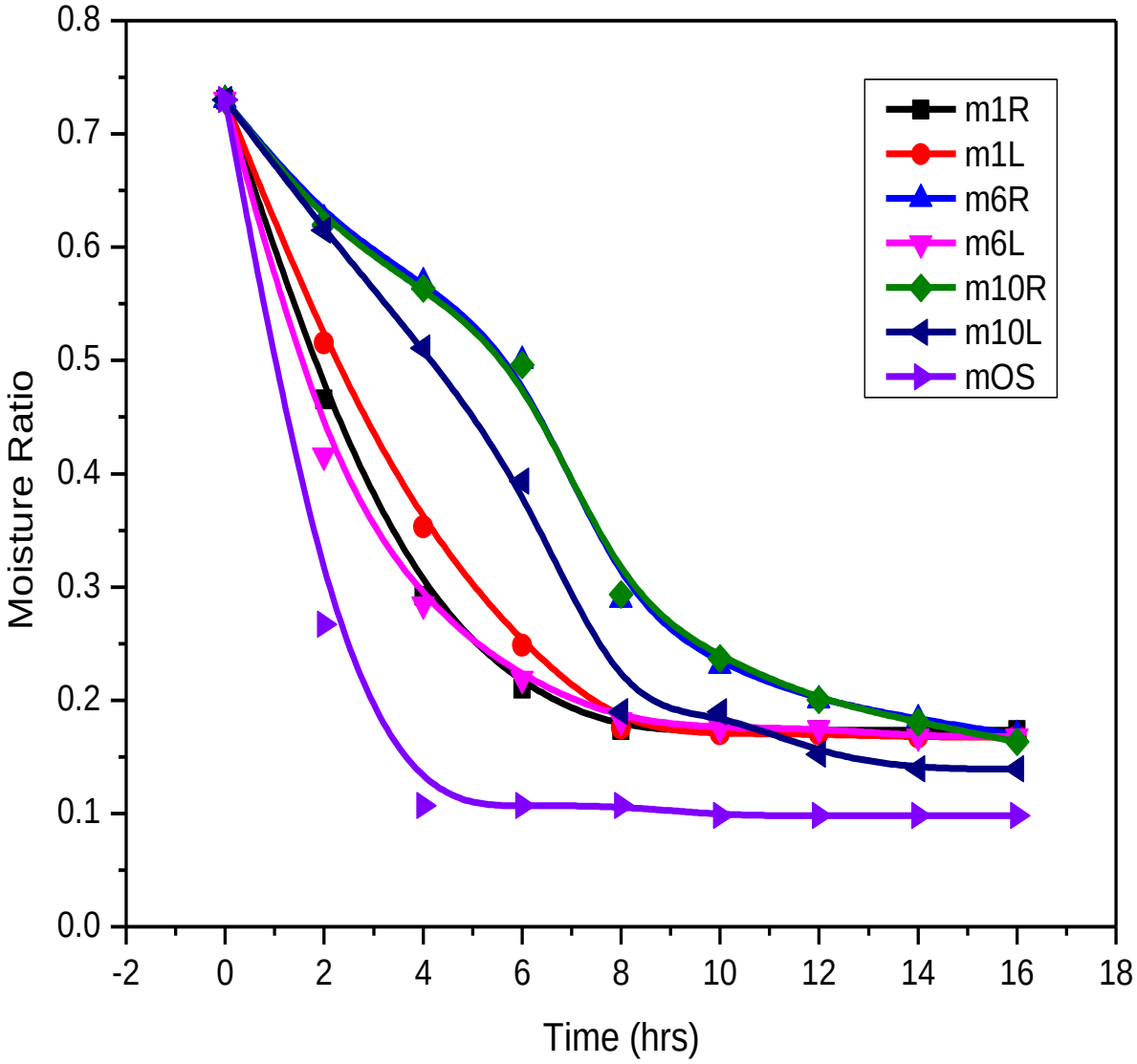

Figure 4.18: Variation of moisture ratios of the fish with time, DS-5

As can be observed for all the open sun (*mOS*) and solar dried fish samples tested, Figures 4.14 -4.18, the moisture ratios of the fish reduces exponentially with increasing drying time, which is consistent with results of previous studies for the drying of most biological materials (Afolabi, 2014). It is further observed that for the three tests that were conducted in the relatively wet season: May- June; WS-**1**, WS-**2** and WS-**3**, the fish in the solar dryer attained a lower moisture ratio of less than 10 % (w. b) for the majority of the samples in a time of 11 hours, which is in

contrast with the open samples that attained 25 % (w. b.) a much higher moisture in the same duration. The majority of the fish samples in solar dryer similarly attained 15 % (w. b.) the safe moisture content, for food products in a comparatively shorter time (between 5 to 9 hours) than the open sun samples. The fish in the solar dryer indicated a greater decrease in their moisture ratio as compared to those in the open sun, in the time interval 0 hours and 7.5 hours for the majority of the tests conducted; WS-**1**, WS-**2**, WS-**3**, DS-**4** and DS-**5**.

However in the case of the experimental tests done in the characteristically dryer season between January and March; DS-**4** and DS-**5**, the lowest moisture ratio of the fish obtained in the solar dryer was about 15 % for the bottom trays in a period of about 14 hours, with the fish in the other trays gradually attaining final moisture ratios of between 15 % and 22 % at the end of the drying period. In contrast the open sun samples attained much lower moisture ratios below 10 % (w. b.) within a period of 8 hours during this drying season.

It was also observed that for all the tests conducted in both seasons, there was a greater decrease in the mean moisture ratio for the fish in the first 8 hours of drying. The mean moisture content of the fish in the solar dryer was reduced from 73 % to 55 %, 47 %, 45 %, 46 %, 37 % and 23 % (w. b.) for the middle trays, top right, top left bottom left, and bottom right trays respectively after the first 6 hrs on a typical day of drying and then to final values of: 8% (w. b.) for the middle right tray and bottom right trays, the bottom left and top right and middle right trays and 9 % (w. b.) for the top left tray and 10% for the middle left tray after another 5 hrs on a continued day of drying. The mean moisture content of the fish was thus reduced from an initial value of 73 % (w. b.) to between 8 and 10 % (w. b.) in the solar dryer in period of about 11 hours where for the final values of moisture content open sun drying took up to 18 hrs. Except in the case of tests conducted in the dryer seasons; DS-**4** and DS-**5**, the drying times were shorter in the

solar dryer than in the open sun because useful solar energy was transferred to air in the collectors raising the temperature which increases the energy available to evaporate moisture from the fish in the drying chambers and hence the higher drying rates in the solar dryer. Further lower moisture contents were obtained for fish in the top and bottom trays compared to the middle, a fact attributed to the increasing humidity profile in drying air from the bottom to top of the chamber so that air at the bottom of the drying chamber has the greater affinity for moisture than that at the top. However the proximity of the top trays to the chimney and the exhaust fan caused higher temperatures and enhanced air flow rates for the top trays which increased their drying rate.

Except for tests conducted in dryer season, (January – March 2015); DS-**4** and DS-**5**, the fish in the solar dryer fish attained a relatively lower final moisture ratio than the open sun samples. The exception is attributable to the operating parameters occurring during this drying season (between January and March 2015) where due to the higher solar radiation intensities the ground and ambient air attained higher temperatures so that increased thermal heat from the ground also enhanced the drying rates. Another factor was the mean the relative humidity of air which was much lower during this particular season of experimental tests. However notable was the fact that for both seasons the fish which was left overnight in the solar dryer at the close of the drying day continued to dry due to the inertia of the drying system. This was detected in the weight measurements of fish in the morning before beginning the second phase of drying day.

The initial phase of drying, where the fish moisture ratio dropped more rapidly at almost constant rate represented the constant rate drying period while the next phase where the rate of moisture loss decreased to almost zero represents the falling rate drying period. The rapid loss in moisture of the fish at the beginning of drying is attributed to the evaporation of moisture on surface of the

fish occurring in both the solar and open sun dried samples. The falling rate drying period represented the stage when all the surface moisture had been evaporated and the rate of moisture loss reduced since the moisture is diffused at a slower rate from the interior of the product first before being evaporated to the surrounding air. Although there was a greater loss in moisture for fish in the top trays as compared to other trays during the first 8 hours, at the end of the drying period, there was no significant difference in the moisture ratio of the fish in the solar dryer as confirmed by the statistical analysis, with the fish in the various trays attaining moisture contents of less than 10 %, a safe value for food products (Ghaba et al, 2007).

The drying of *R. argentea* fish thus occurred in a much shorter time and at lower temperatures than those reported by other studies on drying of fish in solar dryers (Oduor-Odote et al, 2010; Bala and Mondol 2006; Reza et al 2009; Basunia et al, 2011; Sengar et al, 2009). The shorter drying times could be attributed to the fact that smaller fish like *R. argentea* have a high surface area to volume ratio giving rise to higher drying rates even at lower temperatures (Mujaffar and Sankat, 2005).

4.3.6 Variation of the Drying Rates for *R. argentea* Fish

The graphs of the drying rates of *R. argentea* fish against moisture ratio of fish in the solar dryer and open sun have been presented in Figure 4.19 below,

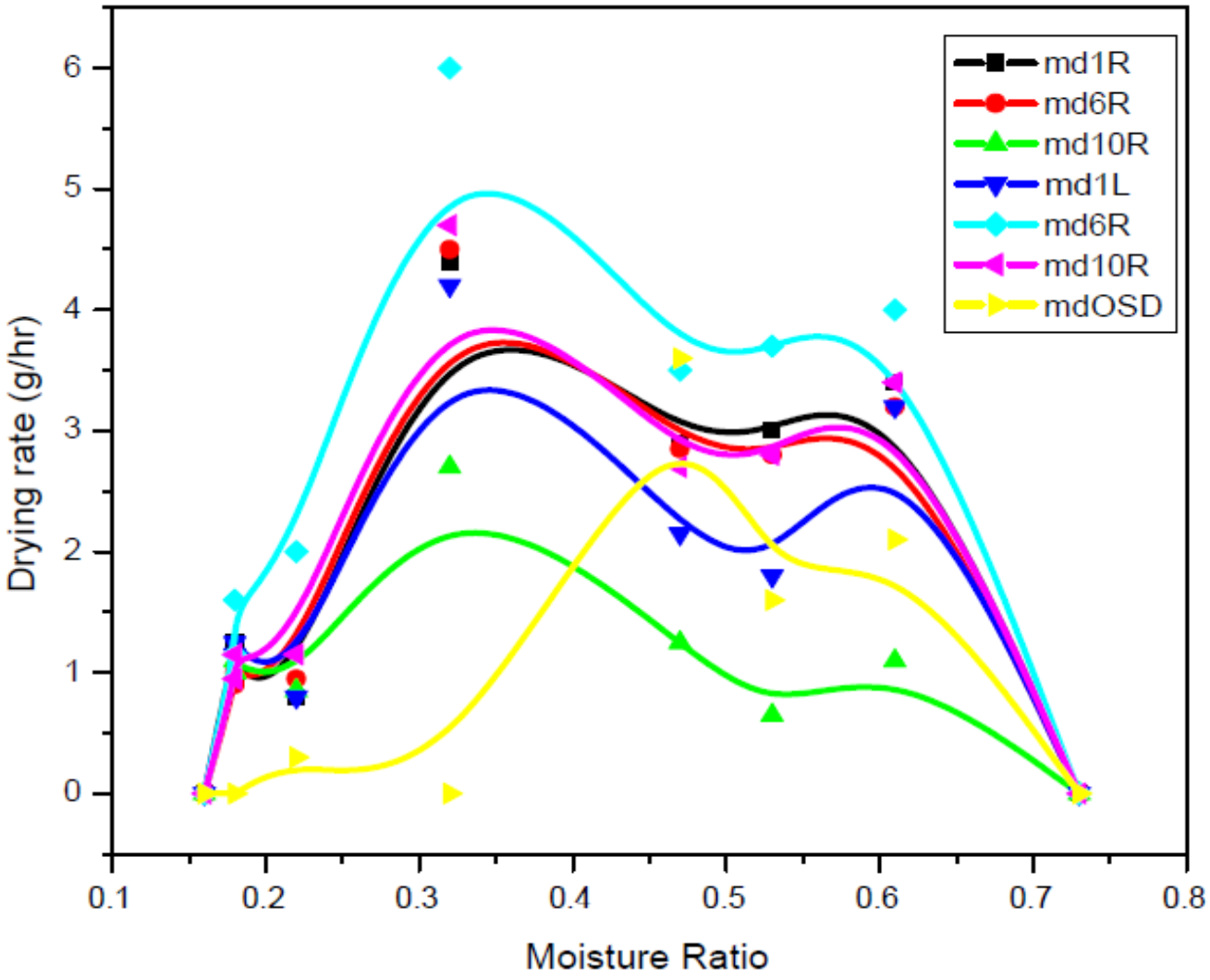

Figure 4.19: Variation of the mean drying rates with moisture ratio of the fish

The variation of the mean drying rate with the moisture ratio of the fish, Figure 4.19, show that the mean drying rates fluctuate with moisture ratio of the fish but are generally higher in the solar dryer than in the open sun. The maximum drying rates occur at about 0.30, the critical moisture content for the fish in the solar dryer as opposed to 0.47 in the case of open sun samples. As the equilibrium moisture content is approached the drying rates decrease. There are three sections in the graph; the left and right knees and a middle section, the right knee (between 0.60 and 0.73 moisture ratios) represents the warming period when the fish is slowly warmed by

the circulating air and water begins to evaporate and then reaches a steady state. This phase is governed by the rate of heat transfer from the surrounding to the fish. The middle section (between 0.30 and 0.60 moisture ratios) represents the constant rate drying in which heat transport to the body of material and evaporation of water from it takes place at steady state, as the temperature of surface of the material remains constant. In this phase there is no internal resistance to mass transfer and the larger cavities within the material are filled with liquid water. However when most of the easily accessible water has evaporated, to below the critical moisture ratio (approx., 0.30) the drying rate decreases hence the falling rate drying period represented by the left knee of the graph (Gullman, 2010).

Below the critical moisture content there is insufficient free moisture to maintain the maximum drying rate since the remaining moisture in the fish is held within its cell structure and more energy is required to break the bonds before evaporating (Ekechukwu, 1999). Therefore as the moisture content of the fish approaches the equilibrium moisture content (E.M.C), the remaining bound moisture cannot therefore move freely through the product to the surface and hence the decrease in the drying rates.

As observed the drying rates in the open sun begin to decrease at higher moisture ratio (approx.., 0.47), this early onset of the falling rate drying period is attributable to the relatively smaller area of the fish exposed to air flow as opposed to the solar dryer in which a larger surface area of the fish is exposed to air to flow leading to longer period of constant rate drying period. The observed fluctuations in the drying rate during the constant rate period (middle section) can be accounted for in terms of the turbulent patterns in the air flow that leads to changes in the rate of heat transfer between the air and the fish product, and changes in porosity and density due shrinkage effects in the fish during drying. This observation has also been made by previous

studies on drying of thick and relatively porous material such as fish, for example a study on the drying process of Sardine fish in a microwave oven (Darvishi et al, 2013). The drying rate being a function of air humidity, temperature, product surface area and convective heat transferred between air and the product per unit area, in the constant rate drying phase is represented by the middle section of the graph, during which the evaporating heat and airflow are the most influential factors. The fluctuations observed in the drying rates in the middle section of the graphs, where linearity is expected (constant rate drying period), are attributed to the non-uniform pattern of distribution in the air flow inside the solar dryer and the ambient, which causes variation in the rate of the convective heat transfer between the product and the hot air.

The decreasing drying rate observed at lower moisture ratios of the fish observed above, is associated with the falling rate drying period of food products in which water is being transferred from the muscle interior of the product to the surface by diffusion which is a function of product structure, temperature and diffusion path length, before being evaporated.

At lower moisture contents the product gets drier the evaporation zone of the moisture shifts to the interior of the material, it therefore takes longer to diffuse moisture to the surface before evaporating to the surrounding air and the heat required for this process has to be conducted through the drier surface and the pore regions both of which are poor thermal conductors. The heat flux from the hot air to sample is thus very low leading to a reduction in the drying rates during this phase.

Further the variations in the drying rates of the fish with time for the solar and open sun dried samples during the five series of experimental tests have been presented in Figures 4.20 - 4.24 below:

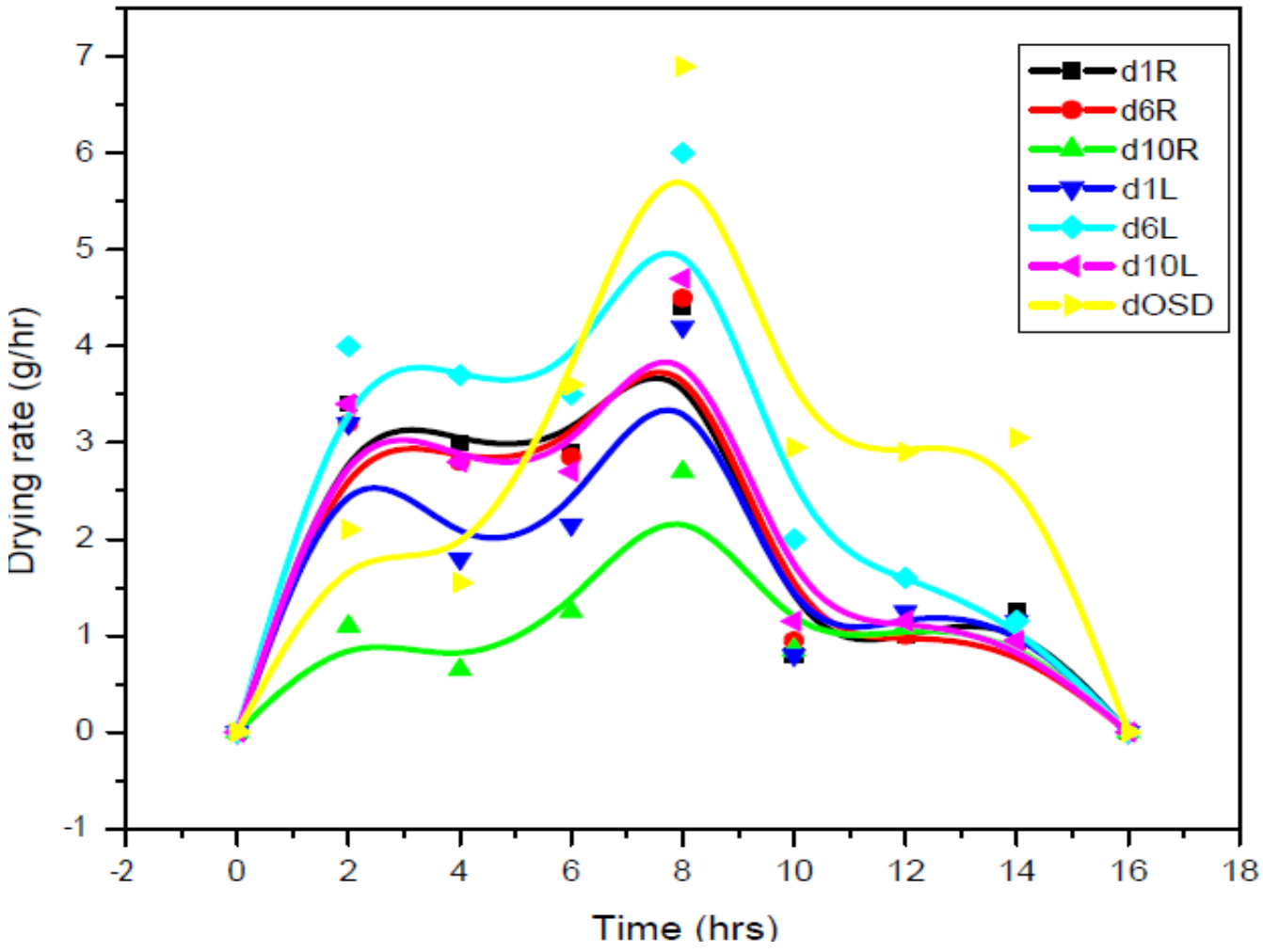

Figure 4.20: Variation of the mean drying rates with time for the top, middle and bottom trays for fish, WS-1

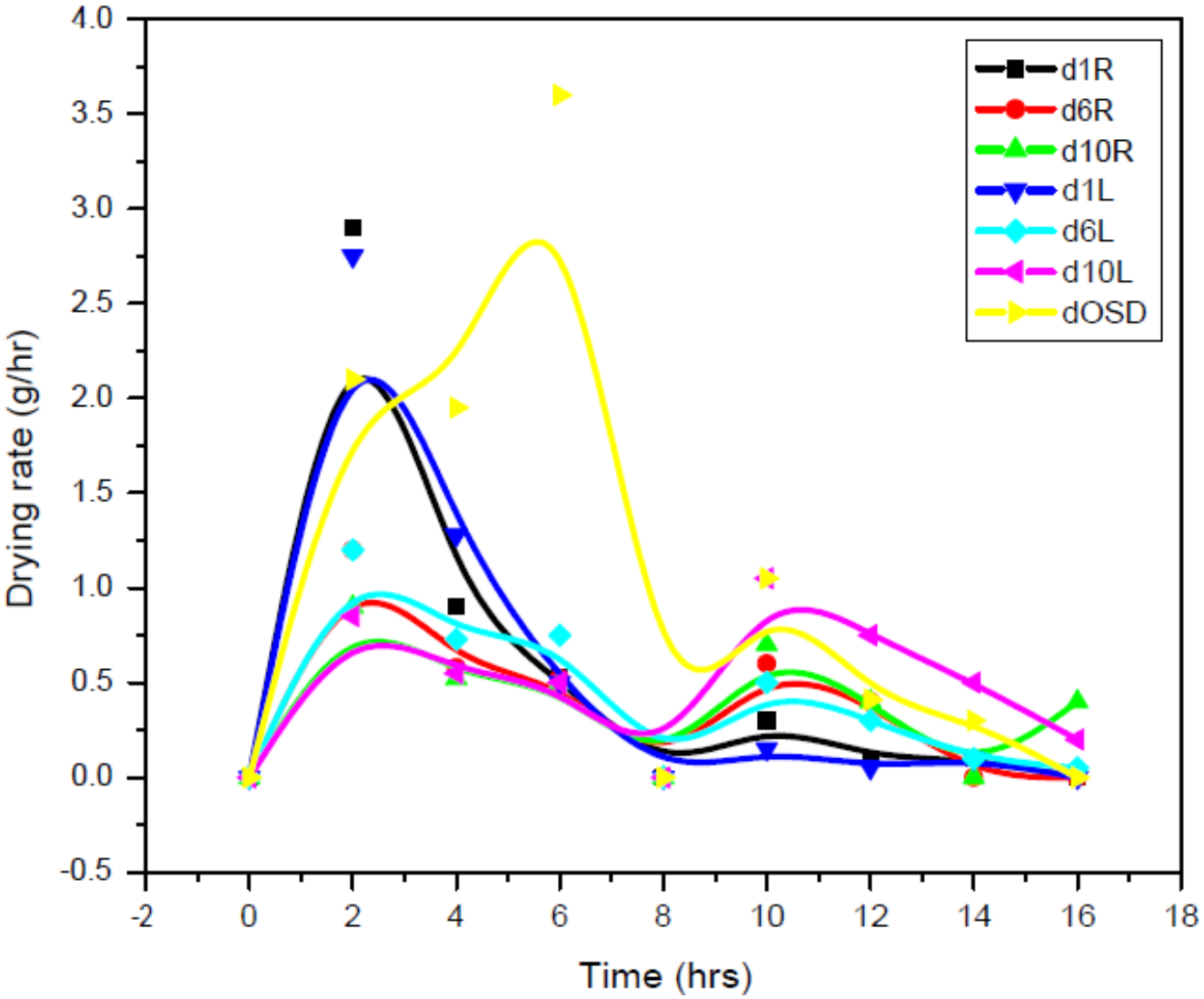

Figure 4.21: Variation of the mean drying rates with time for the top, bottom and middle trays for fish, WS-2

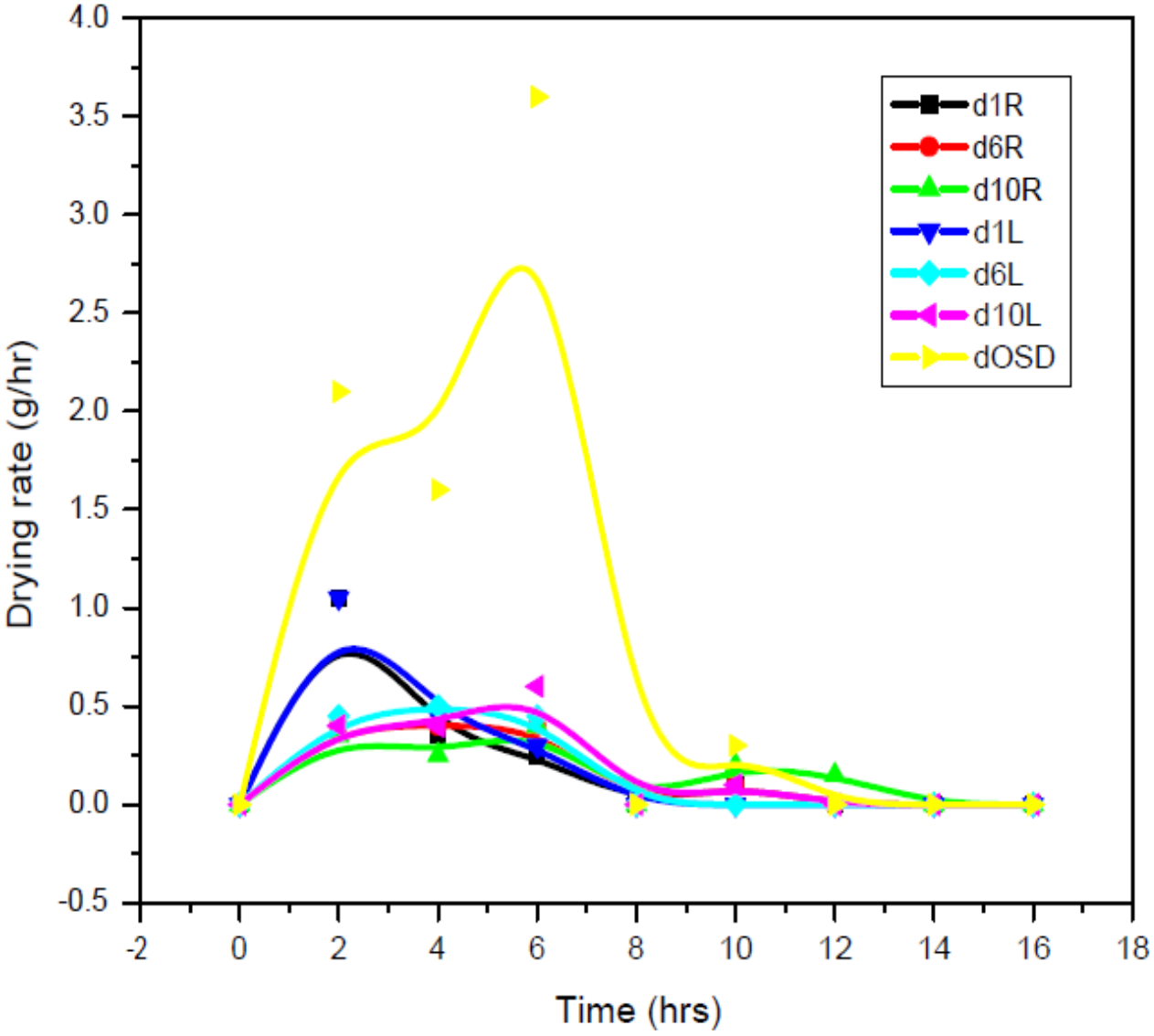

Figure 4.22: Variation of the mean drying rates with time for the top, middle and bottom trays for fish, WS-3

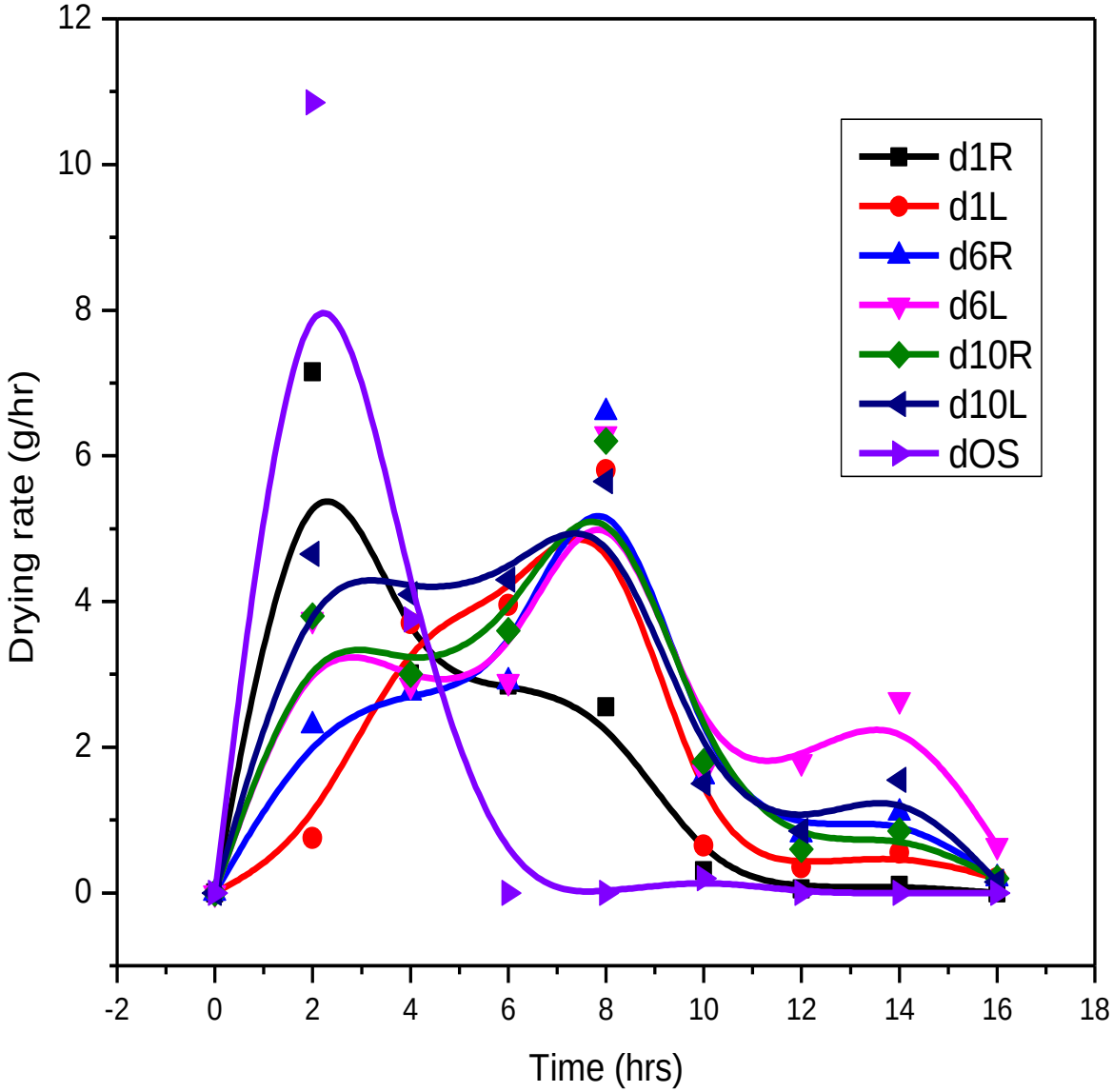

Figure 4.23: Variation of the mean drying rates with time for the top, middle and bottom trays for fish, DS-4

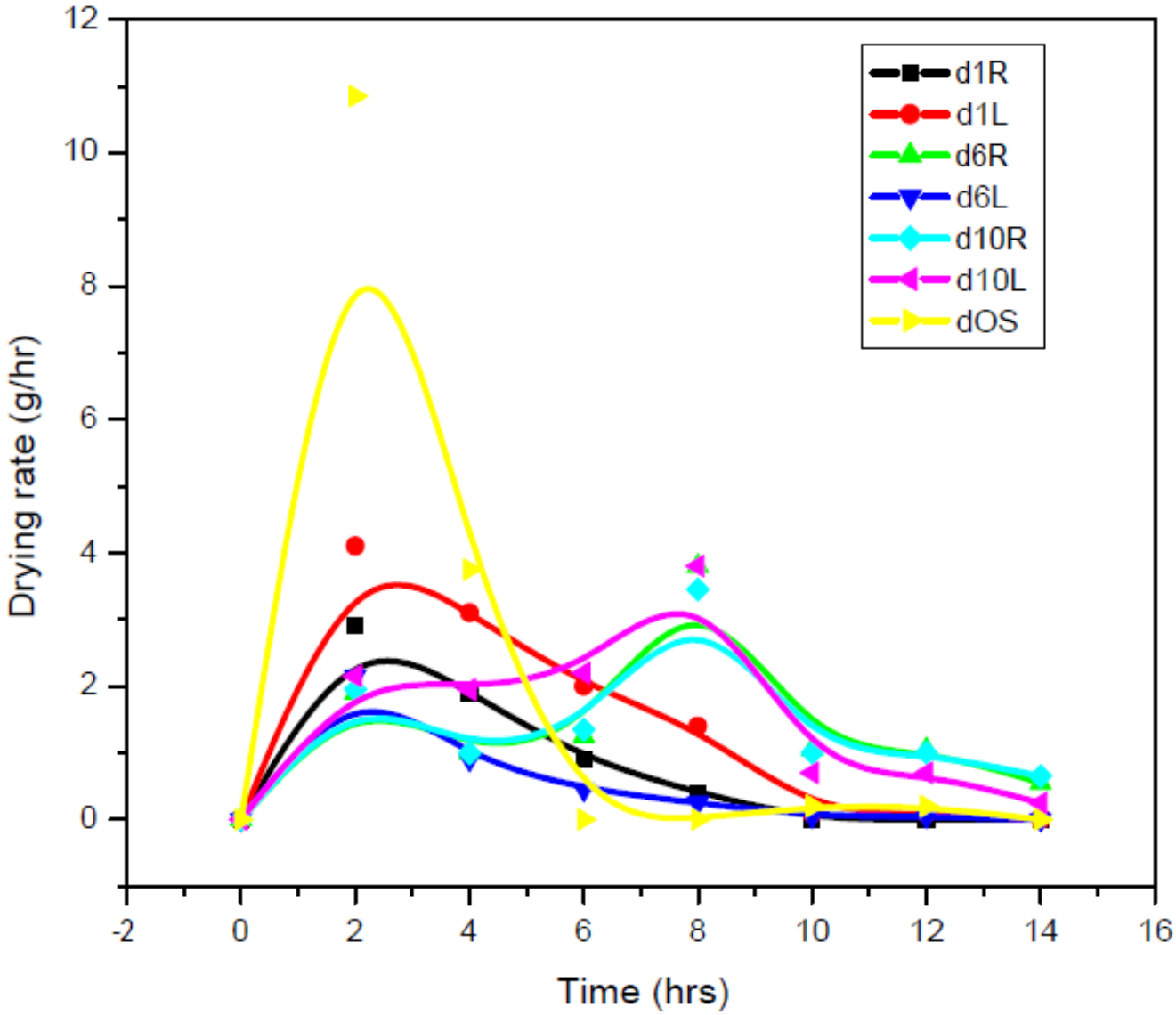

Figure 4.24: Variation of the mean drying rates with time for the top, middle and bottom trays for fish, DS-5

As can be observed in the figures presented above, the drying rates fluctuate with time, are higher at the beginning of drying but gradually approach zero towards the end of drying when the equilibrium moisture content (the lowest amount of moisture that can remain in the solid at the given conditions of the drying process), is reached (Xanthopoulos et al, 2007). It is observed that the highest drying rates are observed in the top trays as compared to the other trays during

the first four hours of drying. At the beginning of drying there is first an increase in the drying rates during the first two hours, followed by a fluctuating rate then finally a decrease towards the end of the drying, when equilibrium moisture content of the fish is finally attained.

The higher drying rates in the top tray of the solar dryer can be associated with the higher air flow rates in this location arising out of their proximity to the exhaust fan which has the effect of enhancing the drying process. The fluctuations in the drying rates of the fish can be attributed to variations in the rate of heat transfer between the hot air and the fish product caused by intermittencies in the air flow rates and temperatures; where the local values of the flow characteristics, air relative humidity and temperatures at different locations in the solar dryer are not homogenous due to the variable speed of the electric fan and in the case of open sun drying, the variations arise from changes in the wind speed and in ambient air temperature and humidities.

As observed the drying rates of the fish samples in the solar dryer and open sun are highest at the beginning of the drying at high moisture contents when the surface is highly saturated with moisture. The drying rate here depends on the rate of evaporation of moisture from the fish surface and is controlled largely by the external heat and mass transfer factors; temperature and air flow rate, and is therefore constant since all the energy received by the product is entirely used to evaporate the moisture. But when all the surface moisture has been evaporated, at later stages of the drying, the rate of transfer of the moisture from the interior of the fish to the surface decreases and hence the observed reduction in drying rates, which also agrees with results of other previous studies (Oduor-Odote et al, 2010).

From the plot of the mean drying rates against moisture ratio of the fish, Figure 4.23, it is observed that the drying rate is higher at larger moisture ratios and decreases at lower moisture

ratios which is in agreement with theoretical expectation since at lower moisture contents the moisture has to be diffused from the interior of the fish before being evaporated, a process which is much slower than the surface moisture evaporation that occurs at higher moisture contents or at beginning of drying. The drying rates at the later stages is much lower and depends on the rate of the diffusion of moisture from the interior of the product to the surface rather than the external parameters, since the evaporation zone moves inside the product (Alonge and Hammed, 2007). As observed in the study, the rate of diffusion decreased at lower moisture content values since it has to be diffused through a longer distance from the interior of the product to the surface before being evaporated to the surrounding, figure 4.23. The moisture thus migrates by both capillarity and diffusion at a constant but lower rate from the interior of product to the surface leading to a reduction in the drying rate.

At the final stages of drying, the surface of the material can be regarded as being effectively free of moisture with all the remaining being contained within the interior. This drying phase is therefore controlled by the temperature gradient from the interior to the surface, which in turn depends on the temperature of the surrounding air or radiation incident upon the surface. But since the rate of moisture removal is now less than in initial stages of drying, the degree of air movement across the surface is of less importance. The higher drying rates for open sun drying in the initial stages can be attributed to the fact that the air movement provided by the natural breezes around the spread fish on the ground is more effective than the air flow within the solar dryer, but where the higher temperatures within the solar dryer have less effect on the drying rates.

It is further observed that although the drying rates were similarly higher for open sun drying during the first phase (first 5 hours) of drying, they are lower in the next phase (next 6 hours) leading to relatively higher final moisture contents in the fish as compared to those of the solar dried samples.

The variation in the drying rates of the open sun dried and solar dried fish in the **right** and **left** hand side trays of the solar dryer have been presented in the Figures 4.25 and 4.26 below;

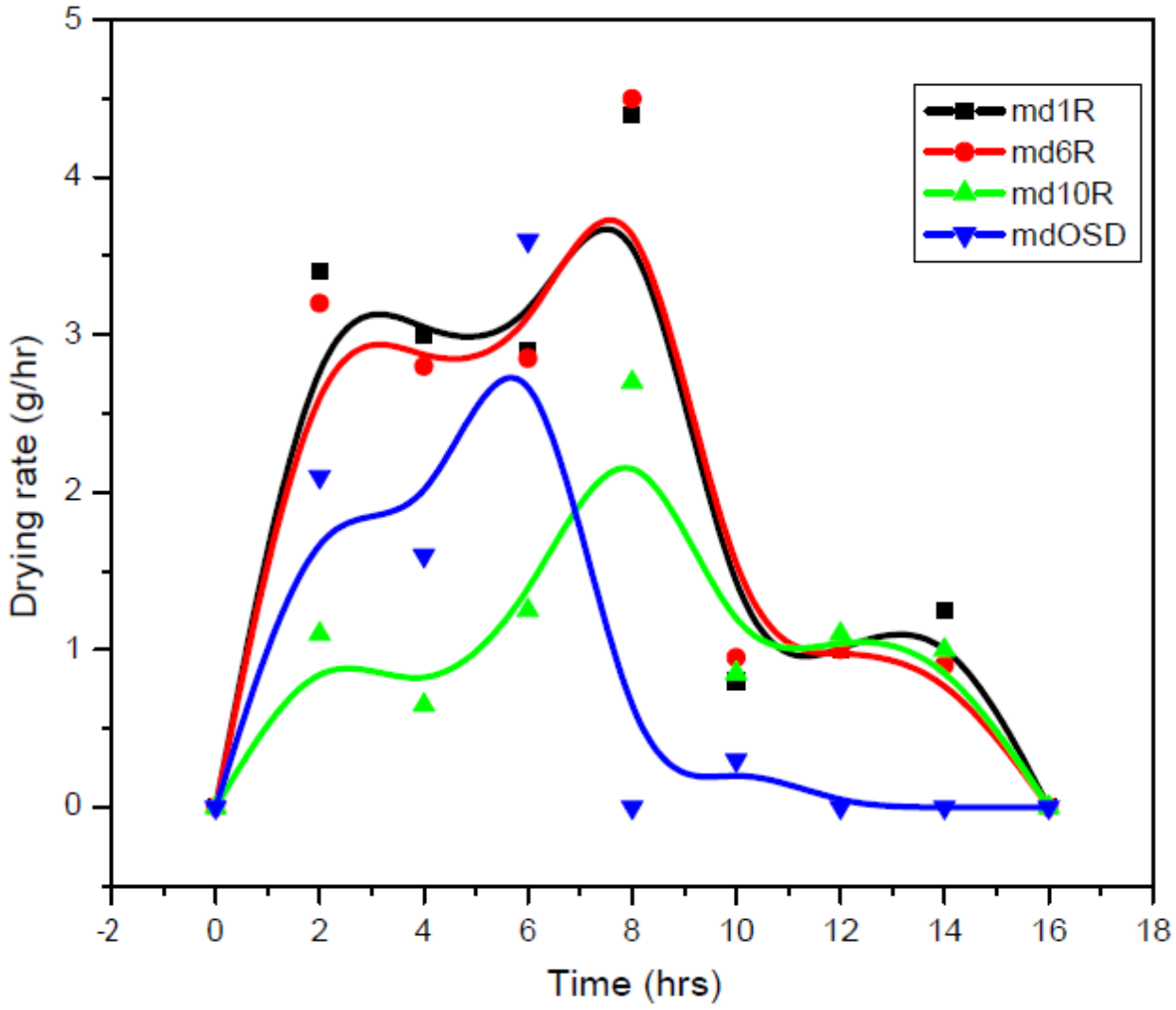

Figure 4.25: Variation of mean drying rates with time for the fish in the right bottom, middle and top trays

The comparative plots of the mean drying rates between the right trays in the solar dryer and open sun drying, Figure 4.25, shows that the top and middle trays are higher than open sun drying.

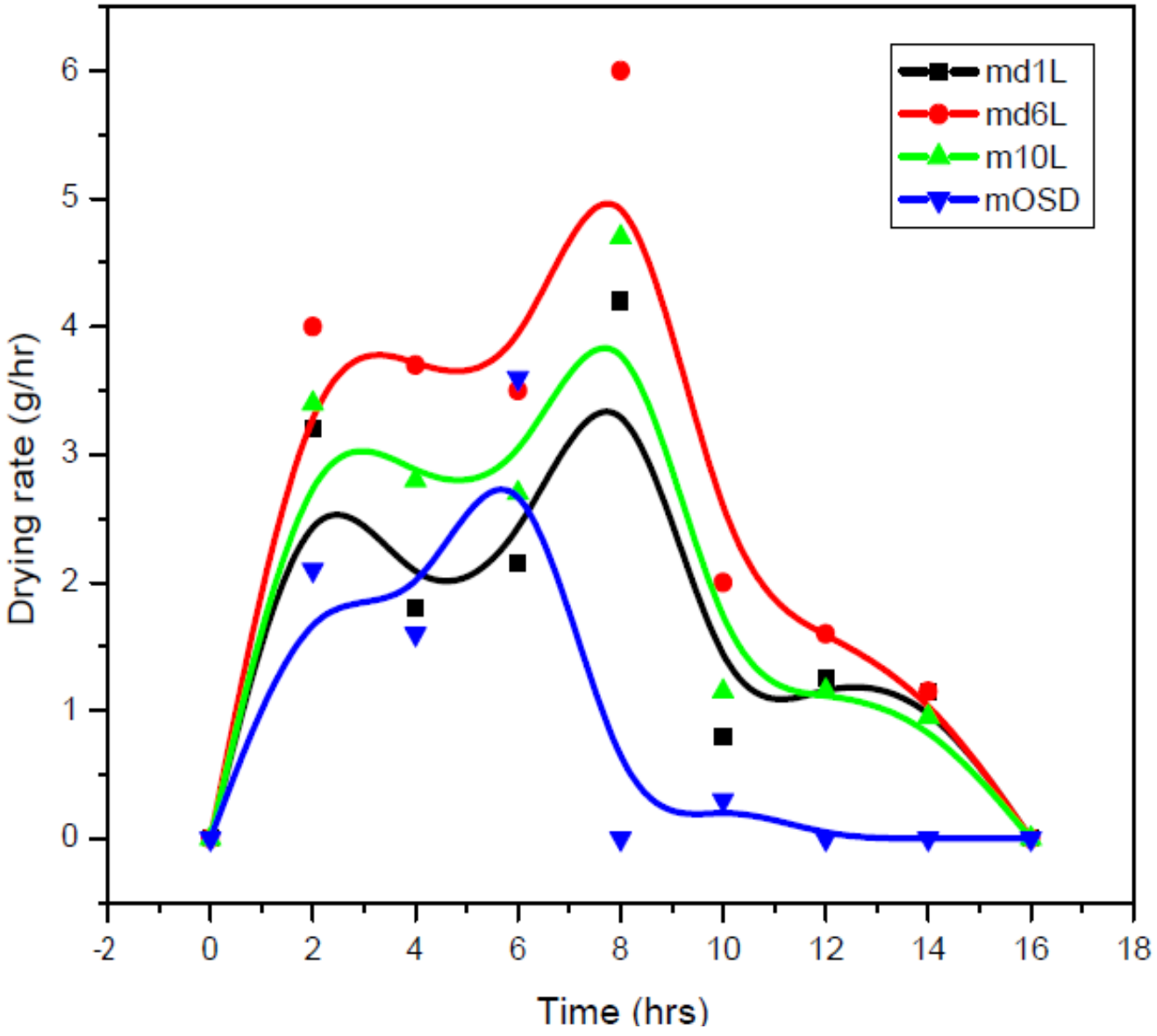

Figure 4.26: Variation of the mean drying rates of the fish in the left bottom, middle and top trays

A similar plot of the mean drying rates of the left trays in the solar dryer and open sun drying, Figure 4.26, shows the middle and bottom left trays are greater than for open sun drying. From these two plots it is observed that the mean drying rates of fish in most of the trays of the solar dryer are higher than for the open sun samples. It is also observed that the drying rates begin to decrease after 8 hours and 6 hours in the solar dryer and open sun respectively. This implies that the constant rate period lasts longer in the solar dryer than in the open sun, which can be attributed to the fact that the fish in the trays of the solar dryer has a larger surface area exposed to the air flow than the fish laid on the ground.

4.3.7 Drying Rate Constant (k) for the *R. argentea* Fish

The experimental drying rate constants for the open sun and solar dried fish samples were computed based on Equation 3.33, as the gradients of the graphs of $-|InMR|$ (natural logarithms of the moisture ratios of the fish) against time, for the five experimental test series, have been presented in the Figures 4.27 – 4.31 below:

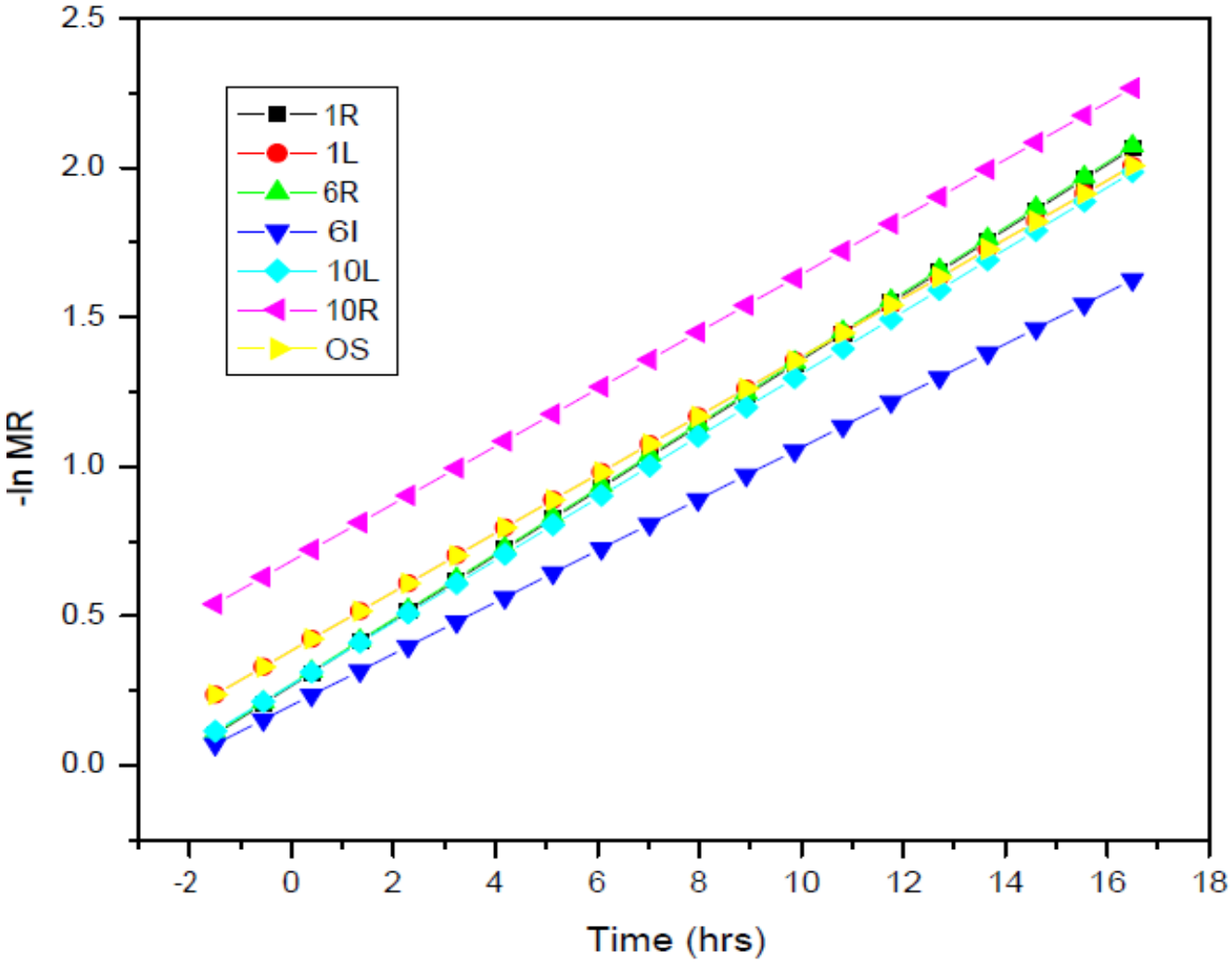

Figure 4.27: Variation of $-|InMR|$ against time for the open sun and solar dried fish, WS-1

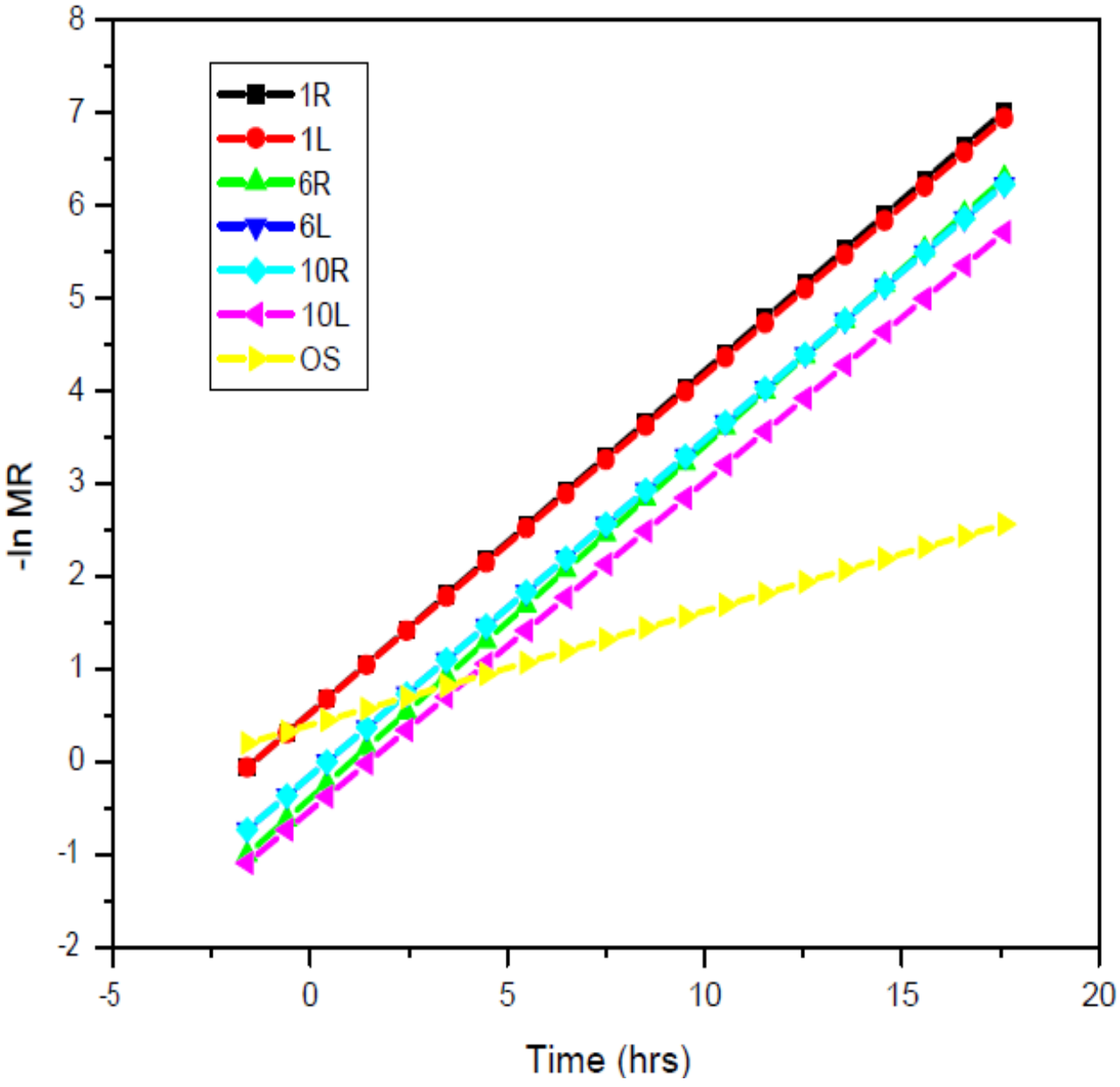

Figure 4.28: Variation of $-|InMR|$ against time for the open sun and solar dried fish, WS-2

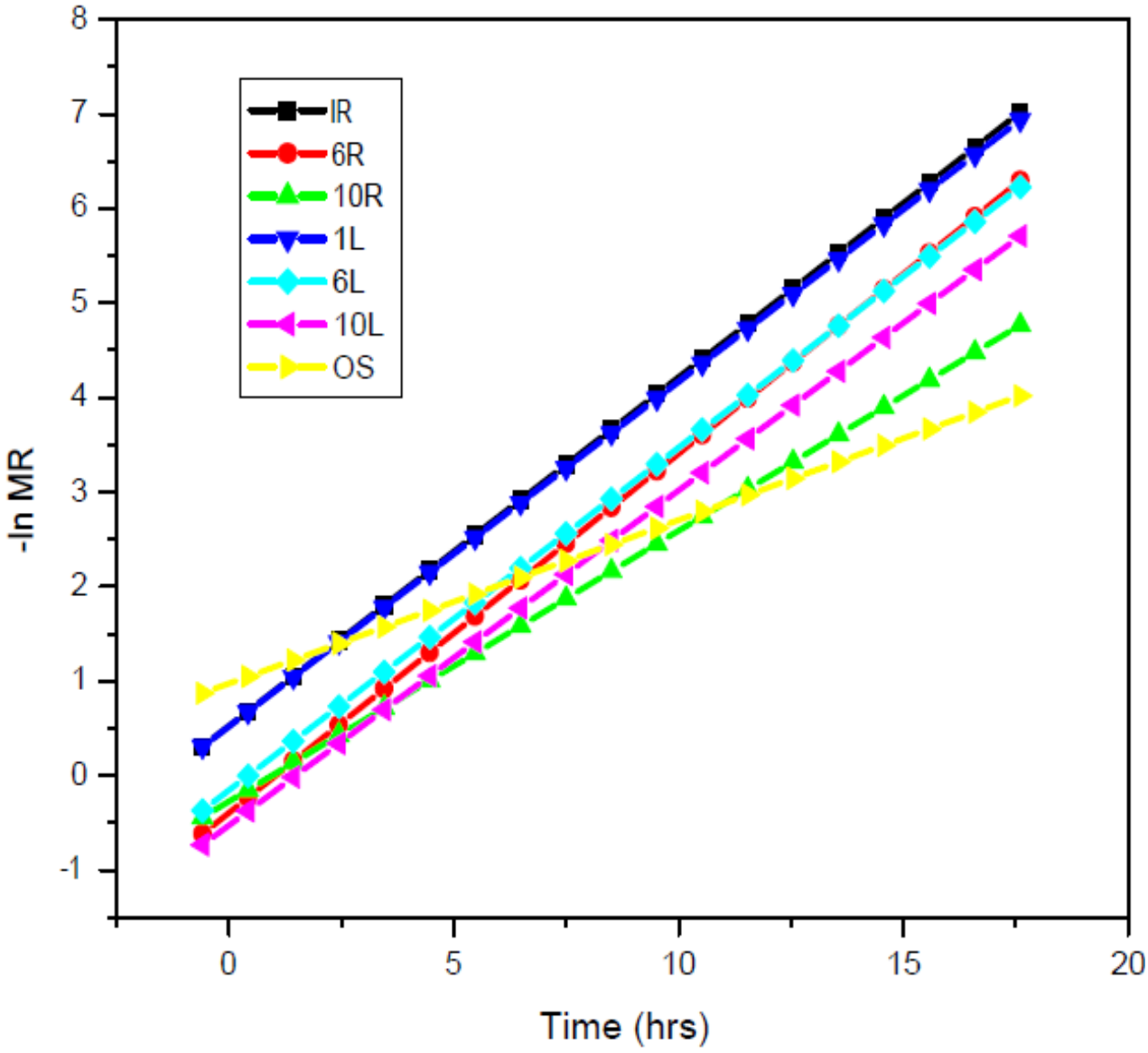

Figure 4.29: Variation of $-|InMR|$ against time for the open sun and solar dried fish, WS-3

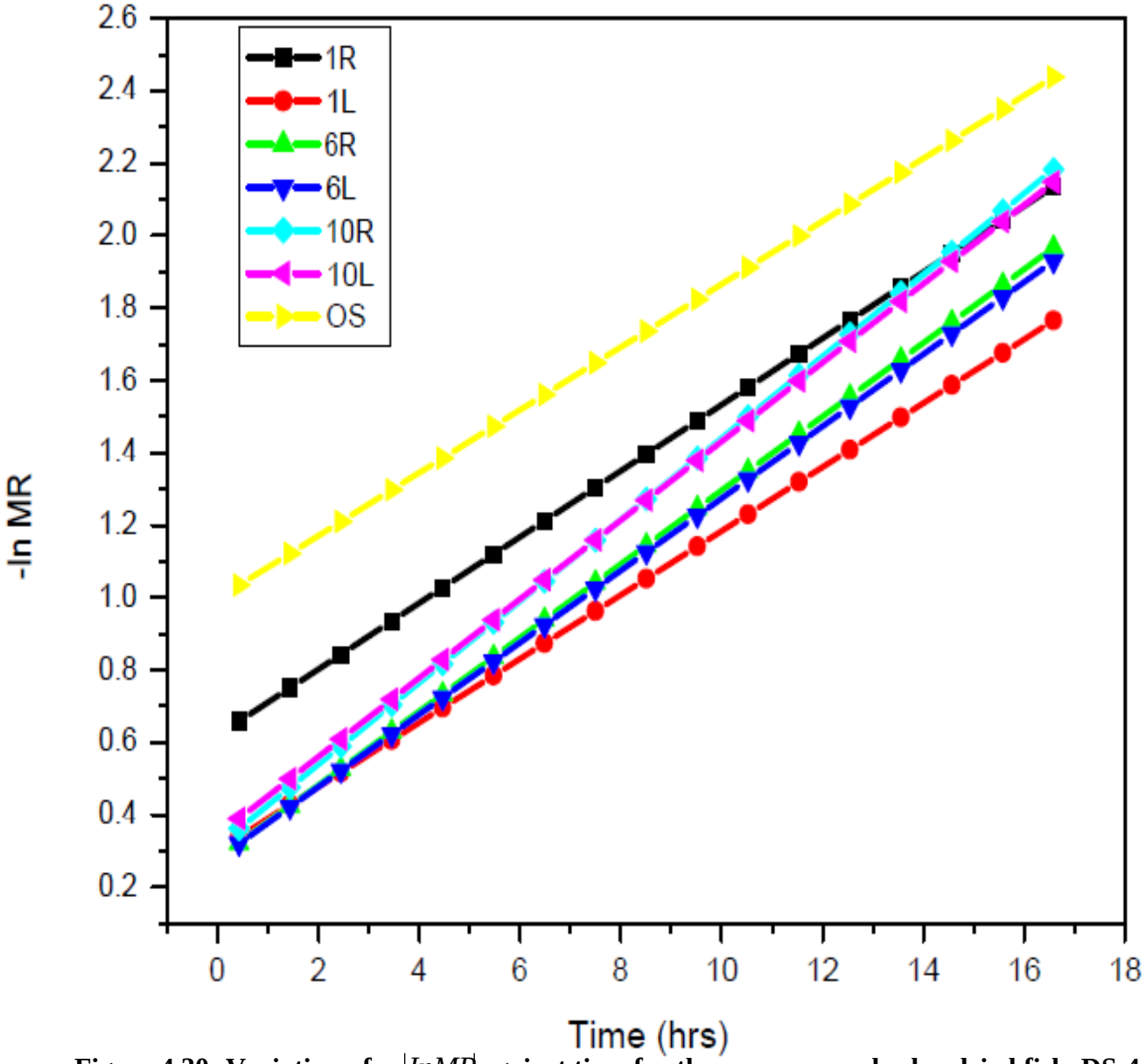

Figure 4.30: Variation of $-|InMR|$ against time for the open sun and solar dried fish, DS-4

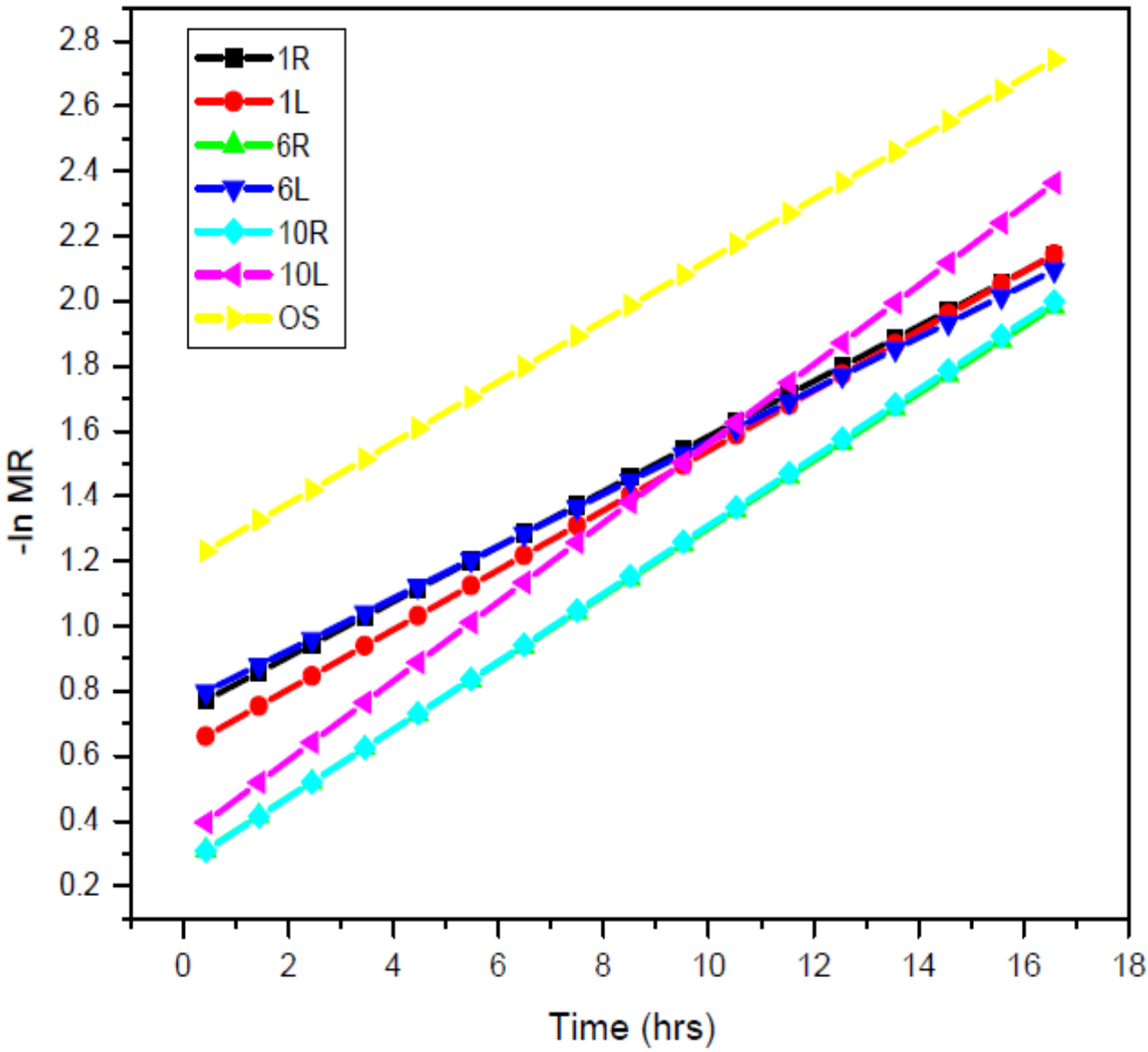

Figure 4.31: Variation of $-|InMR|$ against time for the open sun and solar dried fish, DS-5

The experimental drying rate constants computed from the graphs above for the fish samples in the various trays of the solar dryer and open sun have been summarized in in the table below:

Table 4.6: Experimental drying rate constants for fish samples in the various trays in the solar dryer and in the open sun.

Tray	*k* **(WS-1)**	*k* **(WS-2)**	*k* **(WS-3)**	*k* **(DS-4)**	*k* **(DS-5)**	*mean k*
1R (top right)	0.109	0.369	0.369	0.0913	0.0847	0.205
1L (top left)	0.0984	0.365	0.365	0.0882	0.0918	0.202
6R (middle right)	0.1092	0.380	0.380	0.102	0.1034	0.215
6L (middle left)	0.0864	0.365	0.362	0.0995	0.0802	0.199
10R (bottom right)	0.104	0.280	0.362	0.113	0.105	0.194
10L (bottom left)	0.096	0.365	0.354	0.109	0.122	0.209
OS (open sun)	0.0746	0.131	0.173	0.0868	0.0935	0.112

From the table, it is observed that the mean drying rate constants were obtained as follows: 0.203 $\pm$ 0.141 hr^{-1} for the top trays, 0.207 $\pm$ 0.142 for the middle trays 0.202 $\pm$ 0.123 hr^{-1} for the bottom trays and 0.112 $\pm$ 0.040 hr^{-1} for open sun drying. It is observed that the mean drying rate constants of fish in the solar dryer were higher than in open sun, suggesting that in general the fish was dried more rapidly in the solar dryer than in the open sun. Further a higher mean drying rate constant was obtained for the top trays of the solar dryer as compared to the middle and bottom trays. The experimental values obtained are closer to those predicted by the model at 0.022 kg/s air flow rate, but are lower than 0.220 $\pm$ 0.001 hr^{-1}, obtained by a previous study for the drying of *R. argentea* fish in a direct tunnel solar dryer (Oduor-Odote et al, 2010). This difference can be attributed to the difference in the modes of the solar dryers, where the although

the present study involved an indirect mode model, in the previous study a direct mode dryer was used, moreover it is known that direct mode dryers exhibit higher drying rates than indirect dryers due to the fact that heat energy is absorbed by the product from both the preheated air and the incident direct solar radiation.

4.3.8 Effective Moisture Diffusivities (D_{eff}) for the *R. argentea* Fish

The mean effective moisture diffusivities for the *R. argentea* fish samples were computed from the drying constants according to equation 2.4, for the various trays in the solar dryer and open sun samples and a summary of the results have been presented in the table below:

Table 4.7: Summary of the experimental effective moisture diffusivities for the open sun and solar dried fish *samples*

Tray	D_{eff} **(**WS-**1**) m^2 **/s**	D_{eff} **(**WS-**2)** m^2 **/s**	D_{eff} **(**WS-**3)** m^2 **/s**	D_{eff} **(**DS-**4)** m^2 **/s**	D_{eff} **(**DS-**5)** m^2 /s	mD_{eff} m^2 /s
1R	8.84×10^{-4}	2.99×10^{-3}	2.99×10^{-3}	7.40×10^{-4}	6.87×10^{-4}	1.66×10^{-3}
1L	7.98×10^{-4}	2.96×10^{-3}	2.96×10^{-3}	7.15×10^{-4}	7.44×10^{-4}	1.64×10^{-3}
6R	7.01×10^{-4}	3.08×10^{-3}	3.08×10^{-3}	8.27×10^{-4}	8.38×10^{-4}	1.74×10^{-3}
6L	8.86×10^{-4}	2.94×10^{-3}	2.96×10^{-3}	8.07×10^{-4}	6.50×10^{-4}	1.61×10^{-3}
10R	7.79×10^{-4}	2.94×10^{-3}	2.32×10^{-3}	9.16×10^{-4}	8.51×10^{-4}	1.57×10^{-3}
10L	8.43×10^{-4}	2.87×10^{-3}	2.96×10^{-3}	8.84×10^{-4}	9.89×10^{-4}	1.69×10^{-3}
OS	6.05×10^{-4}	1.06×10^{-3}	1.40×10^{-3}	7.04×10^{-4}	7.58×10^{-4}	9.08×10^{-4}

From the table, it is observed, that the mean effective moisture diffusivities of the fish in the top, middle, bottom trays were: $1.65\times10^{-3}m^2/s$, $1.68\times10^{-3}m^2/s$ and $1.63\times10^{-3}m^2/s$ respectively while that for open sun samples were $9.08\times10^{-4}m^2/s$.

The value of mean effective moisture diffusivity for all the trays in the solar dryer were observed to be slightly higher than that for open sun drying, this observation can be attributed to the higher temperatures, lower relative humidity and increased flow rates of air in the solar dryer, that makes the rate of moisture diffusion from the fish in the solar dryer to be higher than in the open sun samples. No significant difference was observed in the values of effective moisture diffusivities in the solar dryer, an observation which suggests that there is uniform drying in the various trays of the solar dryer. The observed values of effective moisture diffusivity for *R. argentea* fish in this study were much higher than those observed for other food / agricultural products (Hadrich and Kechaou, 2004).

This difference is attributable to the characteristic nature of *R. argentea* fish; namely its small dimensions (0.02 m by 0.002 m) with a larger proportion of unbound surface moisture, so that it has a prolonged duration of constant rate drying by surface evaporation as compared to diffusion of moisture from the interior muscle structure which occurs during the falling rate period. Moreover because of the small diameter, the diffusion path length of the product is much shorter than for other food products. The large values of moisture diffusivities for the fish observed contributed to the relatively shorter overall drying times obtained in the present study.

4.3.9 Activation Energy

The variation of the natural logarithm of effective moisture diffusivity (InD_{eff}) against the reciprocal of the absolute temperature of the drying air ($\frac{1}{T}$) have been presented in Figure 4.32 below:

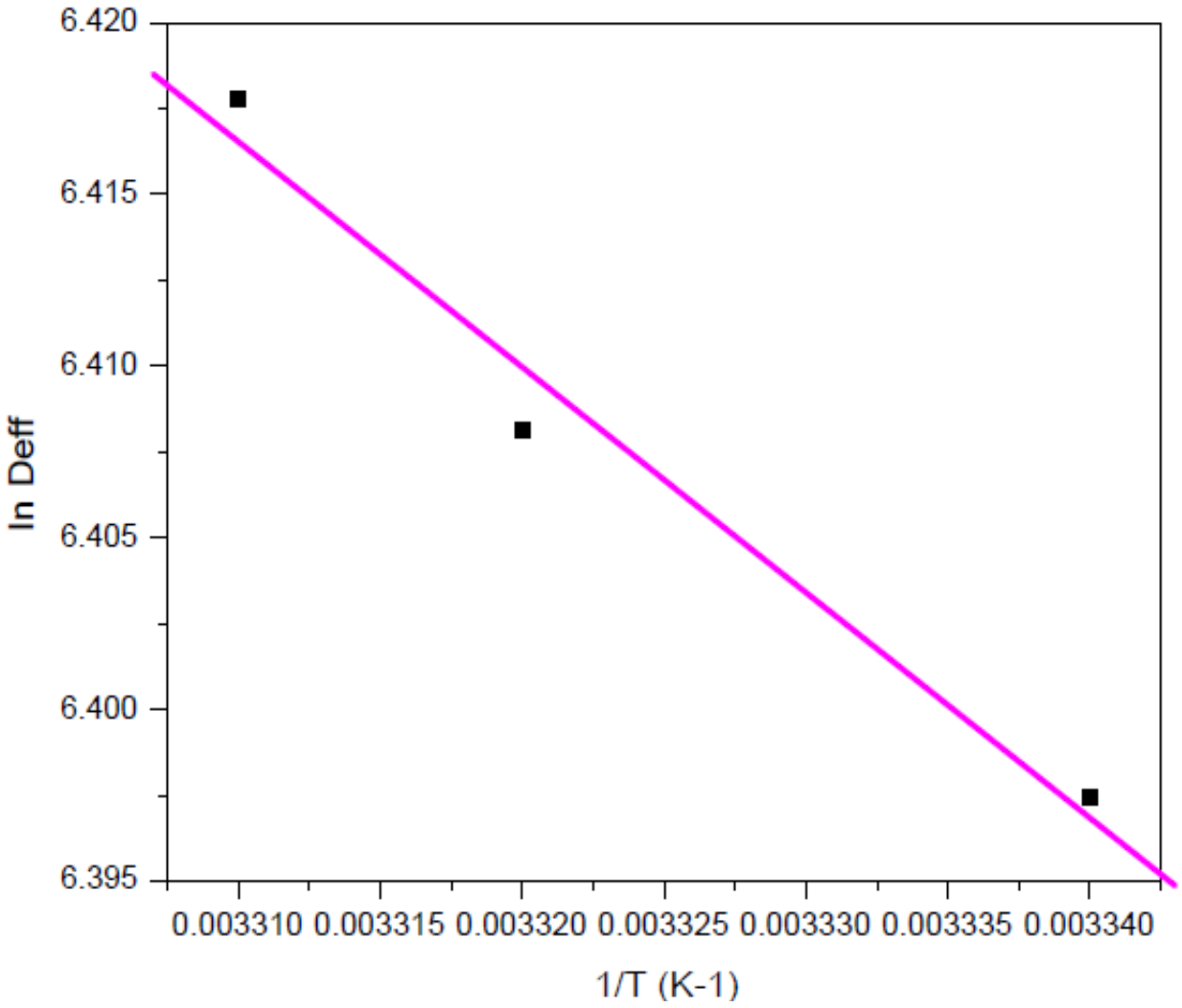

Figure 4.32: Variation of $-\left|InD_{eff}\right|$ against $\frac{1}{T}$

From the figure, it was observed that there is an inverse linear relationship between $-\left|InD_{eff}\right|$ and $1/T$, this phenomena has also been observed by other previous researchers (Karim and Hawlader, 2005).

Based on equation 3.35, the slope representing E_a/R was computed as – 656.64 and from which the value of the activation energy (E_a) for the drying process of *R. argentea* fish was thus derived as -15.954 kJ /mol., similarly the pre-exponential factor in the Arrhenius equation 3.35, represented by the y -intercept of the graph, InD_o was found to be 6.418 and from which the value $D_o = 1.632 \times 10^{-3} m^2/s$ was derived.

The activation energy which represents the minimum energy required to initiate the drying process of *R. argentea* fish obtained in the present study, though comparable to those obtained by past studies for the drying of other food products; - 14.138 kJ/ mol for Sardine fish (Darvishi et al, 2013). But this value of E_a for *R. argentea* fish, was observed to be less than the range of between - 25.26 and - 46.46 k J/ mol reported for water Yams (Falade et al, 2007). The relatively lower value of activation energy for *R. argentea* fish implies that a smaller amount of energy in comparison with other food product is required to initiate its drying process. Thus the activation energy required for drying this fish product can be adequately supplied by the available solar energy.

4.4 Comparison of Model and Experimental Results

4.4.1 The Model versus Experimental Moisture Ratios for the *R. argentea* Fish

The comparison between the mean moisture ratios of *R. argentea* fish as predicted by the model and the experimental tests on the solar dryer and open sun have been presented in Figure 4.33 below:

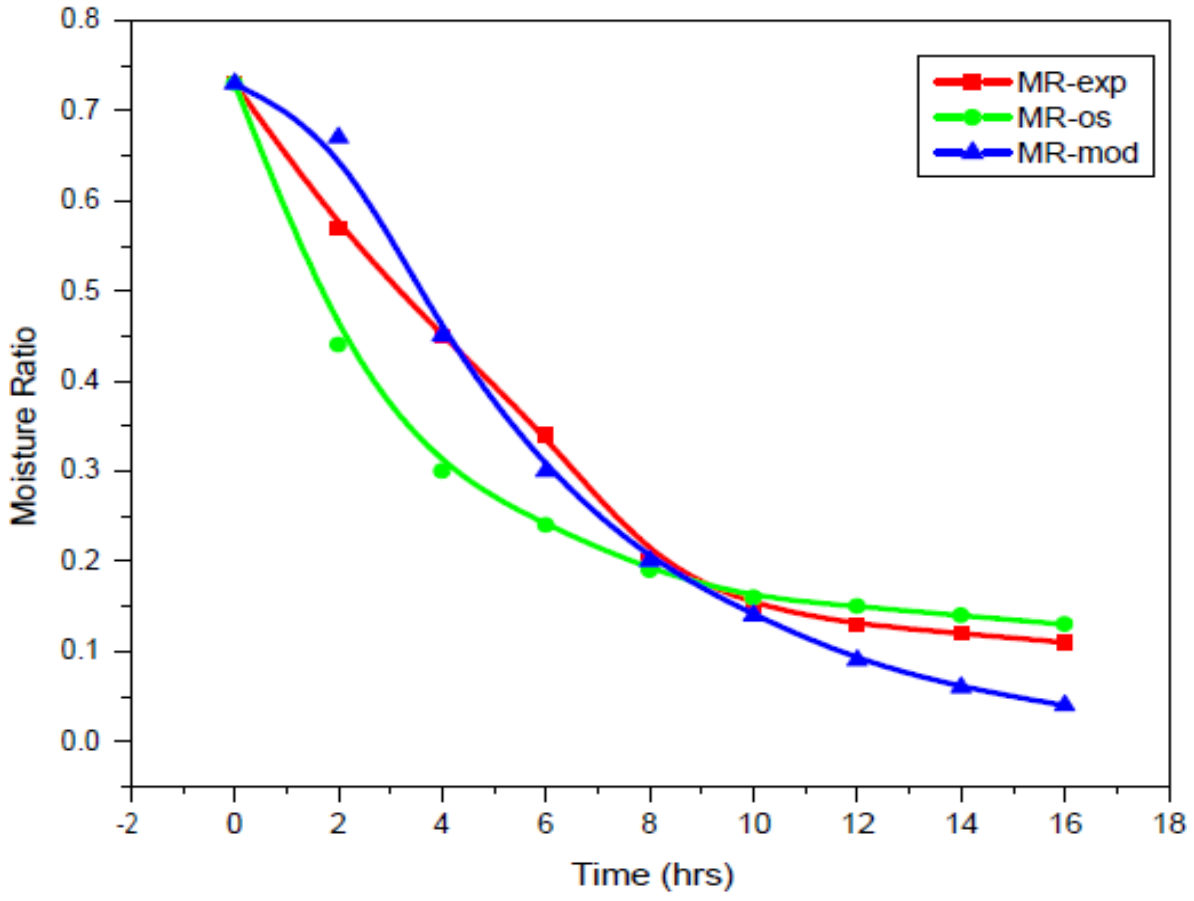

Figure 4.33: Variation of moisture ratio of the model, experimental and open sun fish samples

The figure indicates that there is an initial linear part of the drying curves for the model, solar dried and open sun samples, where in the case of the model and solar dried fish samples it occurs during the first 5 hours while for open sun drying the linearity occurs 2 hours after the start of the drying process. Both the model and solar drying tests reveal that the fish reaches the critical

moisture ratio of 0.30 after about 6 hours. A better correlation was observed between the moisture ratios of the model and solar dried samples as compared to open sun dried fish samples. Further although the open sun samples had a greater moisture loss during the initial hours of drying than the model and solar dried samples, the model and solar dried samples attained lower final moisture content than the open sun samples at the end of drying.

The final moisture ratios of between 8 % and 10 % for the fish in the solar dryer in a time of 11 hours obtained in this study was much lower than between 12.0 % and 12.7 %, in a longer drying time of 14 hours, the values obtained by a previous study on drying of the fish product in a direct solar tunnel dryer (Oduor-Odote et al, 2010). Given that the present dryer was operated in the indirect rather than direct mode it can be postulated that were the present dryer to be operated in direct mode, lower final moisture ratios of fish could be achieved in a much shorter time than observed in the study.

The results of statistical analysis based on moisture ratios for the model and experiments for various trays of the solar dryer, have been presented in the table below:

Table 4.8: The model fitting parameters based on moisture ratio of *R. argentea* fish

Moisture Ratio	**mean** χ^2	**mean** R^2	**mean** $RMSE$
Top trays	0.0028	0.946	0.0383
Middle trays	0.0021	0.752	0.0460
Bottom trays	0.0015	0.839	0.0533

As can be observed from Table 4.8, comparatively a higher coefficient of determination (R^2 = 0.946) was obtained for the fish in the top tray of the solar dryer, indicating a strong correlation between simulated and experimental moisture ratios especially for fish in the top tray of the solar dryer. The least value of root mean square error (*RMSE*) was also obtained for the fish in top tray followed by the middle tray and bottom trays, indicating a higher prediction accuracy of the model especially for the moisture ratio of fish in the top tray. Additionally, the results of the "Student *t* " and one way Anova tests at 0.01 % and 0.05 % levels of significance, (Table A3, Appendix), also indicated that there were no significant differences between the simulated and experimental moisture ratios of the fish in most of the trays in the solar dryer. Thus the model was found to be capable of accurately predicting the moisture ratio of *R. argentea* fish in the solar dryer.

4.4.2 Drying Factor versus Effective Moisture Diffusivity

The drying factor $D_f\,(m^3/s/K)$ in the developed model is analogous to the effective moisture diffusivity coefficient $D_{eff}\,(m^2/s)$ in the diffusion model, both of their magnitudes were of the order; 10^{-3}. Whereas in the diffusion model the drying rate depends on the rate of moisture diffused per unit surface area of the material, in the present evaporation model, it depends on the rate of volume flow of air per unit time and temperature, hence the SI units of the two coefficients are not the same. It is also observed that although D_{eff} in the diffusion model cannot be predicted theoretically, as it depends on the geometry and internal structural properties of the material, D_f was easily computed from Equation 3.9 in which the only variable was the air mass flow rate.

4.4.3 Model and Experimental Drying Rate Constants

It is observed that in the diffusion model, the drying rate constants are derived from experimental moisture curves by plotting graphs of - In *MR* against time according to Equation 4.3, where the drying rate constants are obtained as the gradients of the linear graphs. In contrast, for the present evaporation model the drying rate constants were derived from the relation Equation 3.13, and it was possible to predict the drying rate constants given that all the quantities stated in the equation were known, unlike the case for diffusion models which requires knowledge of the effective moisture diffusivity of the product, which is determinable by experiment.

4.4.4 Model versus Experimental Drying Rates for the *R. argentea* Fish

The comparison between the model predicted and experimental drying rates have been presented in Figure 4.34 below:

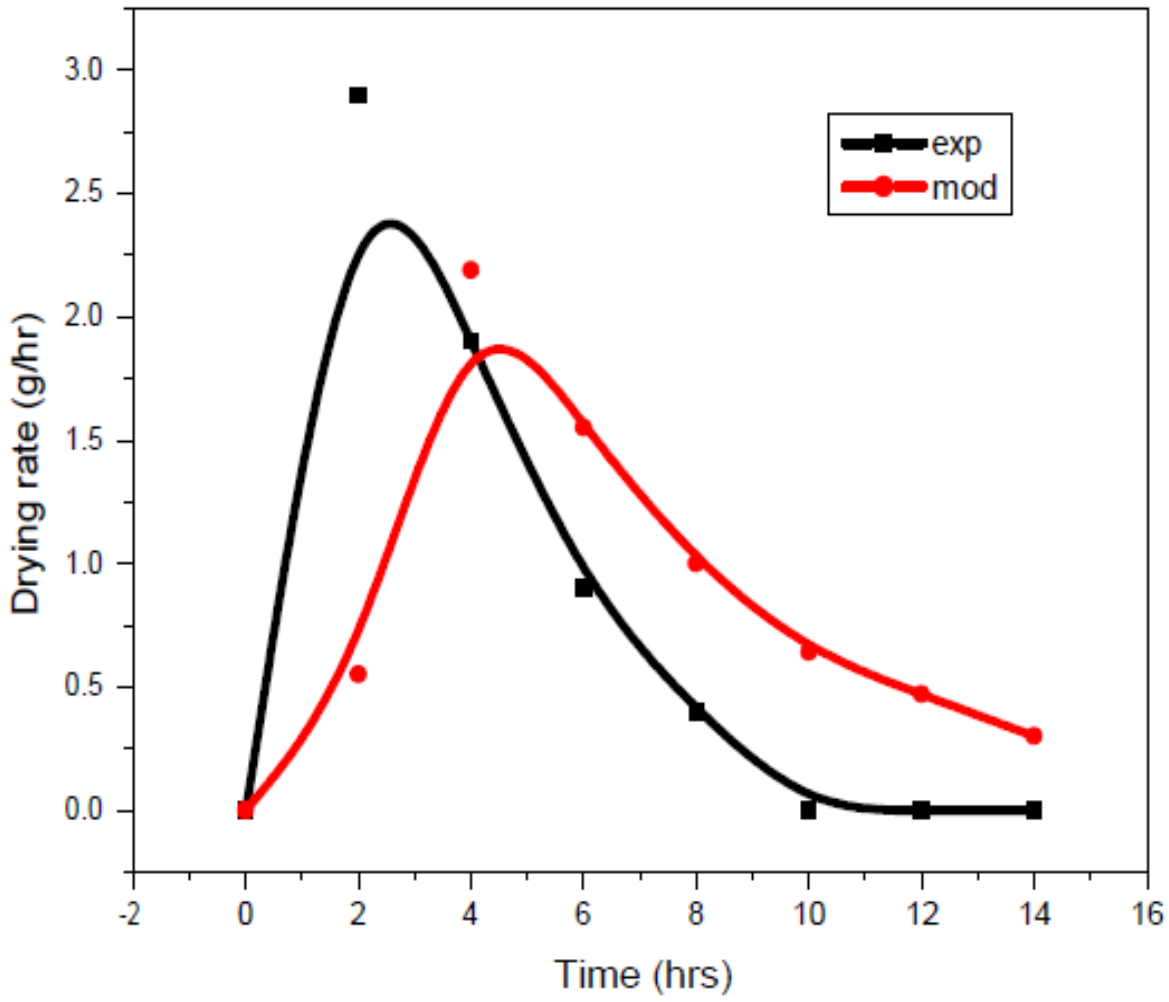

Figure 4.34: Variation of model and experimental drying rates with drying time

It was observed that both the experimental and model predicted drying rates indicated a fluctuating trend with increase in drying time. Although the experimental values were initially higher than those of the model, both had an initial increase at the beginning of drying followed by a decrease and then an almost constant value tending towards zero towards the end of drying. Despite the apparent differences observed in the experimental and model predicted drying rates of the fish, statistical analysis conducted on the model and experimental drying rates, using t-test and one-way Anova at 0.05 % levels of significance, gave the results: $t = 0.1652$; $p = 0.1652$

and $F = 0.0273;\ P = 0.8712$ respectively indicating no significant difference between drying rates of the fish samples in the model and experimental tests. Further, although from the Figures 4.21- 4.27, there are apparent differences in the drying rates of the various trays in the solar dryer for the experimental results, statistical analysis based on χ^2 and one- way Anova tests, conducted at 1 % significance level, revealed chi-square values of $\chi^2 = 0.155$ between the drying rates of top and middle trays, $\chi^2 = 0.606$ between the drying rates of the top and bottom trays and $\chi^2 = 0.135$ between the bottom and middle trays, the fact that all the values of χ^2 between the drying rates of the various trays were less than the limit ($\pm$ 2.33), suggests that there were no significant differences in the drying rates for the different trays in the solar dryer.

The lack of significant differences in the drying rates of the fish in various trays of the solar dryer suggests an almost uniform pattern of distribution of air flow in the solar dryer chamber resulting which resulted in the uniform drying of fish, which is a salient design feature of the present model.

4.4.5 Ambient versus Solar Dryer Chamber Conditions

Further the statistical analysis for the ambient versus drying chamber conditions based on χ^2 test carried out on the measured chamber and ambient parameters, tested at 1 % significance levels, gave $\chi^2 = 1.770$; for the differences between the relative humidity of air in chamber and the ambient, and $\chi^2 = 3.901$; for the difference between ambient and bottom chamber temperatures.

The fact that the value of χ^2 obtained for temperature exceeded the limit, $\pm$ 2.33, indicates that there was a significant difference between the ambient and chamber air temperatures. However

the value of χ^2 obtained for the relative humidity of air was slightly less than the limit, which suggests that the difference between the mean values of the chamber and ambient air relative humidity was not very significant at 1 % significance level.

CHAPTER FIVE: CONCLUSIONS AND RECOMMENDATIONS

5.1 Conclusions

1. The drying model in the study was formulated based on external rather than internal heat and mass transfer factors within the product. Further is was observed that although temperature and air mass flow rates were varied the results revealed that air mass flow rather than temperature was the major parameter which influenced the drying time of R. *argentea* fish. This observation was found to be consistent with findings of other studies conducted on other evaporation models. Further the model results also revealed that when the air mass flow rate was increased to 0.06 kg/s, the drying time of the product was reduced by up to 7 hours with the moisture ratio of the fish being reduced to safe levels of 15 % (w. b.) within a period of about 2.5 hours.

   The model was further used to predict the moisture ratio and drying rates of *R. argentea* fish, where it was found that both the simulated and measured moisture ratios of the fish exhibited a trend of exponential reduction with the drying time, an observation which agrees with those of a previous study (Afolabi, 2014). Additionally, regression analysis showed a strong linear correlation between the simulated and the mean experimental moisture ratio with the model fitting paramaters: $R^2 = 0.995$, $\chi^2 = 0.057$ and $RMSE = 0.6196$). The results of Student- *t* and one-way Anova tests also indicated that there was no significant difference between the simulated and experimental moisture ratios of the fish at 0.05 % and 0.01 % confidence levels, Table A3 (Appendices).

2. The experimental tests revealed a much shorter drying time for the product at much lower temperatures than for a previous study (Oduor- Odote et al, 2010) but at higher air mass flow rates.

   The collector system had a mean thermal efficiency of 12.3 $\pm$ 3.53 % while the overall drying efficiency of the system was found to be 9.93 ± 3.45 %, at average mass air flow rate of 0.0190 ± 0.0048 kg/s for an average incident solar radiation intensity of 571.2 $\pm$ 223.5 W/m^2. Solar energy was used in drying *R. argentea* fish in the prototype indirect forced convection solar cabinet dryer consisting of two solar collectors with a total glazing area of 5.0 m^2. The drying was carried out between 09:00 hrs and 16:00 hrs on each day at mean ambient and drying chamber temperatures of 28.7 $\pm$ 3.23 ^{o}C and 32.0 $\pm$ 9.71 ^{o}C respectively, while the relative humidity of air in the drying chamber was reduced by an average value of 23.4 % below the ambient value on the days of drying. With full load tests conducted with 10 kg batches of *R. argentea* fish, the results revealed that the moisture content of fish in the solar dryer was reduced from an initial value of 73 % w. b. to between 8 % and 10 % (w. b.) in about 11 hrs where open sun drying took 18 hours to attain the same moisture contents. The solar dried fish were also found to have a better appearance as compared to the sun dried samples.

   The mean drying rate constants for *R. argentea* fish was found to be: 0.204 $\pm$ 0.135 hr^{-1} in the solar dryer and 0.112 $\pm$ 0.040 hr^{-1} in the open sun, which indicated higher drying rates in the solar dryer as compared to open sun. The mean effective moisture diffusivities of the fish in the in the solar dryer was: $1.65 \pm 0.02 \times 10^{-3} m^2/s$, while that for open sun was: $0.908 \pm 0.052 \times 10^{-3} m^2/s$ which also indicated that the moisture diffusivity rate in the fish was higher in the solar dryer than in the open sun. The mean activation energy for the drying

process of *R. argentea* fish was obtained as; - 15.953 k J/ mol, which was within the expected range of - 12 kJ/ mol and - 110 kJ/ mol for agricultural and food products (Falade et al, 2007).

Although the drying rates and effective moisture diffusivities obtained for *R. argentea* fish in the study were observed to be much greater than for other food products, the activation energy needed to start the drying process of the product was observed to be comparatively lower than for other high moisture products.

Over all the study achieved its objectives yielding critical parameters for the design of solar dryer, the product (*R. argentea* fish) as well as the operating parameters required for optimizing the solar drying process. The drying parameters of *R. argentea* fish product obtained were: mean drying rate constant; 0.204 $\pm$ 0.135 hr^{-1}, the critical moisture contents; 30 % or 0.30 moisture ratio, mean effective moisture diffusivity; $(1.65 \pm 0.02) \times 10^{-3} m^2/s$ and activation energy; - 15.954 kJ /mol.

Through mathematical modeling and simulation of the solar drying process of the fish in the solar dryer, the study also predicted the mean drying temperature and air mass flow rate of; 340 K and 0.06 kg/ s, respectively and relative humidity of ambient air range of between 25 % and 65 % as the conditions required to optimize the thin layer drying of *R. argentea* fish. Thus the information obtained in this study would thus be useful in the development process of an optimized commercial scale solar dryer for *R. argentea* fish. The experimental results revealed that drying of *R. argentea* fish occurred in the constant and falling rate periods with the former period lasting longer than the latter in contrast with other food products which have been found to exhibit falling drying rate periods and shorter or no constant drying rate periods. This

observation therefore suggests that the drying of *R. argentea* fish may be adequately described by an evaporation based rather than diffusion based model.

5.2 Recommendations of the Study

1. With the experimental results having revealed that a lower and safe moisture level could be achieved by drying *R. argentea* fish in a solar dryer rather than in open sun, in a significantly reduced drying time of less than 5 hours, the study recommends that the stakeholders in the fishing sector adopt the use of the solar dryers rather than traditional preservation methods as this would lead to significant improvement in quality and reduction of post harvest losses that currently occur due to prolonged drying periods associated with open sun drying, the main preservation method applied by the fish farmers in Lake Victoria.

2. Since results of the study have revealed that the model developed for the drying process of *R. argentea* fish, in an indirect solar dryer can be used to accurately predict the moisture ratio and drying times of the product, as confirmed by the statistical analysis, the study recommends the adoption of the drying model for *R. argentea* fish by the stakeholders and its use in the scaling up to a commercial solar dryer with the capability of drying the fish product in a period of less than five hours.

5.3 Recommendations for Further Work

1. Arising from the limitation of the short time span of the experimental tests in the present study it is suggested that further work on experimental drying tests on *R. argentea* fish could be carried over a much longer cycle to capture the seasonal variation in the operating parameters.

2. Further work could also be conducted on the effect of adopting the present drying model of *R. argentea* fish on drying time for a mixed or direct mode solar dryer.

REFERENCES

Abalone, R., Cassinera A., Gaston A. and Lara M. A., (2006). Thin layer drying of Amaranth seeds, *Biosystems Eng*. 93 (2): 179-188.

Abila, O. R., (2003). Food safety in food security and food trade Case study: Kenyan fish export, 2010 Vision for food agriculture and the environment, Focus 10, Brief 8 th September.

Afolabi, T. J., (2014). Mathematical modelling and simulation of the mass and heat transfer of batch convective air drying of tropical fruits, *Chemical and Process Eng. Resear*., 23: 9-19.

Afriyie, J. K., Rajakauna H., Nazha M. A. A. A. and Forson F. K., (2013). Mathematical modeling and validation of the drying process in a chimney dependent solar crop dryer, *J. Ener. Conv. and Mgt*. 67: 103-116.

Afzal, T. M. and Abe T. (2000). Simulations of moisture changes in barley during far infrared radiation drying, *Comput. Electron Agric*. 26: 137-145.

Aghbasho, M., Kianmehr M. H. and Akhijahani H., (2008). Influence of drying conditions on the effective moisture diffusivity, energy of activation and energy consumption during the thin layer drying of berberis fruit, *Energy Convers. Mgt.* 49: 2865-2871.

Ahmed, A. G., (2011). Design and construction of a solar drying system, a cylindrical section analysis of the performance of the thermal drying system, *African J. Agri*. 6 (2): 343-351.

Akoy, E. O. M., (2007). Mathematical modeling of solar drying of mango slices, PhD Thesis, University of Khartoum.

Akpinar, E. K., (2010). Drying of mint leaves in a solar dryer and under open sun modeling performance analyses, *Energy Conver. and Mgt* 51: 2407-2418 process of long green pepper in solar dryer under open sun, *Energy Conv. and Mgt*., 49 (6): 1367-1375.

Akpinar, E. K. and Bicer Y., (2008). Mathematical modeling of thin layer drying process of long green pepper in solar dryer under open sun, *Energy Conv. and Mgt*., 49 (6): 1367-1375.

Akipnar, E. K., Bicer Y. and Midilli A., (2003). Modeling and Experimental study on drying of apple slices in a convection Cyclone Dryer, *J. Food Proc. Eng*. 26 (6): 515-541.

Ali, S. A. and Bahnasawy A. H., (2011). Development of a simulation model for hybrid solar dryers as alternative sustainable drying system for herbal and medicinal plants, Proc. C.I.G.R section IV, Int. Symp. on Food Process, Bio- processing and Food quality Mgt.

Al-Juamily, K. E. J., Khalifa A. J. N. and Yassen T. A., (2007). Testing of Performance of fruit and vegetable solar drying systems in Iraq, *Desalination*, 209: 163-170.

Al-Juamily, K. E. J., Khalifa A. J. N., Yassen T. A., (2007). Testing of performance of fruit and vegetable solar drying systems in Iraq, *Desalination* 209: 163-170.

Alonge, A. F. and Hammed R. O., (2007). A direct passive solar dryer for crops. African Science Conf. Proc. Vol 8: 1643-1646.

Amer, B. M. A., Hossain M. A. and Gottschalk K., (2010), Design and performance evaluation of a new hybrid solar dryer for banana, *Ener. Convers. and Mgt*., 51 (4): 813-820.

Amedorme, S. K., Apodi J. and Agbeudor K., (2013). Design and construction of forced convection indirect solar dryer for drying moringa leaves, *Scholars J. of Eng. and Technol.* 1 (3): 91-97.

Arata, A., Sharma V. K. and Spagna G., (1993). Performance evaluation of solar assisted dryers for low temperature drying applications II: experimental results, *Energ. Conver. and Mgt*. 34 (5): 417-426.

Arbhosseni, A., Huisman W., Van Boxtel A. and Muller J., (2008). Modeling of thin layer drying of Tarragrin (Artenusa dracunclus L.) *Industrial Crop and Products* 28 (2): 53-59.

Awadalla, H. S. F., El-Dilo A. F., Mohamad M. A., Reuss M. and Hussein H. M. S., (2004). Mathematical modeling and experimental verification of wood drying process, *J. Ener. Conver. and Mgt.* 45 (2004): 197-207.

Bahnasawy, A. H. and Ali S. A., (2011). Development of a simulation model for the hybrid solar dryers as an alternative sustainable drying system for Herbal and Medicinal plants, CIGR Int. Symposium on towards a sustainable food chain process *Bio processing and Food quality Mgt*., France.

Babalis, S. J. and Belessiotis V., (2004). Influence of drying conditions on the drying constants and moisture diffusivity during mono- layer drying of figs, *J. Food Eng*., 65 (3): 449-458.

Baghari H., Arabhosseini A., Kianmehr M. H., Chegini C. R., (2013). Mathematical modeling of thin layer solar drying of tomato slices, *Agric. Eng. Int. C.I.G.R. J*. 15 (1): 146-153.

Bala, B. K. and Janjai S., (2009). Solar drying of fruits, vegetables, spices, medicinal plants and fish: Developments and Potentials, Proc. Intern. Conf. on Solar food processing, Bangladesh Agricultural University.

Bala, B. K. and Mondol M. R. A., (2009). Solar drying of fruits, vegetables, spices, medicinal plants and fish: Development and Potentials: International solar Food Processing Conference, http//www.solarfood.org/solarfood/page/solar food 2009/3 Full papers/ Technologies/145 Bala pdf (accesed 12/ 07/ 2010 at 12:00)

Bala, B. K. and Mondol M. R. A., (2001). Experimental investigation on solar drying of fish using a solar tunnel dryer, *Drying Technol*. 19: 1532-1537.

Bala, B. K. and Mondol M. R. A., (2006). Experimental investigation on solar drying of fish in a solar tunnel dryer, Drying Technol. 19 (2): 427-436.

Basunia, M. A., Handali H.H., Bahish M. T., Rahman M. S. and Mahgoubo O., (2011). Drying of fish sardines in Oman using solar tunnel dryers, *J. of Agric. Sci. and Technol*., BI (2011): 108-114.

Bentayab, F., Bekkioui N. and Zeghmati B., (2008). Modeling and simulation of a wood solar dryer in Moroccan Climate, *Ren. Ener*. 33: 501-506.

Berruti, F. M., Klaas M., Briens C. and Berutti F., (2009). Model for convective drying of carrots for pyrolysis. *J. of Food Eng*. 92 (2): 196-201.

Bicer, Y., Akpinar E. K. and Yildiz C., (2003). Thin layer drying of red pepper, *J. Food Eng*., 59 (1): 99-104.

Bolaji, B. O. and Olalusi A. P., (2008). Performance evaluation of a mixed mode solar dryer, *AU Journal of Technol*. 11(4): 225-231.

Brooker, D. B., Bakker-Arkema F. W. and Hall C. W., (1978). Drying cereal grains, AVI Publishing Co.

Buchinger, J. and Weiss W., (2002). Solar drying, Austrian Development Co-operations, Institute for Sustainable Technologies.

Chandrakumar, B. P. and Jiwanlal L. B., (2013). Development and performance evaluation of mixed mode solar dryers with forced convection, *Int. J. of Energ. and Enviromental Eng*. 4: 23.

Christie J. G., (2008). Transport Processes and Separation Process Principles, 4th Ed., New Jersey; Prentice Hall.

Chukwuka, T. N., Ejimofor R. and Onyemaobi O.O., (2009). Mathematical Analysis of Evaporation of the duration and conditions of latent drying of wet clays, *New York Science Journal* 2(7): 38-41.

Darvishi, H., Azadbakht M., Rezgeias A. and Farhang A., (2013). Drying characteristics of sardine fish dried with microwave heating, *Journal of Saudi Society of Agricultural Sciences* 12 (2): 121-127.

Davies, R. M., (2009). Traditional and Improved fish processing technologies in Bayelsa State Nigeria, Eikiatden J. European *J. Scientific Resear*. 26 (4): 539-548.

Doymaz, I. (2005). Drying characteristics and kinetics of Okra, *J. Food Eng*., 69: 275-279.

Ekechukwu, O. V. (1999). Review of solar energy drying systems I: an overview of drying principles and theory, Energy Conver. and Mgt. 40 (6): 593-613.

El-Beltaji, A., Gamea C. R. and Essa A. H., (2007). Solar drying characteristics of Strawberry, *J. Food Eng*., 78: 456-464.

Falade, K.O., Olurin T. O., Ike E. A. and Aworh C. O., (2007). Effect of pretreatment on air drying of Dioscorea alata and Doiscorea rotundata slices , *J. Food Eng*., 80 (4): 1002-1010.

Forson, F. K., Nazha M. A. A., Akuffo F. O. and Rajokauna H., (2007). Design of mixed mode natural convection solar crop dryers applications of principles and rules of thumb, *Ren. Ener*. 32: 2306 -2319.

Ghassan, M. T., Mohamad J., Shadi Z. and Mohamad A., (2014). A mathematical model of indirect solar drying of diary products (Jameed), *Energy and Env. Eng*., 2 (1): 1-13.

Ghaba, P., Andoh H. Y., Saraka j. K., Kona B. K. and Toure S., (2007), Experimental investigation of a solar dryer with natural convective heat flow, *J. Ren. Ener*. 32: 1817-1829.

Giner, S. A., (2009). Influence of internal and external resistances to mass transfer on constant drying rate period in high moisture foods, *J. Biosystem Eng*. 102 (1): 90-94.

Gokan, G., Necdet O. and Gungor A., (2009). Solar tunnel drying characteristics and mathematical modelling of tomato, *J. Therm. Sc. and Technol*., 29 (1):15-23.

Guarte, R., (1996). Modeling the "Drying behavior of Copra and development of a natural convection dryer for production of high quality Copra in the Philippines", PhD Thesis, Dissertation, 287 Hohenheim, University, Stuttgaut, Germany.

Gullman, R. G.,(2010). Development of Evaporation models for CFD applications within drying process simulation, MSc. Thesis, Dept. of Chemical Reactions Engineering, Chalmers University, Goteberg.

Hadrich, B. and Kechaou N., (2004). Mathematical modelling and simulation of heat and mass transfer phenomena in shrinking cylinder during In: Proceedings of the 14th International Drying symposium (IDS 2004) Sao Paulo, Brazil 22nd-25th Aug. Vol. A, pp. 533-541.

Hossain, M. A., Woods J. L. and Bala B. K., (2005) Optimization of solar tunnel dryer for drying of chilli without color loss, *Ren. Ener*. 30: 729-742.

Iguaz, A., Esnoz A., Martinez G., Lopez A. and Virseda P., (2003). Mathematical modeling and simulation for the drying process of vegetable wholesale by-product in a rotary dryer, *J. Food of Eng*., 59: 151-160.

Janjai, S., Sristipokekun N. and Bala B. K., (2008). Experimental investigation and modeling performances of a roof-integrated solar drying systems for drying herbs and spices, *J. Ener*. 33 (1): 91-103.

Janjai, S. and Tung P., (2005). Performance of a solar dryer using hot air from roof-integrated solar collectors for drying herbs and spices, *Ren. Ener*. 30 (14): 2085-2095.

Jindal, V. K. and Gunasekaran S., (1982). Estimating air flow and drying rate to natural convection in solar rice dryers, *Renewable Energy review*, 4 (2): 1-9.

Kaplanis, S. N., (2006). New Methodologies to estimate hourly global solar radiation: comparison with existing models, *Ren. Ener*. 31: 781-790.

Karim, M. A. and Hawlader M. N. A., (2005). Mathematical modeling and experimental investigation of tropical fruits drying, *Int. J. of Heat and Mass transfer* 48 (23- 24): 4914-4925.

Kavak, E. A., (2010). Drying of mint leaves in a solar dryer and under open sun: modeling performances analyses, *J. Ener. Conver. and Mgt*. 51 (12): 2407-2418.

Kemp, I. C. and Oakley D. E., (2002). Modeling of particulate drying in theory and practice, *Drying Technol*. 20 (9): 1699-1750.

Kenya Bureau of Standards, (KBS), (1998), Specification for dried *Rastrineobola argentea* (Omena/ Dagaa).

Kenya Industrial Research and development Institute, (KIRDI), (2008) Analysis of nutritional value of solar dried fish from L. Victoria, GTZ-PSDA stoves cluster Project on solar fish drying Draft Report.

Kituu, G. M., Shitanda D., Kanali C. L., Mailutha J. T., Njoroge C. K., Wainaina J. K. and Silayo V. K., (2010). Thin layer drying model for simulating the drying of Tilapia fish (*Oreochromis niloticus*) in a solar tunnel dryer, *J. of Food Eng*., 325-331.

Madhlopa, A., Jones S. A. and Saka J. D. K., (2002). A solar air heater with composite absorber systems for dehydration, *Ren. Ener*. 27: 27-37.

Midilli, A. and Kucuk H., (2003). Mathematical modeling of thin drying of Pistachio by using solar energy, *Ener. Conver. and Mgt*. 44 (7): 1111-1122.

Mohamed, L. A., Kouhila M., Jamali A., Lahsasni S., Kechaou N. and Mahrouz M.,(2005). Single layer drying behavior of Citrus Aurantium leaves under forced convection, *Energy convers. and Mgt,* 46: 1473-1483.

Morris, S., (1981). "Retrofitting with Natural convection collectors, In Wilson T., (Ed). Home Remedies": A Guidebook for Residential Retrofit, Philadelphia PA: Mid Atlantic Solar Energy Association, 152 -161.

Mujaffar, S. and Sankat C. K., (2005). The mathematical modeling of the osmotic dehydration of shark fillets at different brine temperature, *Int. J. of Food Sci. and Technol*., 41 (4): 405-416

Mustapha, M. K., Ajibola T. B., Salko A. F. and Ademola S. K. (2014). Solar drying and organoleptic characteristics of two tropical African fish species using improved low- cost solar dryers, *Food Sci. Nutri.* 2 (3): 244-250.

Murthy, M. V. R., (2009). A Review of new technologies, modes and experimental investigations of solar dryers, *J. Ren and Sust. Ener. Rev*. 13 (4): 835-844.

Nyeko, D., (2008). Challenges in sharing of L. Victoria fisheries Resources: Policies Institutions and Processes. L. V. F. O. Regional Stakeholders Conf., 27th -29th Oct. 2008, Imperial Royal Int. Hotel, Kampala.

Oduor-Odote, P. M., Shitanda D., Obiero M. and Kituu G., (2010). Drying characteristics and some quality attributes of *Rastrineobola argentea* (Omena) and *Stolephorous delicatulus* (Kimarawali), *African J. of food Agriculture, Nutrition and Development* 10 (8): 2998-3014.

Onyinge, G. O., Oduor A. O. and Othieno H. E., (2014). Investigating the thin layer drying characteristics of vegetable kales in a natural convection solar cabinet dryer under the climatic conditions of Maseno, Kenya, *Int. J. of Eng. Reser. and Technol*., 3 (8): 1527-1535.

Owaga, E. E., Mumbo H., Aila F. and Odhianbo O., (2011). Kenyan Artisanal fish industry, *Int. J. of cont. Bus*. 2 (12): 32-38.

Ozdemir, M. and Devres Y., (1999). The thin Layer Drying characteristics of Hazelnuts during Roasting, *J. Food Eng*., 42 (4): 225-233.

Rahman, M., (1998). Description isotherm and heat pump drying of peas, *Food Res., Int*. 30 (7): 485-491.

Pangevhane, D. R., Sawheng R. L. and Sarsavadia P. N., (2002). Design, development Performance testing of a new convection Solar dryer, *Ener*. 27: 579-590.

Panwar, N. L., Kaushik S. C. and Surendra K. (2013). Thermal modelling and experimental validation of solar tunnel dryer: a clean energy option for drying surgical cotton, *Int. J. of Low Carbon Technol*., pp. 1-13.

Raju, S. V. R., Meenakshi R. R. and Siva R. E., (2013). Design and fabrication of efficient solar dryers, *Int. J. of Ener. Resear. Appl*i. 3 (6): 1445-1458.

Reza, MD S., Jafor MD A. F. B., Nazrul I. and Kamal MD, (2009). Optimisation of marine fish drying using solar tunnel dryer, *J. Food Processing and Preservation* 33 (1): 45-59.

Sacilik, K. and Elicin A. K., (2006). Thin layer drying Characteristics of Organic apple slices, *J. Food Eng*., 73 (3): 281-289.

Sagagi, A. D. and Enaburekhan J., (2007). Review of simulations studies for grain drying in indirect sun and solar dryers, *Continental J. Eng. Sc*., 1: 27-35.

Saleh, A. and Badran I., (2009). Modeling and experimental studies on domestic solar dryer, *J. Renew*., 34(10): 2239-2245.

Saveda, M. S., (2012). Design and development of walk-in type hemi-cylindrical solartunnel dryer for industrial use, *ISRN, Ren. Energ*., 10: 5402-5411.

Sengar, S. H., Khandetod Y. P. and Mohod A. G., (2009). Low cost solar dryer for fish, *African J. of Envir. Sci. and Technol*. 3 (9); 265-271.

Simante, I. N., (2003). Optimisation of mixed mode and indirect mode natural convection solar dryers, *Ren. Ener*. 28: 435-453.

Smitabindhu, R., Janjai S. and Chakong V., (2008). Optimization of a solar assisted drying system for drying bananas, *Ren. Ener*. 33(7); 1523-1531

Sobukola, O., (2009). Effect of pre-treatment on the drying characteristics and kinetics of okra (*Abelmoschus esculentus* (L.) Moench) slices. *International Journal of Food Engineering*, 5 (2): 1-20.

Srikiatden, J., (2007). Moisture transfer in solid food materials: A review of mechanisms, models and measurements, *Int. J. of Food Properties*, 10: 739-777.

Tripathy, P.P. and Kumar S., (2009). A methodology for determination of temperature dependent mass transfer coefficients form drying kinetics: Application to solar drying, *Applied Thermal Eng* 90 (2): 212-218.

Tunde- Akirtunde, T. Y., (2011). Mathematical modeling of sun and solar drying of chilli pepper, *Ren. Ener*. 36 (8): 2139-2145.

Wakjira, M., (2010). Solar drying of fruits and windows of opportunities on Ethiopia, *African Journal of Food Sci*. 4 (13): 790-802.

Westerman, P. and White W., (1973). Relative humidity effect on the high temperature, drying of shelled corn. *Transaction of ASAE,* 16: 1136-1139.

Xanthopoulos, G., Lambrino G. and Manolopoulos H., (2007). Evaluation of thin layer models for Mushrooms (*Agricus bisporus*) drying, *Drying Technol*., 25: 1471-1481.

Yagcioglu, A., Degirmencioglu A. and Cagatay F., (1999). Drying characteristics of Laurel leaves under different drying conditions, *Proc. of the 7th Intern. Conf. on Agri. Mech. and Energy*, 565-569, 26-27.

Yaldiz, O. and Erteken C., (2001). Thin layer Solar drying some different vegetables, *Dry. Technol*., 19 (3): 583-596.

Yaldiz, O., Erteken C. and Uzun H. I., (2001). Mathematical modeling of thin layer solar drying of sultana grapes, *Ener*. 26: 457-465.

Youcef, I. K., Messaoudi H., Desmons J. Y. and LeRay M., (2001). Determination of the average coefficient of internal moisture transfer during the drying of a thin bed of poatato slices, *J. Food Eng*., 48 (2): 95-101.

Zomorodian, A. and Dadeishzadeh M., (2009). Mathematical modeling of forced convection thin layer solar drying of Cuminium Cyminium *J. Agric Sci. Technol*. 11: 391-400.

Zomorodian, A. and Moradi M., (2010). Mathematical modeling of a forced convection thin layer solar drying of Cuminium Cyminium, *J. Agric. Sci. Technol*. 12: 401-408.

APPENDICES

Table A1: The theoretical values used in the mathematical model of the solar dryer

Quantity	Description	Value
M_s	Mass of product to be dried	10.0 kg
m_i	Initial moisture content of product	73%
m_f	Final moisture content of product	15%
t	Total time of drying	14 hours
m_w	Mass of water evaporated	6.8 kg
V_a	Volume of air needed to evaporate moisture	1526.3 m^3
$\dot{v}_a$	Volume air flow rate	0.022 m^3 /s
η_c	Collector system efficiency	43.5 %
η_d	Drying efficiency	12.1 %
X_e	Equilibrium moisture content	13.42 %
ρ_a	Density of air	1.17 kg/ m^3
P_a	Partial pressure of air in atmosphere	101 k Pa
C_{pa}	Specific heat capacity of air	1007 J/ kg K
L_t	Latent heat of vaporization of water	2260 kJ/ K
T_{a2}	Temperature of air leaving dryer	301.5 K
T_{a1}	Temperature of air leaving collectors	311 K
[illegible]	Ambient air temperature	298 K
I_m	predicted mean value of solar radiation incident on collectors	496 W/m^2
A_c	Total surface area of collectors	5.0 m^2
l_s	Length of chamber	1.9 m
w	Width of collector	1.29 m
l	Characteristic length	2.0 cm
P_f	Power used to operate fan	40.3 W

Table A2: The mathematical drying models of various agricultural products

	Model Name	Model Equation	Reference
1.	Newton	$MR = \exp(-kt)$	(Westerman and White, 1973)
2.	Page	$MR = \exp(-kt^n)$	(Guarte, 1996)
3.	Modified Page	$MR = \exp(-kt)^n$	(Yagcioglu et al, 1999)
4.	Henderson and Pabis	$MR = a.\exp(-kt)$	(Yaldiz and Erteken, 2001)
5.	Logarithmic	$MR = a.\exp(-kt) + C$	(Yagcioglu et al, 1999)
6.	Two term	$MR = a.\exp(-kt) + b.\exp(-k_1 t)$	(Akipnar et al, 2003)
7.	Exponential two term	$MR = a.\exp(-kt) + (1-a)\exp(-kat)$	(Rahman, 1998)
8.	Wang and Singh	$MR = 1 + at + bt^2$	(Yaldiz et al, 2001)
9.	Thompson	$t = aInMR + b[InMR]^2$	(Guarte, 1996)
10.	Approximation of diffusion	$MR = a.\exp(-kt) + (1-a)Exp(-kbt)$	(Rahman, 1998)
11.	Midilli et al	$MR = a.\exp(-kt^n) + bt$	(Ozdemir and Devres, 1999)
12.	Verma et al	$MR = a.\exp(-kt) + (1-a)Exp(-gt)$	(Sacilik and Elicin, 2006)
13.	Gokan et al	$MR = at^3 + bt^2 + ct + 1$	(Gokan et al, 2009)

where a, c and n are drying coefficients and k is the drying constant.

Table A3: Statistical tests based on Moisture ratios of the fish in the top, middle and bottom trays

	Student " t "		**One way Anova test**		
	t	*p*	*t*	*p*	
Top left tray / model	0.327	0.7481	0.1068	0.7481	Not significant
Top right tray / model	- 0.4236	0.6775	0.1794	0.678	Not significant
Middle left tray/ model	0.0483	0.9621	0.00233	0.9621	Not significant
Middle right tray/ model	0.02857	0.9776	0.000816	0.9776	Not significant
Bottom right tray/ model	- 0.1622	0.8732	0.02629	0.8732	Not significant
Bottom left tray/ model	0.1465	0.8853	0.02147	0.8853	Not significant